LAWRENCE
LIVERMORE
NATIONAL
LABORATORY

LLNL-TH-725751

Enhancing Electrophoretic Display Lifetime: Thiol-Polybutadiene Evaporation Barrier Property Response to Network Microstructure

C. C. Cook

March 2, 2017

Disclaimer

This work performed under the auspices of the U.S. Department of Energy by Lawrence Livermore National Laboratory under Contract DE-AC52-07NA27344.

ENHANCING ELECTROPHORETIC DISPLAY LIFETIME: THIOL-POLYBUTADIENE EVAPORATION BARRIER PROPERTY RESPONSE TO NETWORK MICROSTRUCTURE

A Thesis
presented to
the Faculty of California State Polytechnic State University,
San Luis Obispo

In Partial Fulfillment
of the Requirements for the Degree
Master of Science in Polymers and Coatings Science

by
Caitlyn Christian Cook
March 2017

COMMITTEE MEMBERSHIP

TITLE:	Enhancing Electrophoretic Display Lifetime: Thiol-Polybutadiene Evaporation Barrier Property Response To Network Microstructure
AUTHOR:	Caitlyn Christian Cook
DATE SUBMITTED:	March 2017
COMMITTEE CHAIR:	Shanju Zhang, PhD Assistant Professor of Chemistry
COMMITTEE MEMBER:	Andrew J. Pascall, PhD Lawrence Livermore National Laboratory
COMMITTEE MEMBER:	Raymond Fernando, PhD Kenneth N. Edwards Endowed Chair

ABSTRACT

Enhancing Electrophoretic Display Lifetime: Thiol-Polybutadiene Evaporation Barrier Property Response To Network Microstructure

Caitlyn Christian Cook

An evaporation barrier is required to enhance the lifetime of electrophoretic deposition (EPD) displays. As EPD functions on the basis of reversible deposition and re-suspension of colloids suspended in a solvent, evaporation of the solvent ultimately leads to device failure. Incorporation of a thiol-polybutadiene elastomer into EPD displays enabled display lifetime surpassing six months in counting and catalyzed rigid display transition into a flexible package. Final flexible display transition to mass production compels an electronic-ink approach to encapsulate display suspension within an elastomer shell. Final thiol-polybutadiene photosensitive resin network microstructure was idealized to be dense, homogeneous, and expose an elastic response to deformation.

Research at hand details an approach to understanding microstructural change within display elastomers. Polybutadiene-based resin properties are modified via polymer chain structure, with and without added aromatic urethane methacrylate difunctionality, and in measuring network response to variation in thiol and initiator concentration. Dynamic mechanical analysis results signify that cross-linked segments within a difunctionalized polybutadiene network were on average eight times more elastically active than that of linked segments within a non-functionalized polybutadiene network. Difunctionalized polybutadiene samples also showed a 2.5 times greater maximum elastic modulus than non-functionalized samples. Hybrid polymer composed of both polybutadiene chains encompassed TE-2000 stiffness and B-1000 elasticity for use in encapsulating display suspension. Later experiments measured kinetic and rheological response due to alteration in dithiol cross-linker chain length via real time Fourier transform infrared spectroscopy and real-time dynamic rheology. Distinct differences were discovered between dithiol resin systems, as maximum thiol conversion achieved in short and long chain length dithiols was 86% and 11%, respectively. Oscillatory real-time rheological experiments confirmed a more uniform network to better dissipate applied shear in short chain length dithiol systems, as long chain length dithiols relayed a steep internal stress build-up due to less cross-links and chain entanglements. Thorough understanding of network formation aids the production of a stronger and impermeable elastomeric barrier for preservation of EPD displays.

Keywords: thiol-ene, displays, evaporation barrier, elastomer, polybutadiene

ACKNOWLEDGEMENTS

First, I would like to thank Lawrence Livermore National Laboratory for providing me with my master's project and internship opportunity. Never have I worked at an establishment where I have felt so supported and encouraged by my entire department, while working on and with state-of-the-art technologies. A big thank you to my mentor, Dr. Andrew Pascall, who initially brought me on board as an intern and proceeded to provide guidance throughout my entire project. Andy invests his time in helping a broad range of projects around the lab, and meets with individual members to ensure all questions have been answered to the best of his ability. I have been honored to receive the same treatment throughout my project as he has been invested in my success in obtaining my master's degree, as well as in my success at the lab.

Concurrently, my team, the "Hammer" team, has been a strong support system. We had biweekly meetings where members encouraged me to provide updates on my project as to ensure all was progressing smoothly, and because they were sincerely interested in the results I was obtaining. Thank you to Dr. Joshua Kuntz, Dr. Marcus Worsley and Dr. Elaine Lee for your random check-ins to discuss and help with my project plans and needs, and for generally caring about my well-being. Thank you for constantly sharing your technical wisdom and providing constructive criticism, which I greatly appreciate. Without you all, my project experience would not have been the same.

A big thank you to my advisor, Dr. Shanju Zhang, for working with me from a distance. Dr. Zhang realizes potential in each of his students and works to maximize that potential in all work performed. At a distance, Dr. Zhang has been extremely flexible in receiving presentations and updates via video calls and screen sharing. Thank you for keeping me on track to fulfill all thesis requirements.

Dr. Raymond Fernando has also been an encouragement and help during my masters project, and in the year prior. He hired me as a research assistant for a barrier coating project that provided me with some experience and knowledge when stepping into my internship. Additionally, Dr. Fernando also helped in ensuring all graduation paperwork was submitted to make obtaining my Master's degree a smooth process.

Last but certainly not least, I would like to thank my Heavenly Father for presenting this project opportunity and giving me strength to finish my master's project to the best of my ability. Thank you to my friends and family who constantly encouraged, prayed, and believed in me every step of the way. I could not have succeeded in this project without you all!

LLNL-TH-725751

Prepared by LLNL under Contract DE-AC52-07NA27344.

TABLE OF CONTENTS

Page

List of Tables…….. viii

List of Figures……. ix

Chapter

1. INTRODUCTION..…… 1

1.1. Longevity Enhancement of Electrophoretic Displays…… 1

1.1.1. Electrophoretic Display Technology at Present…… 1

1.1.2. Edge Sealing & Encasing Displays…….. 3

1.1.3. Micro-encapsulation of Display Media…… 5

1.2. A Short History of Thiol-ene Chemistry in Rubbers…….. 7

1.3. Advantages of Multifunctional Thiols as Cross-linking Agent……..… 8

1.4. Mechanical & Physical Properties of Thiol-Ene Networks…… 10

1.5. The Mechanism of Photo-cross-linking Thiol-Polybutadiene……...…….. 19

1.5.1. Step-Growth Radical Addition Mechanism…… 19

1.5.2. Photo-cross-linking Kinetics of Thiol-Polybutadiene…..……... 25

1.5.3. Complications of Cross-linking High Molecular Weight Polybutadiene

..... 28

1.5.4. Photoinitiator Selection…… 31

2. EXPERIMENTAL PROCEDURE…… 34

2.1. Resin Constituents…….. 34

2.2. Device Preparation…….. 36

2.2.1. Sealing……..... 36

2.2.2. Spacing..... 37

2.2.3. Encasing..... 37

2.3. Encapsulation via Microfluidics..... 39

2.4. Instrumental Methods of Analysis..... 40

2.4.1. Dynamic Mechanical Analysis..... 40

2.4.2. Swell Testing..... 41

2.4.3. Real-Time Fourier Transform Infrared Spectroscopy..... 42

2.4.4. Rheology..... 44

3. RESULTS AND DISCUSSION..... 46

3.1. Preliminary Investigation..... 46

3.2. Effect of Thiol and Initiator Concentration on Functionalized and Non-Functionalized Polybutadiene..... 50

3.2.1. Cross-linking Density Determination..... 52

3.2.2. Compressive Material Properties..... 55

3.3. Hybrid Polymer..... 59

3.4. Cross-linking Variation Among Dithiol Carbon Chain Length..... 65

3.4.1. Real-time Fourier Transform Infrared Spectroscopy..... 66

3.4.2. Real-time Rheology..... 78

3.4.3. Internal Network Stress Variation 82

4. RESEARCH OUTLOOK..... 86

5. CONCLUSIONS..... 89

6. REFERENCES..... 91

LIST OF TABLES

Table Page

Table 2.1. Respective dithiol molecular weight differences ……..... 36

Table 3.1. Rate, conversion and relative reactivity ratio comparison between dithiol systems ……..... 71

Table 3.2. Dithiol resin system initial viscosities at $1x10^3$ s^{-1}…….. 72

Table 3.3. Stage II polymerization network stress build-up as a function of thiol conversion…….....……..... 80

LIST OF FIGURES

Figure Page

Figure 1.1. EPD schematic within a display with no applied electric field (left) and with an applied electric field (right)..... 2

Figure 1.2. Cross-section of display stacking architecture of rigid (top) and flexible (bottom) devices. Sealant and encasing preservation application of elastomer within EPD displays..... 4

Figure 1.3. Electronic ink-like microencapsulated NP suspension with photo-initiated elastomer shell..... 5

Figure 1.4. Double-emulsion microfluidic cell for polymer shell encapsulation [9].... 6

Figure 1.5. Schematic of first normal stress calculation components..... 13

Figure 1.6. Isotropic network prior to shear (left) and after shear (right). Compressed segments in yellow cause a greater positive axial force than elongated segments identified in red [41]..... 14

Figure 1.7. Measure stress and strain as a function of time during dynamic loading of a viscoelastic material [45]..... 15

Figure 1.8. DMA with increasing temperature graph portrays network uniformity [11]. 17

Figure 1.9. Comparing molecular structures of rigid Kevlar vs elastic polybutadiene..... 18

Figure Page

Figure 1.10. Increasing degree of crosslinking as functional groups react in step-growth and chain-growth polymerization methods..... 20

Figure 1.11. Radical step-growth mechanism for common thiol-polybutadiene chemistries..... 21

Figure 1.12. Homopolymerization (left) vs cross-linking (right) reaction pathway that each 1,2-butadiene unit can take with a difunctional thiol compound..... 22

Figure 1.13. Cross-linking reaction possibilities of both 1,2-units and 1,4 "trans" butadiene units..... 23

Figure 1.14. Oxygen reaction during thiol-ene chemistry may produce oxygen radicals or hydroxysulfoxides..... 24

Figure 1.15. Steps composing the thiol-polybutadiene cross-linking reaction..... 27

Figure 1.16. Translational diffusion of two radicals leading to diffusion-controlled termination..... 29

Figure 1.17. Gel effect demonstrated via double bond (–) and thiol (---) conversions within multiple dimethacrylate oligomer and monofunctional thiol formulations. From [46]..... 31

Figure 1.18. Initial bond cleave of DMPA at α-carbon upon illumination..... 32

Figure 1.19. Exciplex formation of BP upon illumination and radical formation with thiol..... 33

Figure 2.1. B-1000 and TE-2000 PB representative molecular structures..... 35

Figure Page

Figure 2.2. Sealant polymer with kapton tape spacer (left) and spacer polymer replacement (right)..... 37

Figure 2.3. Illustrated procedure of encasing flexible electrodes with elastomer resin..... 38

Figure 2.4. NP suspension encapsulation schematic via microfluidics..... 40

Figure 2.5. Horizontal absorbance apparatus used for RT-FTIR experimentation 43

Figure 2.6. Thiol (A.), PB vinyl (B.), and benzyl radical peak (C.) conversions with UV exposure time..... 43

Figure 2.7. RT-Rheology diagram of bottom-up curing of resin between two parallel plates. From TA Instruments product guide..... 44

Figure 3.1. Spacer elastomer layer uniformity comparison of spin coating deposition (left) vs doctor blade deposition (right)..... 46

Figure 3.2. Imperfections in capsule shell surface due to high viscosity of TE-2000 and voids..... 49

Figure 3.3. Increased polymerization stress from a two second cure with 2.5 W/cm^2 light (left) opposed to a five minute cure from a 550 $\mu W/cm^2$ light (right) 50

Figure 3.4. Radical reaction pathway in difunctionalized PB after excitation via UV light..... 51

Figure 3.5. Swell percentage comparison between B-1000 (A) and TE-2000 (B) 53

Figure 3.6. Gel percentage comparison between B-1000 (A) and TE-2000 (B).... 54

Figure Page

Figure 3.7. Tan delta values displaying more elastic modulus dominated B-1000 samples in comparison to TE-2000 samples..... 57

Figure 3.8. Average compressive elastic moduli values for TE-2000 and B-1000 matrix samples..... 59

Figure 3.9. Decreasing hybrid polymer viscosity with increasing B-1000 concentration at 1000 s^{-1}..... 60

Figure 3.10. Cross-linking density determination via swell testing shows a decrease in swelling with increasing thiol percentage and subsequent increase in gel percentage..... 61

Figure 3.11. Stiffness and loss tangent properties of hyrbid polymer falling between those of TE-2000 and B-1000 samples..... 62

Figure 3.12. Encapsulation with HP lacking dithiols resulted in stable capsules in the continuous fluid (left) and concaved capsules after drying (right). Shell thickness ~ 17 μm..... 63

Figure 3.13. HP with 0.05 molar thiol ratio encapsulating boron suspension when suspended in DI water (left) and spherical capsules post drying (right)..... 64

Figure 3.14. Cracking within flexible EPD cell resin encasing, as a result of long dithiol CL (left) in comparison to short CL dithiol resin (right)..... 66

Figure 3.15. Thiol Conversion comparison of increasing carbon CL as a function of time..... 67

Figure 3.16. Displaying step-growth trend in thiol conversion for 1,5-pentanedithiol resin system..... 68

Figure 3.17. Linear slope transition from stage I polymerization (~20 seconds) to stage II in representative HD resin system..... 69

Figure Page

Figure 3.18. Vinyl vs thiol conversion graph displaying an increased C=C reactivity for higher molecular weight dithiols..... 71

Figure 3.19. Copolymerization vs homopolymerization of 1,2-butadiene vinyl groups..... 75

Figure 3.20. Double peak due to oxygen side reaction with thiols in PD (left) and DD (right) resin systems..... 77

Figure 3.21. No significant initiator benzyl radical inhibition when compared to that of thiol conversion during early exposure times..... 77

Figure 3.22. Representative dynamic oscillatory rheology plot vs. UV exposure time, displaying the gelation point of when G' crosses G"..... 78

Figure 3.23. Representative plots portraying positive values of calculated shear stress distribution with time (left) and elastic shear modulus increase with increasing thiol conversion (right)..... 80

Figure 3.24. Complex viscosity as a function of thiol conversion for PD and DD resin systems follow similar trends to that of increasing G' as a function of thiol conversion..... 81

Figure 3.25. Axial force change due to increasing dithiol CL displaying greater network contraction in short CL dithiols, and greater stress in long CL dithiols.... 83

Figure 3.26. Greater shrinkage stress in HD compared to DD, verified via first normal stress measurements..... 84

Figure 4.1. Preliminary DSC characterization of TE-2000 without thiol and with 0.05 molar ratio thiol:vinyl addition..... 87

1. INTRODUCTION

1.1. Longevity Enhancement of Electrophoretic Displays

Today, electrophoretic displays compete in the drive for thin, low-powered display technology. By far the most common, recent example of electrophoretic display technology is found in electronic paper (e-paper), or electronic ink (e-ink), of e-readers (i.e. Amazon Kindle or Sony's Reader), and also used in watches and cell phones [1]–[3]. These displays support long battery life and are reflective, meaning they do not require a backlight. Although electrophoretic deposition (EPD) based display technology will be elaborated on, one major challenge in producing flexible EPD displays is preserving the display lifetime. As display media is composed of a suspension of colloids, preserving the suspension solvent is of vital importance to the display usability. The following study presents the advancement of thiol-polybutadiene photosensitive elastomer formulations to act in preserving EPD active display media. The applied methods of display preservation are discussed in detail, along with chemical, mechanical, and physical elastomeric property requirements.

1.1.1. Electrophoretic Display Technology at Present

EPD is a process by which colloid particles suspended in a solvent are deposited on an electrode via the application of an applied electric field [4]. Colloid surface charge and the magnitude of an applied electric field drives EPD, and Brownian motion re-suspends the colloids when the field is removed [4]. Conventionally, low power EPD displays desire bistability, where an image remains visible even with removal of power [1]. However, the display application for this work requires an image to be erased without

applied power. Display image must be reversible by applying a electric field to produce the image, and erasing the image as colloids re-suspend when the electric field is removed (Figure 1.1). When deposition occurs on an optically transparent electrode, suspensions are able to strongly diffract visible light as colloid particles self-assemble into a photonic quasi-crystal [5], [6]. Reflective photonic displays use the structural and pigmentary color of dielectric particles to provide tunable color in a single pixel. Structural color of a photonic crystal is the result of light interference with its periodic structure, which can be tuned by manipulating the periodicity and/or refractive index of the crystal [7].

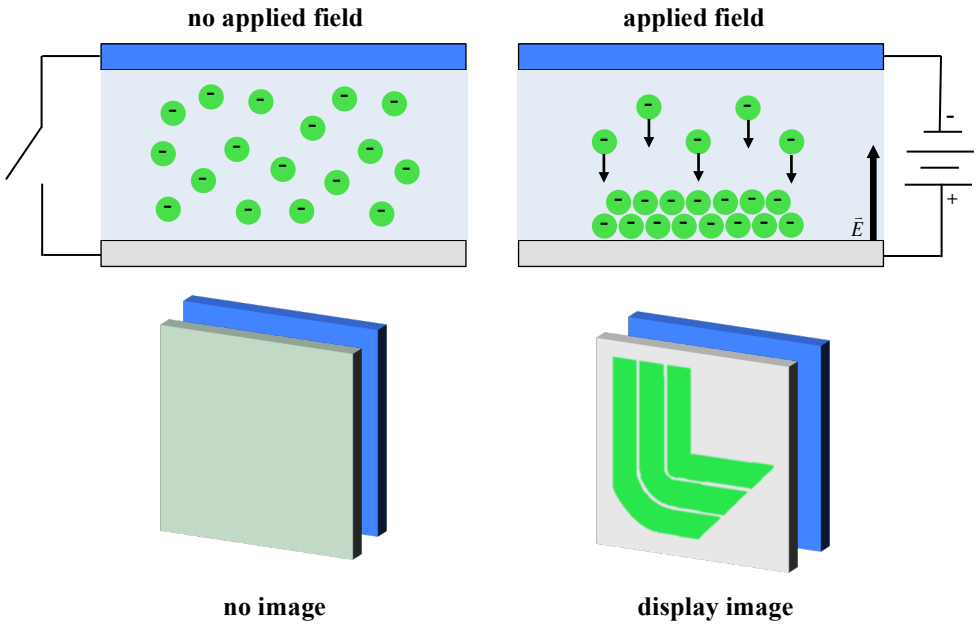

Figure 1.1. EPD schematic with a display with no applied electric field (left) and with an applied electric field (right).

EPD suspension utilized in the display is composed of α-Fe_2O_3/SiO_2 core/shell nanoparticles (NPs) in propylene carbonate (PC) solvent. Without the solvent, colloids are unable to deposit and re-suspend, thus terminating device functionality. PC has a low

vapor pressure (0.13 mmHg @ 20°C), is low in toxicity, and requires low voltages to actuate the nanoparticles (NPs) to the attractive electrode. Although PC has a low volatility, display lifetime was shown to be two to three days until solvent evaporates. EPD displays are required to last for at least 10 years without any degredation of EPD performance. To enhance device lifetime, three methods have been proposed: utilization of polymer to edge seal the device, complete encasing of displays within a barrier polymer, and micro-encapsulation of the suspension within a thin elastomer shell. No matter the method, the photo-sensitive elastomer formulation is required to be immiscible with PC and unreactive when cured. As PC has a polarity (6.1 P') similar to that of water (10.2 P') [8], the elastomer system was required to be entirely non-polar. Prior work determined 1,2-polybutadiene (PB) to be an appropriate base polymer. The present work has developed PB-based elastomer formulations to cure within 10 seconds of UV light exposure. Additionally, all elasomer formulations cure transparent, enabling the display area to be the only colored region of the device.

1.1.2. Edge Sealing & Encasing Displays

Initial stages of display development utilized a top indium tin oxide (ITO)/glass electrode and a bottom electrode of platinum/silicon, aluminum/silicon, or ITO/glass. Ultimately, the desired display will be composed of flexible transparent conductive electrodes, with complete device stacking architecture not to exceed 35 μm in thickness. ITO coated polyethylene tetraphthalate (PET, 150 μm thickness) electrodes comprised electrodes in initial attempts in producing flexible displays. Display sealing is localized around the perimeter of the gap separating opposing electrodes (Figure 1.2), where spacer

material determines the thickness separating the electrodes and sets the maximum allowable volume of NP suspension in the display window area. Kapton tape of 25-μm thickness was initially employed as the spacer material, mainly for usage of the known thickness. This thickness was found to provide high contrast images of colors changing from green to purple when turning the applied electric field off and on, requiring only 0.18 Watts of power. Thus, 25 μm was set as the maximum thickness that an elastomeric spacer should succeed. Ideally, a spacer would produce a 10-25 μm gap between device electrodes, with a lesser gap requiring a lower voltage to be applied. Kapton tape was an issue because the α-Fe_2O_3/SiO_2 core/shell suspension had a high affinity towards Kapton, driving media out from display window area and the Kapton was undesirably yellow in color.

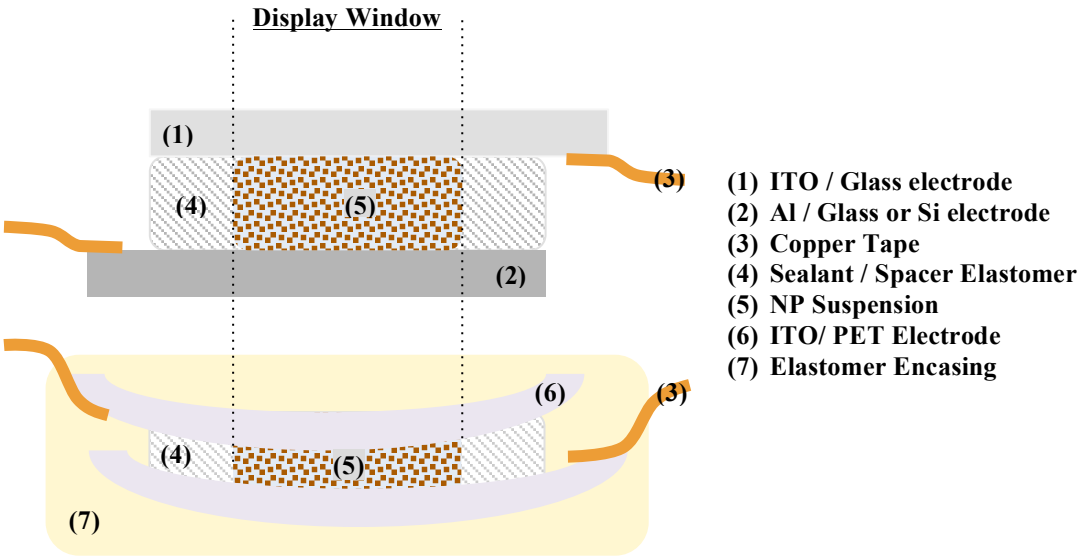

Figure 1.2. Cross-section of display stacking architecture of rigid (top) and flexible (bottom) devices. Sealant and encasing preservation application of elastomer within EPD displays.

Sealant/spacer elastomer must be impermeable to propylene carbonate and act to adhere the two electrodes together. For rigid electrodes, sealing is straightforward as

electrode positions are fixed. Sealing NP suspension with the elastomer on flexible electrodes is more challenging. With the flexible electrodes, it is more difficult to coat a uniform surface thickness, which is necessary for even color distribution across the display window area.

Encasing is developed to reinforce flexible display durability as well as attempt to easy flexible display fabrication. For encasing flexible electrodes, elastomer network must be strong enough to endure tensile and compressive forces of the underlying PET electrode and withstand constant deformation applied by the user. As the encasing may be thicker than the 25 μm spacer, formulations must be able to evenly cure throughout the entire thickness.

1.1.3. Micro-encapsulation of Display Media

Microencapsulation of the NP suspension allows for manufacturing methods such as rotogravure printing, as microcapsules can be formulated into inks. Similar to e-ink in a Kindle or other low-power portable displays, EPD of NP suspension will occur within the core of elastomer capsule shell (Figure 1.3).

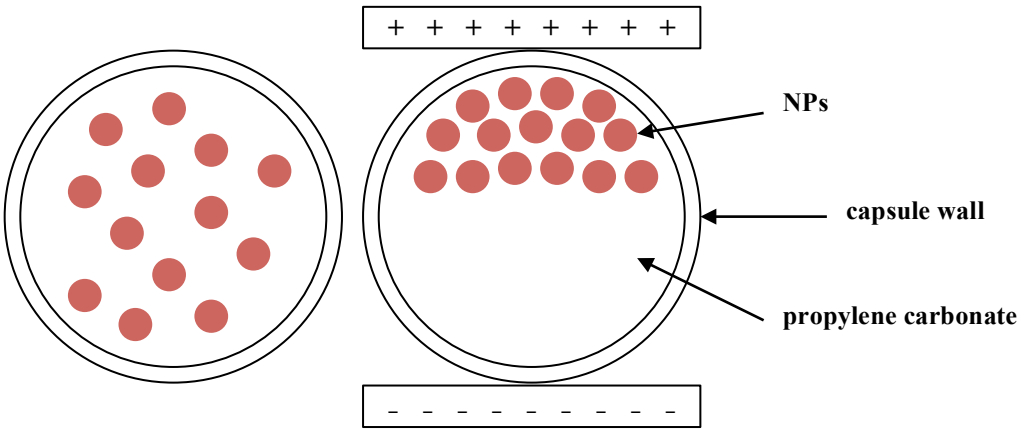

Figure 1.3. Electronic ink-like microencapsulated NP suspension with photo-initiated elastomer shell.

Microcapsules are made via a double emulsion microfluidic cell, where three fluids are input into the device at one time: the NP suspension core, shell elastomer resin, and continuous fluid (Figure 1.4). Coaxial capillaries face each other, with outlet diameters, flow parameters, and inlet fluid viscosities dictating the final size of the whole capsule, as well as the thickness of the cured elastomer shell [9]. NP suspension is pumped through the inside of the left capillary, with elastomer resin flowing in the same direction in the outside of the capillary. Continuous fluid opposes the flow when entering from the outside of right capillary, hydrodynamically pinching the flow from the left capillary into double emulsion droplets. Droplets continue flowing through the right capillary until reaching a ultraviolet (UV) light chamber. Capsules experience approximately 10 seconds of UV light exposure while flowing in the outlet tube, until cured capsules are captured in a vial of deionized (DI) water. Capsule fabrication rates range from 200 to 5000 drops s^{-1} dependent on the size of the capillaries (usually 20 to 400 μm diameter) and the parameters mentioned previously [9].

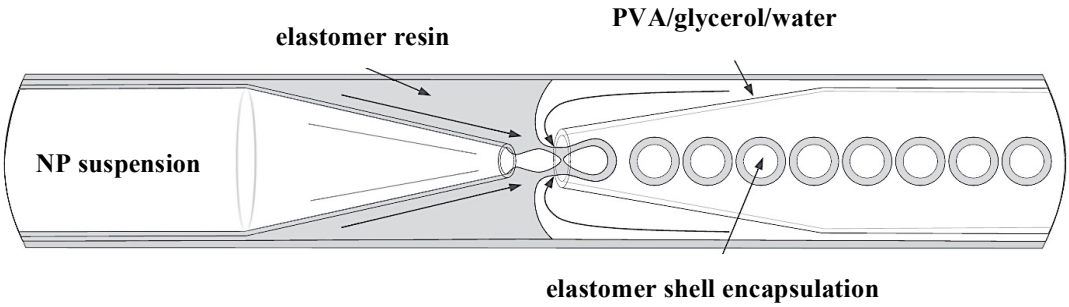

Figure 1.4. Double-emulsion microfluidic cell for polymer shell encapsulation [9]

Elastomer resin viscosity dramatically affects flow rates necessary to encapsulate the NP suspension. Maximum microfluidic cell input fluid viscosity is around 500 mPa.s at shear rates of at least 10^3 s^{-1}. If utilizing monomer species, resin viscosities should meet microfluidic viscosity criteria. However, 1,2-polybutadiene is not commercially available as a monomer in liquid form, but rather as a gas. Manipulating resin viscosity is essential for forming EPD microcapsules, without deteriorating cross-linking density or network strength.

Dense cross-linking density is vital for elastomer shell to withstand high loads of compression during printing methods such as rotogravure. This requires capsules to be flexible and entirely elastomeric in order to undergo elastic deformation when subject to applied force. Polybutadiene has been utilized in rubbers and shown to be an ideal elastomer base material for thiol-ene chemistry.

1.2. A Short History of Thiol-ene Chemistry in Rubbers

Although not a novel idea, thiol-ene chemistry became popular when Charles Goodyear patented the vulcanization of natural rubber, poly(cis-isoprene), by sulfur in the mid-19th century [10]. During this time, poly(isoprene) was utilized for consumer products with the downside of acquiring sticky and soft properties during summer months, hard and brittle properties during winter, and a high degradation rate. Goodyear's introduction of the synthetic polymerization method of 'vulcanization' was simply adding sulfur or an oxidizing agent and heat. By performing this process and recording sulfur ratios used, properties of the synthetic rubber remained the same throughout cold (generally above -40°C) and heat. At lower sulfur ratios of about 5 to 8

parts in 100 parts of rubber, a “high” tensile strength and elongation was achieved. Goodyear observed that tensile strength remained relatively the same with the loss of elongation when increasing sulfur to 30-50 parts. The exact chemical mechanism of thiol-ene vulcanization was not well understood due to lack of accurate analytical methods; however, much progress has been made since then.

The first photo-initiated thiol-ene industrial films and coating applications were presented by Morgan and Ketly in 1975, to produce conformal coatings on electronics and relief plates [11], [12]. Since then, Norland Products produced thiol-ene optical and electronics adhesives that were successfully input into industry [13], followed by an increased interest by the National Science Foundation to fund research by Bowman and Cramer [14]–[16] and Hoyle [11]. In-situ experimentation by Chiou et al. also sparked interest to investigate radical step-growth polymerization kinetics [17], [18]. Today thiol-ene polymerization is utilized in a wide range of applications, including coatings to dental materials, contact lenses, and photolithographic processes [19]–[24].

1.3. Advantages of Multifunctional Thiols as a Cross-linking Agent

Along with the academic interest in thiol-ene chemistry, industrial interest was piqued due to the large improvement in mechanical and physical bulk properties. The inherent chain-transfer step within thiol-ene propagation enables a longer gelation point compared to acrylate based resins, leading to a reduction in shrinkage stress, a more uniform network, and a reduction in oxygen inhibition [25]. Additionally, reduction of internal network stress leads to an increase in adhesive strength [11]. Controlling the

cross-linking density to maintain adhesive properties and not harden significantly is an important measure when using thiol-ene chemistry as an adhesive or sealant [26].

Specifically, in relation to dental resins and composites shrinkage and de-bonding have significant effects in applications such as tooth fillings, which have been improved on with thiol-ene chemistries [19]. Current dimethacrylate dental resins cross-link via chain-growth polymerization, resulting in polymerization shrinkage, incomplete conversion, and shrinkage stress [19]. Although the development of shrinkage stress due to the reduction in molecular spacing from previous van der Waal separation between polymer chains to covalent bonds [27] is inevitable, significant shrinkage stress restricts resin usage in dental composites. Low conversions are due to oxygen inhibition as oxygen attacks carbon radicals, producing an oxygen radical that further propagates to diminish the degree of cross-linking. Attempting to overcome oxygen inhibition by introducing higher acrylate functionalities or an increase in initiator concentration results in an even higher degree of shrinkage stress, thus catalyzing the interest towards alternative photo-initiated resin chemistries like that of thiol-ene. Reduced oxygen inhibition in thiol-ene resins functions on the bases of chain-transfer, as oxygen radicals are deflected by hydrogen abstraction, and a thiyl radical is produced to further the cross-linking reaction (see sec 1.5.1 for reaction scheme) [28].

Radical step-growth of thiol-ene chemistry also leads to an increase in depth of cure, adaptable formulation chemistry related to altering thiol monomer structure and functionality, a decrease in toxicity when compared to acrylate based formulations, and the ability to start-and-stop reaction by addition and removal of UV light [29]. In the application of photolithography, high-resolution geometries can be achieved after

washing away residual uncured polymer resin as only the absorbing species in the exposed areas initiate cross-linking. Cross-linking can be controlled to a specific location by utilizing a photomask or high resolution projection or laser, enabling production of fine features down to the nanoscale [30]. Curing thick samples of photosensitive resin is challenging as light penetration is insufficient and cannot initiate all radical species within the bottom layer of the sample. This phenomenon is referred to as the inner filter effect, as absorbing species close to the irradiated surface absorb UV light preventing activation of species towards the substrate [31]. However, as thiol-ene chemistry propagates via step-growth mechanism, irradiation at the surface of the sample has been shown to be sufficient to continue throughout thick samples (exceeding 10 cm) [32].

1.4. Mechanical & Physical Properties of Thiol-Ene Networks

Studies have shown that altering thiol-ene monomer functionality, molecular structure, and stoichiometric balance of formulation chemistry will admit significant changes in physical and mechanical bulk properties [14], [17], [33]. Thiol-ene elastomeric structure consists of a dense cross-linked network. Cross-link density and network homogeneity that a formulation achieves directly influences bulk properties, with a higher degree of conversion typically providing a higher mechanical strength [34]. For cross-linking to occur, both thiol and ene constituents must have a functionality of at least two, although many studies use monomers with three to four functional groups to obtain higher cross-linking densities [35]. However, with high functionalities of monomer A (f_A) and monomer B (f_B) and total functionaliy ratio r, Flory-Stockmayer theory (Equation 1.1) hypothesizes a lower critical conversion (x_c) to reach the gelation

point, leading to an ultimately higher shrinkage stress [36]. Shrinkage stress within a polymer network is directly proportional to conversion during curing [20], [37].

$$x_c = \frac{1}{[r(f_A-1)(f_B-1)]^2} \quad (1.1)$$

Real time-rheology has been utilized to determine the gelation point (GP), quantify stress at the GP, shrinkage stress, and network deformation via dynamic oscillatory experimentation. In 1986, Winter and Chambon developed equations for quantitative analysis of linear viscoelasticity of a cross-linked polymer at GP that have become a staple throughout rheological studies. To their definition, GP is the point at which G', the storage or elastic modulus is equal to G", the loss or viscous modulus, when subjected to a constant frequency and strain in an initially linear viscoelastic region of the polymer resin [38], [39]. Approaching the GP signifies the appearance of insoluble chemical cross-linked regions, or gel regions, which later will form an infinitely cross-linked network at full conversion. The strength (S) of the network at gel point is determined by G' when equal to G" at constant oscillation frequency (ω_o) (Equation 1.2). As in Chiou's study, measuring the strength at GP provides insight to the network microstructure that is forming as the resin is exposed to UV light.

$$S = G'[\frac{\pi\omega_o}{2}]^{-1/2} \quad (1.2)$$

Shrinkage stress development occurs directly after reaching the gelation point (GP), or the point at which a sufficient number of covalent bonds form insoluble regions, during conversion. The GP distinguishes the irreversibility of a thermosetting reaction and marks the point at which the elastic properties dominate viscous properties. Multiple studies have performed real-time Fourier infrared transform (RT-FTIR) spectroscopy in combination with real-time dynamic rheological experimentation in order to compare the

GP of a select matrix of resins to better understand how manipulating thiol-ene chemistries defers conversion until GP. Chiou et al. measured conversion vs. GP differences at multiple temperatures of reacting a trifunctional allyl monomer with either a trifunctional or tetrafunctional thiol monomer. Room temperature (25˚C) GP results for trifuntional and tetrafunctional thiol monomer formulations were 2160 and 310 seconds at conversions of 0.50 and 0.41, respectively. Strength at the gel point was calculated by the Winter-Chambon criterion, indicating a greater strength in the trifunctional thiol system due to a higher conversion and thus a higher cross-linking density [18].

Measuring the force or stress on the upper parallel plate geometry during real-time rheological experiments can aide understanding to the degree of shrinkage stress during network formation and a qualitative measure to internal network stress post network formation. For example, shrinkage stress due to cross-linking can be quantified by measuring the first normal stress as a result of curing without applied shear. Normal stress (N_1) acting on the upper parallel plate geometry of the rheometer (Figure 1.5) is calculated by subtracting the stress measured along the y-axis (σ_{YY}), or normal to the plate geometry, from the stress detected along the axis of applied shear (σ_{XX}) (Equation 1.3) [40]. As a resin cures and the network volume shrinks, σ_{YY} increases, resulting in a "negative" normal stress values. Further curing results in an increasing number of cross-links in the network and an increased σ_{XX} due to large molecule displacement.

$$N_1 = \sigma_{XX} - \sigma_{YY} \tag{1.3}$$

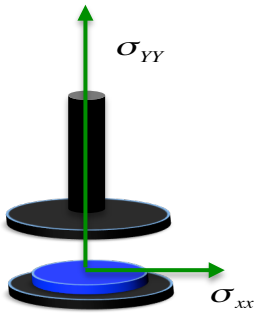

Figure 1.5. Schematic of first normal stress calculation components.

Axial force can be measured on the upper parallel plate geometry during an oscillatory test, as a means to measure network response when experiencing shear. Applying shear increases the internal stress of a network, as three-dimensional deformation occurs. Axial force when utilizing parallel plate geometries is a much more complex calculation that involves three-dimensional stresses and will not be utilized throughout this work [41]. Janmey et al. characterized an isotropic network of semiflexible polymers, attributing an increase in positive axial force to compressed segments and a negative axial force to segments that were elongated in the direction of shear (Figure 1.6) [42]. Entanglements within the network contribute to greater positive axial force response as a greater internal friction between linked segments results [43]. Thus network homogeneity can be compared between similar resin chemistries to depict how formulation change can alter network ability to dissipate shear.

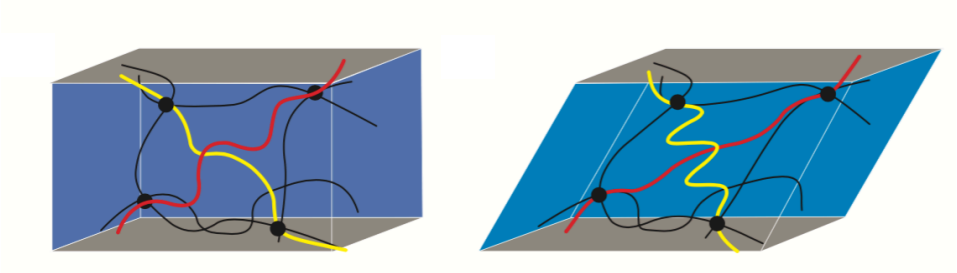

Figure 1.6. Isotropic network prior to shear (left) and after shear (right). Compressed segments in yellow cause a greater positive axial force than elongated segments identified in red [42].

Molecular structure differences within polybutadiene or thiol molecular structure will modify viscoelasticity, pertaining to how rigid, glassy, flexible or elastic the final network becomes. Elastomers possess both elastic and viscous behaviors at room temperature. A better understanding of the material results from decoupling and studying the two responses separately. Following the "continuum approach", mechanical behavior of solids is described by the laws of elasticity and the rheological properties of liquids [36]. Viscoelasticity in materials is defined as a relationship between stress and strain that depends on time or frequency [44]. Dynamic rheology and dynamic mechanical analysis (DMA) are effective methods to measure molecular mobility between cross-links in a network when subject to a given stress or strain. Greater cross-link mobility in response to deformation acts in a more viscous-like behavior, similar to how a rubber ball reacts when impacting a hard, rigid surface, where a rigid network is unable to deform. In dynamic oscillatory tests, the loss tangent (tan δ) represents the phase angle (δ) between stress and strain measured during sinusoidal deformation in time (Figure 1.7) [44]. A degree of dampening of the phase angle occurs when subjecting materials to sinusoidal

deformation, resulting in a phase angle shift (Δt) at period T (Hz) (Equation 1.4). A greater phase angle shift alludes to a greater chain mobility within a network.

$$\Delta t = \frac{T\delta}{2\pi} \tag{1.4}$$

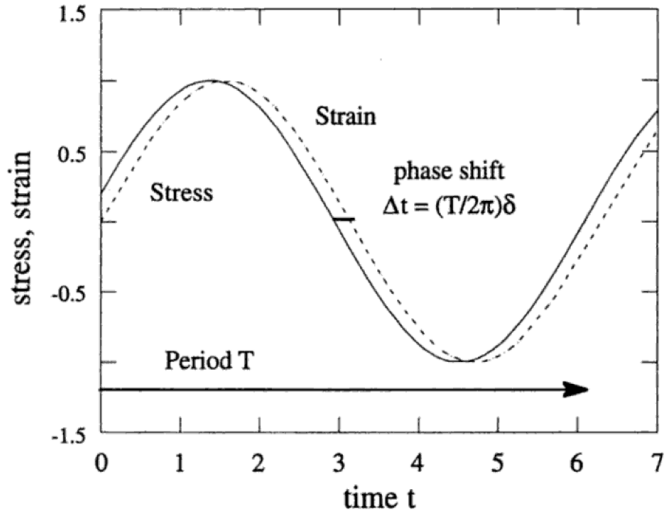

Figure 1.7. Measure stress and strain as a function of time during dynamic loading of a viscoelastic material [45].

For tensile and compressive testing with DMA, the loss tangent can be represented as the ratio of the loss modulus, E", to the storage modulus E', where each moduli represent the imaginary and real components of the complex modulus E^*, respectively (Equation 1.5) [45]. This is also applied similarly to the shear modulus in rheology experiments, differing in complex shear modulus, G*, as opposed to normal compression or tensile experiments commonly applied during DMA.

$$E^* = E' + iE'' \tag{1.5}$$

Studies have performed DMA dynamic oscillatory tests in conjunction with increasing temperature gradients, to simultaneously measure the glass transition temperature (T_g) with changing loss tangent [11], [14], [46]. Although elastomers are physically solid,

their mechanical responses act more similarly to a liquid. In general, cured elastomers have a T_g below room temperature, signifying a high mobility within the network.

DMA with increasing temperature is advantageous as T_g is directly related to the free-volume (V_f), or unoccupied volume, within a polymer system. In liquid resins, the concept of free volume is a measure of the diffusion of polymer chains. Free volume is defined as the difference between the total macroscopic, or specific volume (v), and the physically "occupied" molecular volume (v_o) (Equation 1.6) [47].

$$V_f = v - v_o \tag{1.6}$$

Polymer molecules can change their center of gravity via bond rotation, where synchronized movement of neighboring bonds can function similarly to mitigate sufficient chain displacement. Molecular motion is dependent on the free volume provided by neighboring molecules, as well as the viscosity of the system. Williams, Landel and Ferry (WLF) derived an equation from Doolittle (more information can be found elsewhere [45], [48]) relating mechanical relaxation times of one temperature (T) to the T_g via the respective viscosities η_T and η_{T_g} and specific heats C_1^g and C_2^g (Equation 1.7). Relaxation time is the time a polymer takes to adjust to a new configurational position [36]. It depends on the viscosity, temperature gradient, and specific heat of the polymer system at hand. An in depth discussion will not be given on these theories, except to obtain a basic understanding that cross-links in a cured network can be modeled with a cooperative bond motion theory when subject to stress and increased temperature. Higher free volume allows greater cooperative molecular motion to dissipate and relieve applied oscillatory stress. Similarly, increasing temperature of a polymer network increases molecular oscillations, resulting in bulk thermal expansion of the material.

$$\log \eta_T = \log \eta_{T_g} + \frac{C_1^g (T - T_g)}{C_2^g + (T - T_g)} \qquad (1.7)$$

An elastomeric structure must be near entirely amorphous and have a low T_g to enable cooperative molecular motion when subject to stress. Increasing chain mobility within a cross-linked network allows large deformations to be irreversible at low stresses [49]. Hoyle et al. detected a narrow glass transition temperature via DMA in a sample produced from a 1:1 molar ratio of trifunctional thiol and allyl triazine (Figure 1.8). Uniform cross-link density is not only essential for the performance of dense elastic networks, but also ensures a higher free volume for molecular movement and few dangling chain-ends left once reaction has terminated. When a difunctional acrylate 1,6-hexanedioldiacrylate (HDDA) was reacted with increasing amounts of the same trifunctional thiol, an increase in network homogeneity was recorded by a decrease in rubbery modulus (the steady-state storage modulus above the T_g) and T_g [11]. Another study of reacting a difunctional thiol and difunctional acrylate have relayed an increase in network homogeneity reduces the storage modulus and subsequent value of the rubbery modulus [33]. Dramatic alterations can thus be performed to the physical and mechanical properties by varying stoichiometric ratios within thiol-ene formulations.

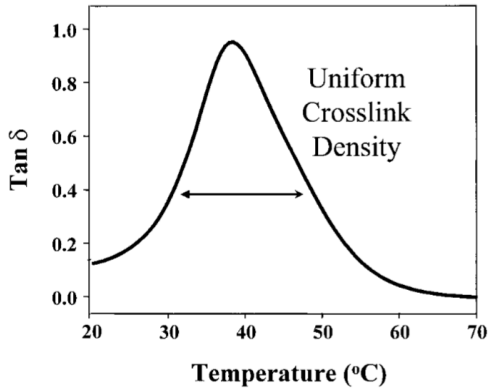

Figure 1.8. DMA with increasing temperature graph portrays network uniformity [11].

Individual polymer or monomer microstructure can also dictate bulk mechanical and physical properties of a cured product by how restricted, or how little free volume, polymer chains have to move and deform when subjected to deformation. For example, aromatic rings along a Kevlar fiber backbone provide high crystallinity that provides high resistance to deformation (Figure 1.9). Restricted chain mobility has been observed in polycarbonate as ring methyl groups restrict rotation of the carbonate group, evoking stiffer mechanical properties in the direction parallel to aromatic ring arrangement, and brittle in other directions [50]. Higher crystallinity is a result of the high degree of order as rigid polymer chains can better align themselves and pack more closely together, resulting in a more glassy and rigid network. Rigidity restricts the free volume available, resulting in higher elastic moduli. Bond rotation in elastomers composed of polybutadiene or polyisoprene is simple, as carbon atoms do not deter mobility. Greater free volume is present as these polymer networks are amorphous, where chain relaxation is quick in comparison to crystalline rigid networks when elastically deformed.

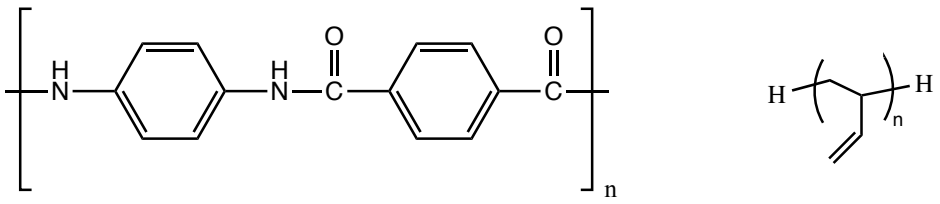

Kevlar 1,2-Polybutadiene

Figure 1.9. Comparing molecular structures of rigid Kevlar vs elastic polybutadiene.

Improving aging capabilities of thiol-ene elastomers is also necessary for long-term stability in the cured product. Few extensive studies have been performed on long-term

hydrolytic stability of thiol-ene films. Norland's thiol-ene chemistries for optical adhesives have been age tested at 50˚C for 3 years, finding no chemical change within the network and no visible discoloration. The claim was then made that their product could last for 24 years if used at room temperature, assuming each 10˚ increase doubles aging effects [13]. It is well known that dangling vinyl bonds or unreacted thiols left trapped within the network pose a threat to long-term stability of thiol-ene network properties, requiring full conversion of all thiol compounds to mitigate aging effects. Unreacted thiols may further react with impurities such as oxygen, potentially initiating degradation.

1.5. The Mechanism of Photo-cross-linking Thiol-Polybutadiene

1.5.1. Step-Growth Radical Addition Mechanism

Traditionally, there are two common methods of cross-linking polymerization: step-growth and radical chain-growth. The main differentiating factor of the two methods is that radical chain-growth polymerization utilizes an active species in order to propagate a polymer chain, whereas step growth is dependent on the functionality and reactivity of functional groups present on the monomers [36], [49]. Photo-activated polymerization follows the chain-growth process, whereby an active species is produced by a photoinitiator (PI) upon irradiation of UV light. Dense cross-linked networks are formed within seconds when utilizing vinyl and thiol monomers with multifunctionality during chain-growth reactions as all activated radicals attack C=C double bonds present and available. Step-growth polymerization occurs by a step-wise process of monomers with functionality group A bonding with functionality group B, or through self polymerization of A with A. As the process proceeds, monomers combine to form dimers, trimers,

oligomers, until a high molecular weight polymer chain is formed and no accessible monomers are left. [49] Figure 1.10 displays the polymerization trend of step-growth versus chain-growth, as the degree of cross-linking increases with conversion.

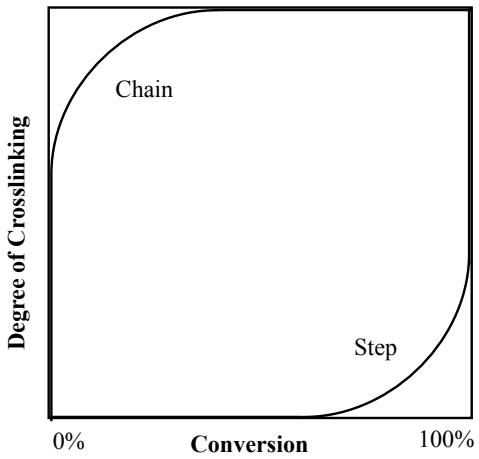

Figure 1.10. Increasing degree of cross-linking as functional groups react in step-growth and chain-growth polymerization methods.

Photoinitiation of thiols and olefins, like chain-growth polymerization, undergoes three distinctive steps from the beginning and end of polymerization: initiation, propagation, and transfer or termination. For reference, a complete thiol-ene reaction overview is given in Figure 1.11. Initiation is a two-step process, which involves first producing an active species (PI*) via homolytic dissociation, followed by the interaction of an active species with a carbon-carbon double bond or thiol to produce a chain initiatiated radical or thiyl radical, respectively. However, one past study involving radical step-growth polymerization of PB indicated that butadiene units could not be initiated via an initiator active species [28]. Therefore, in considering the most basic 1,2-polybutadiene resin system, only direct initiation of thiols via a initiator active species will be considered.

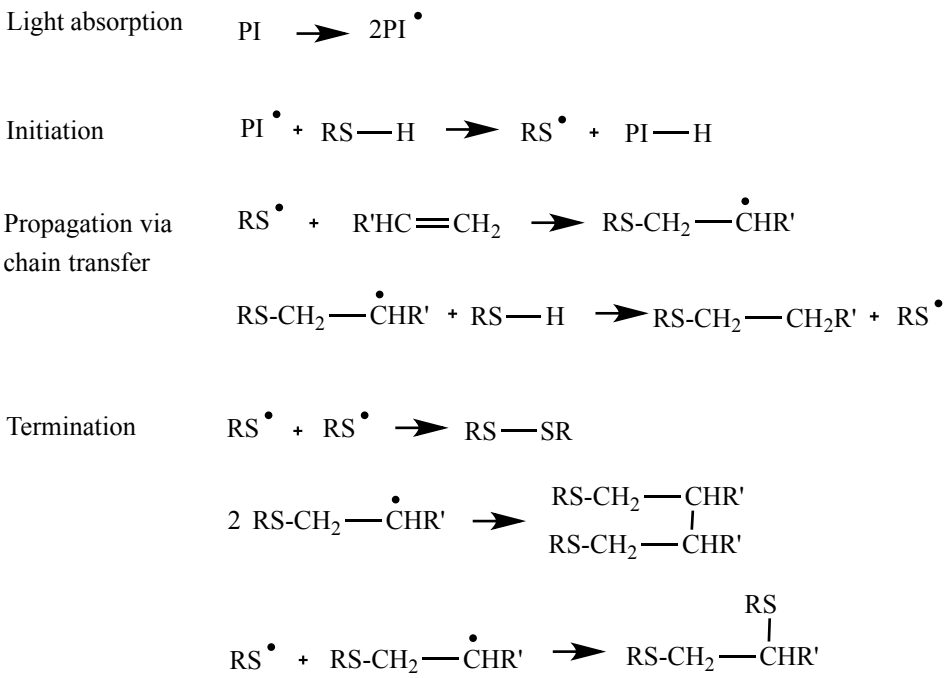

Figure 1.11. Radical step-growth mechanism for common thiol-polybutadiene chemistries.

Radical step-growth cross-linking of thiol and vinyl group is considered to propagate via a step-growth mechanism due to the inherent chain transfer step specific to reactions involving thiols. Chain transfer is advantageous as multifunctional thiol compounds enable each functional group to be accessible for cross-linking via radical addition [51]. During the propagation reaction of thiyl radical to C=C bond, the beta carbon is activated into a radical species. In a perfectly efficient cross-linking system, hydrogen abstraction will occur with a thiol compound, replacing the carbon radical with hydrogen and generating another thiyl radical. This thiyl radical can then proceed to propagation, covalently linking PB chains in an intermolecular fashion. However, in a 1,2-polybutadiene system with close neighboring butadiene units, homopolymerization may also occur. Homopolymerization proceeds when a neighboring C=C bond reacts with the carbon radical, forming an intramolecular ring (Figure 1.12) [26], [52]–[54].

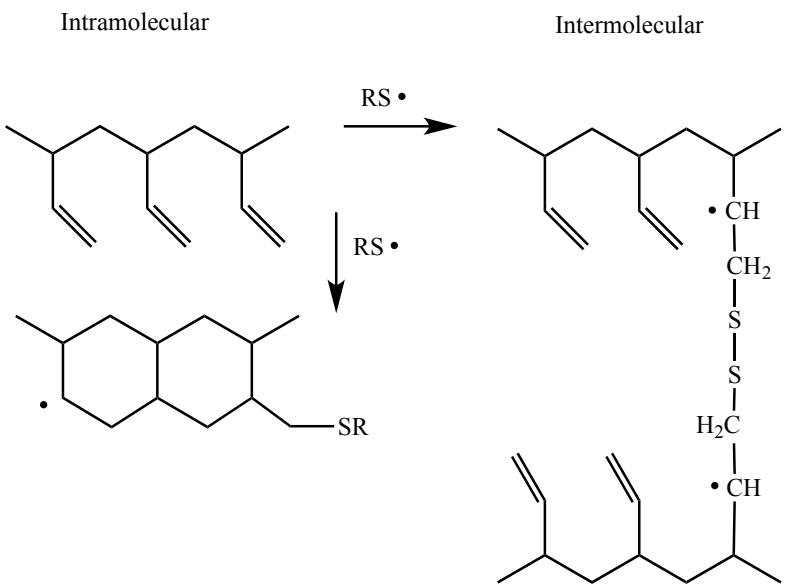

Figure 1.12. Homopolymerization (left) vs cross-linking (right) reaction pathway that each 1,2-butadiene unit can take with a difunctional thiol compound.

In a 1,2-polybutadiene chain, some 1,4-butadiene units in the trans conformation may also be present. Literature states that an initiator radical activates neither conformation, leaving the thiol compound to be the primary means of activation. Typically, an anti-markovnikov reaction of thiol and 1,2-PB vinyl is executed, while the in-chin vinyl is attacked by the thiyl radical to propagate cross-linking (Figure 1.13). Vinyl reaction with the thiyl radical poses a high probability of intermolecular cross-linking, unless chain entanglement or a dramatic increase in system viscosity results. Termination may then follow in two radical species, disabling further cross-linking from occurring. Major termination reactions are shown in Figure 1.11, although other reactions may also cause termination.

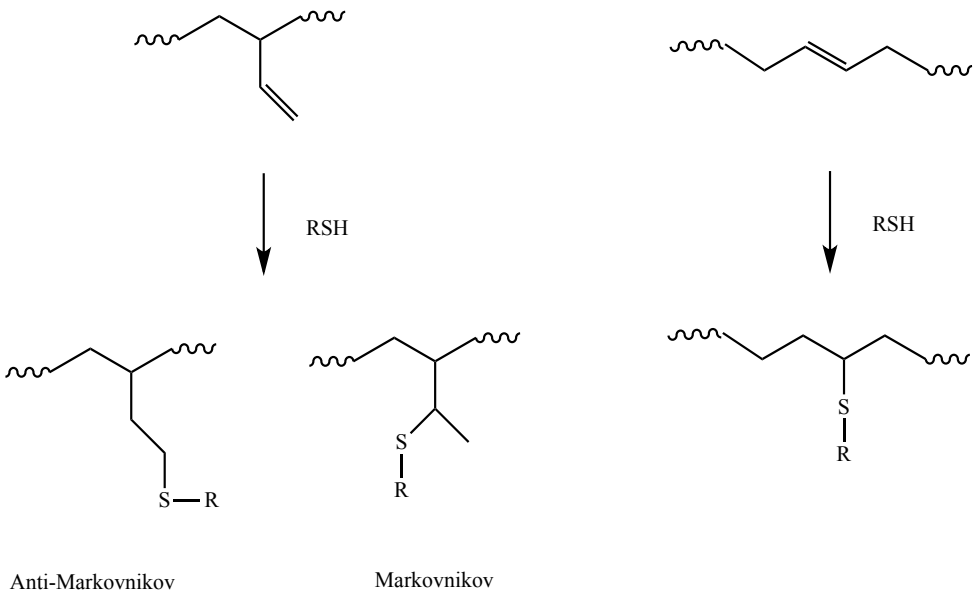

Figure 1.13. Cross-linking reaction possibilities of both 1,2-units and 1,4 "trans" butadiene units.

Oxygen side reactions may interfere with thiol-polybutadiene cross-linking, although as discussed, thiol-ene chemistry is not as prone to oxygen inhibition in comparison to entirely inhibited acrylate polymerizations. However, in the presence of oxygen, oxygen may attack the beta carbon radical, producing a peroxide radical. An additional thiol can then remove the oxygen radical via hydrogen abstraction during chain transfer, thus producing a thiyl radical to continue propagation. This is a single added step that could induce a minor delay in the cross-linking reaction. In the presence of excess oxygen, a co-oxidation reaction between a thiol, olefin and oxygen can form a hydroxysulfoxide as well (Figure 1.14) [55].

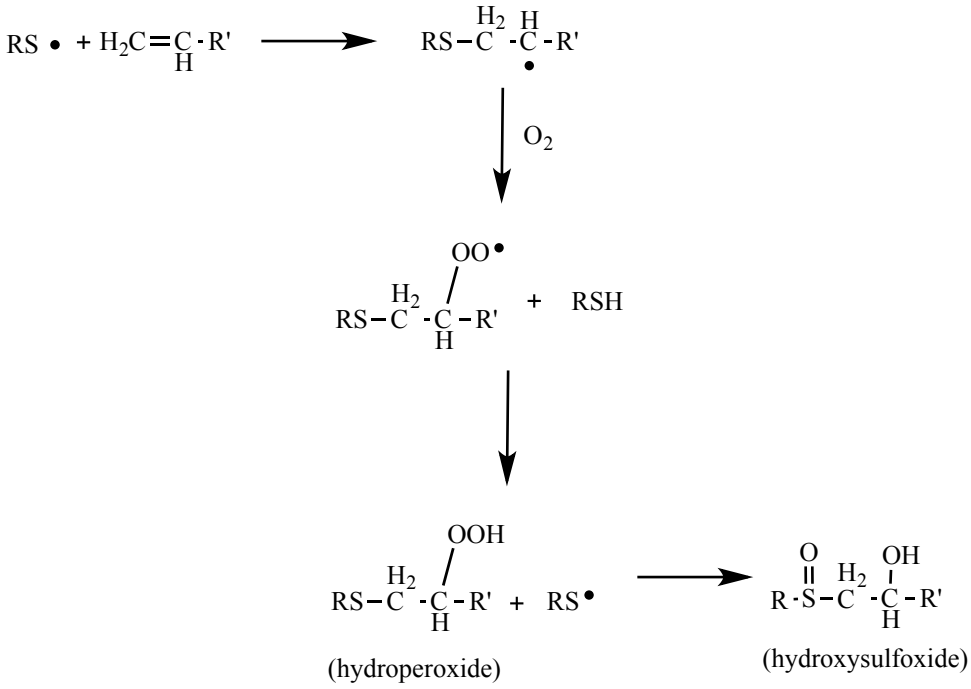

Figure 1.14. Oxygen reaction during thiol-ene chemistry may produce oxygen radicals or hydroxysulfoxides.

Studies have also found that thiol-ene chemistries are capable of photo-initiation without an initiator species, as well as without light present [56], [57]. Cramer and Bowman presented a study with thiol/acrylate systems, displaying conversion of thiols and acrylates in an initiatorless system utilizing both 365nm and 254nm UV light. A slower reaction rate persisted for 365nm light, however 254 nm light propagated at a rate equivalent to that of the thiol-ene system using a photo-absorber [56]. Without light present, sulfur-centered radical cations have been found via ^{1}HNMR to be produced by a single electron transfer. Charge-transfer complexes between thiol and C=C bond formed prior to UV exposure can be oxidized, resulting in a sulfur cation. Although studies have found this reaction to be slow, yielding in mostly a disulfide termination produce, overall thiol conversion and thus cross-linking may be impacted [29].

1.5.2. Photo-cross-linking Kinetics of Thiol-Polybutadiene

Photochemical initiation rate (R_i) is dependent upon the intensity of absorbed light (I_a) and the quantitiy of propagating chains, $\emptyset$, initiated per photon absorbed (Equation 1.8) [49].

$$R_i = 2\emptyset I_a \tag{1.8}$$

As most commonly two radical species dissociate from the photo-sensitive initiator compound, a factor of two is included. I_a is also referred to as the photon absorption rate, which is dependent on the initiator efficiency (f), molar absorptivity ($\in$), initial concentration of the initiator species ([I]), light intensity (I_o), peak wavelength of light λ, Avogadro's number (N_{AV}), Planck's constant (h), and the speed of light (c). After Lovestead's computer modeling experiment in the photo-initiation of optically clear thin films, he derived a more precise factor of 2.303 in calculating the rate of photochemical initiation (Equation 1.9) [58].

$$R_i = -\frac{d[PI]}{dt} = \frac{2.303f\in[I]I_o\lambda}{N_{AV}hc} \tag{1.9}$$

Initiator efficiency and molar absorptivity varies from system to system, where molar absorptivity can be experimentally derived from utilizing the Beer-Lambert law in combination with ultraviolet visible spectroscopy (UV-Vis) (Equation 1.10) [51].

$$\in = \frac{A}{d[I]} \tag{1.10}$$

More complex methods are needed to experimentally measure initiator efficiency, methods such as electrospray-ionization mas spectroscopy, where initiator efficiency is broken down as the rate of initiation of propagating chains divided by the rate of primary radical formation [59].

Following photolysis of initiator species is the initiation of the thiol compound. Thiol initiation rate is dependent on the reaction order of experimentally derived thiol conversion data. For thermosetting systems, either order involves a rate constant, k, and the conversion of the reacting compound of interest, x. First order reaction kinetics involves data lacking an inflection in conversion (Equation 1.11), where second order reaction kinetics presents a change in the conversion rate (Equation 1.12) [60]. Second order reaction kinetics is typical of thiol-ene curing, as autoacceleration (discussed in the following section) is characteristic of the radical step-growth mechanism and causes an increase in the propagation rate. Degree of conversion, or degree of cross-linking, is calculated from the integral of the reaction order equation. Rate constants are thus the calculated slope of the degree of conversion against time graph [17]. Thiol consumption rate (R_s) can then be calculated by multiplying k_s by the concentration of thiols ([SH]) and concentration of photoinitiation ([PI]) (Equation 1.13).

$$\frac{dx}{dt} = k_s(1-x) \tag{1.11}$$

$$\frac{dx}{dt} = k_s(1-x)^2 \tag{1.12}$$

$$R_s = -\frac{d[SH]}{dt} = k_s[SH][PI^*] \tag{1.13}$$

There are no standard equations that can directly be applied for calculating the rate of vinyl consumption (R_v) via propagation and chain transfer steps, as these equations are dependent on the ability of vinyl bonds to be initiated (or not) on the PB chain. As already discussed, 1,2-butadiene vinyl units on a simple PB chain without additional functionality added to end groups have been found unable to be initiated by initiator radicals. Thus, vinyl consumption has been assumed to occur via three main steps (Figure 1.15) [56]. Step 1 pertains to the dithiol reacting with the vinyl groups

protruding off the PB backbone. Resulting carbon radical can then either undergo chain transfer with an additional thiol compound (step 2), or react with a neighboring vinyl group, performing homopolymerization (step 3). As chain transfer is the sole reaction pathways of thiols to propagate, the rate at which thiyl radicals react with vinyl groups (step 1) and the rate at which chain transfer occurs to produce a new thiyl radical (step 2) was assumed to be nearly equal. Thus, step 2 can be defined as the rate-limiting step.

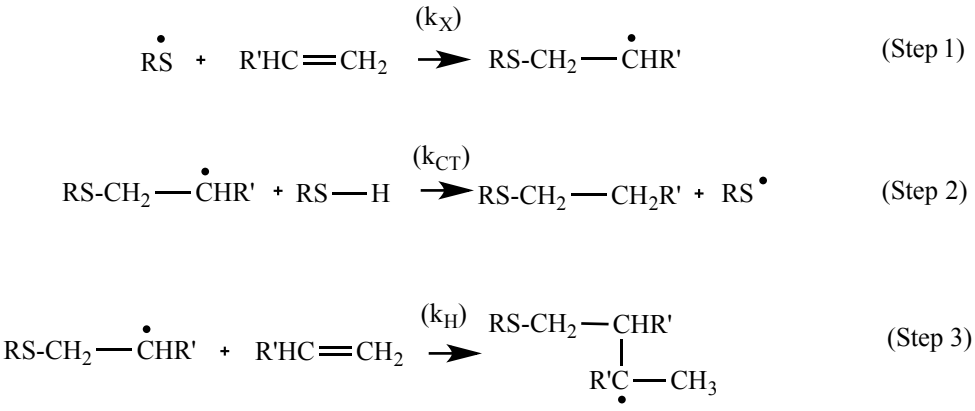

Figure 1.15. Steps composing the thiol-polybutadiene cross-linking reaction.

Thiyl radical reaction can follow step 2 or be consumed via a termination reaction. Cramer and Bowman assumed termination reactions were negligible in their thiol-ene system of monomers, as thiyl radicals to have a high affinity to C=C bonds [56]. However, for a system commencing with PB polymer chains, this cannot be true as thiol-polybutadiene reaction introduces diffusion-limitations of high molecular weight PB chains. Calculating termination kinetic constant is much more complex, as termination embodies multiple reaction pathways. Addition of a multifunctional thiol monomer acts as a reactive diluent in order to combat diffusion restraints. However, as the reaction proceeds thiol monomer diluent ability decreases, causing an overall increase in resin

system viscosity. As will be discussed in the next section, diffusion limitations may be particularly high in systems that begin with high molecular weight polymers of low mobility, which can lead to diffusion related terminations.

1.5.3. Complications of Cross-linking High Molecular Weight Polybutadiene

Only a few reports have studied the thiol-polybutadiene reaction to date [26], [28], [61], [62]. Cross-linking of PB polymer chains is complex, as thiol-polybutadiene reaction neither follows step-growth nor radical chain-growth polymerization directly, although propagation is best understood to be via step-growth mechanism due to the chain-transfer step. P. J. Flory's assumption in step-growth polymerization kinetics is that the reaction rate is independent of monomer molecular weight, as each functional group is the sole driving force in a reaction with an equal number of reacting groups per unit volume [36]. For example, if a difunctional thiol compound of low molecular weight were to propagate in a reaction with equal numbers of C=C bonds, Flory's theory says that a dithiol of high molecular weight would propagate at the same rate with equal reactivity. Systems in which this theory applies provides facile reaction kinetics and, as seen in the Flory- Stockmayer Equation 1.1, provides an accurate means of calculating the GP prior to experimentation. However, Flory's assumption is not valid in fast reacting, high viscosity systems as diffusion dominates the reaction, preventing an equilibrium between the reaction of thiols and vinyl groups. Reactivity of the functional groups do not change, but the rate of collisions between thiol and C=C bond decreases, thus decreasing the probability of reaction [54], [63].

Thiol-polybutadiene chemistry is a rapid reaction between thiyl radicals and C=C bonds in butadiene units, assumed to be partially controlled by the proximity of each reactant to another, or otherwise said to be partially diffusion controlled. For formulations initially dilute in radical species, diffusion can occur via two independent processes: translational diffusion or segmental diffusion. Translational diffusion is the movement of two radicals diffusing towards one another through solution, starting at an initial distance ℓ_o from the center of gravity of radical A and radical B. The two radicals may near each other until colliding at a distance ℓ. Termination occurs if radicals are in contact for a sufficient amount of time, or if the reaction per unit time at that distance is probable (Figure 1.16) [64]. During cross-linking, the overall viscosity of the system increases as the thiol monomer reactive diluent is consumed and gel formation increases. Unreacted thiyl monomer mobility slows with increasing viscosity, decreasing the reaction rate constant. As thiyl monomers may come sufficiently close to each other at a distance ℓ, the reaction becomes translationally diffusion-controlled [54].

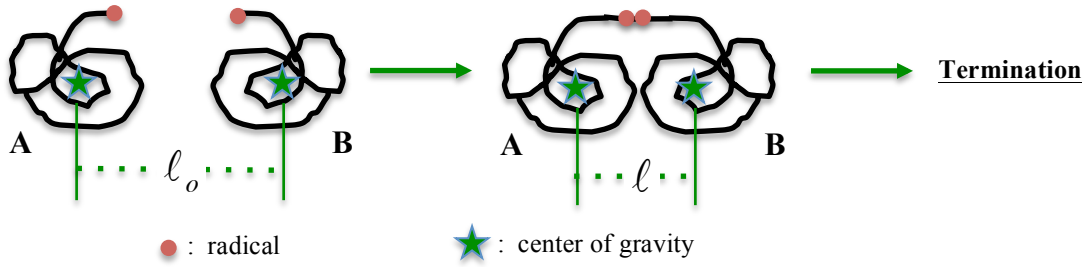

Figure 1.16. Translational diffusion of two radicals leading to diffusion-controlled termination.

PB chain vinyl group mobility is restricted prior to the commencement of the radical step-growth reaction, as 1,2-butadiene units are attached to the PB backbone. Although this bond restriction could be advantageous as the PB chain could act similarly

to radical template polymerizations where thiyl radicals can readily attack 1,2-butadiene units [65], the relative closeness of 1,2-butadiene vinyl units may also introduce segmental diffusion limitations. For segmental diffusion to occur, restrained radical segments must be approximately 3 Å apart for radicals to combine and terminate [64]. In comparison to translational diffusion where radicals A and B are dependent on monomer diffusion coefficients, segmental diffusion is dependent on the restricted mobility of one segment end bound to a polymer chain. In the thiol-polybutadiene reaction, two main routes for segmental diffusion related termination may proceed. For a thiol compound of multifunction, following thiyl propagation reaction with a 1,2-butadiene vinyl unit can lead to a thiyl radical on another open site. In the common circumstance that two neighboring 1,2-butadiene units react with a multifunctional thiol compound and two thiyl radicals are sufficiently close, the multifunctional thiol compound may become segmentally diffusion-controlled. Additionally, although much less likely, if neighboring beta carbon atoms are initiated following a 1,2-butadiene vinyl unit reaction with a thiyl radical, an intramolecular radical termination reaction may occur between radical beta carbons. The later case of segmental diffusion related termination is less likely due to an increase in bond angle strain in cyclic conformations [49], [54].

Although the chain-transfer step during propagation reaction follows a step-growth trend, radical initiation of thiols presents the gel or autoacceleration effect characteristic of radical chain-growth reactions. In radical-chain growth reactions, the reaction rate increases with conversion, attributing to the dramatic increase in resin system viscosity. This increase has been directly correlated to translational diffusion decreasing faster than the increase in segmental diffusion [49]. As in the case of thiol-

polybutadiene reaction, increasing conversion results in a greater entanglement of PB chains as less thiol monomers act to dilute the reaction system. Lecamp observed this autoacceleration effect in his study of dimethacrylate oligomers and monofunctional thiol reaction (Figure 1.17), where a dramatic increase in the rate of both double bond and thiol conversion occurred after approximately seven seconds of UV exposure [46]. Studies have shown that an increase in segmental diffusion decreases the rate of termination [66], due to the glass or vitrification effect. Conversion begins to level off as cross-linking time proceeds if the network T_g exceeds that of ambient temperature. As PB chains are entangled prior to UV exposure, this glass effect may appear sooner in comparison to reacting vinyl and thiol containing monomers.

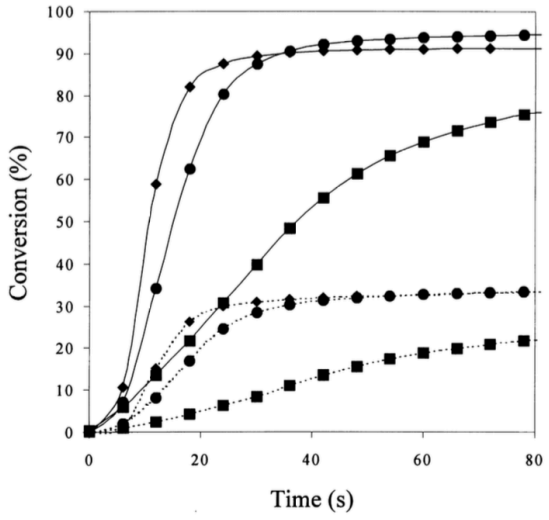

Figure 1.17. Gel effect demonstrated via double bond (–) and thiol (---) conversions within multiple dimethacrylate oligomer and monofunctional thiol formulations. From [46].

1.5.4. Photoinitiator Selection

PIs can produce either a free radical or ionic type of active species, depending on the chromophore position in the molecule. In producing a radical active species, there are

two types of PI compounds available. Type I unimolecular cleavage PI initiates direct fragmentation at a α or β carbon to produce two subsequent active species: a benzoyl radical and a tertiary carbon radical. One of the most commonly used Type I PI's for use with 365 nm light is 2,2-dimethoxy-2-phenylacetophenone (DMPA) (Figure 1.18). DMPA has been found to be an efficient PI for acrylic based resins and thiol-ene chemistry as dissociated radicals are able to attack both olefins and thiols. In particular, one study found that using DMPA in thick layers (~2 mm) of methacrylate resins produced fast reactions with high conversion at low concentrations of 0.25 wt% [31]. Another common Type I PI sensitive to 300-400 nm light is 2-Hydroxy-2-methyl-1-phenyl-propan-1-one, or Irgacure 1173 [67]. Irgacure 1173 is advantageous when compared to DMPA as it is readily available in liquid form at room temperature to provide facile mixing into polymer resins. Additionally, Irgacure 1173 has been promoted for high storage stability and non-yellowing characteristic when compared to DMPA [68].

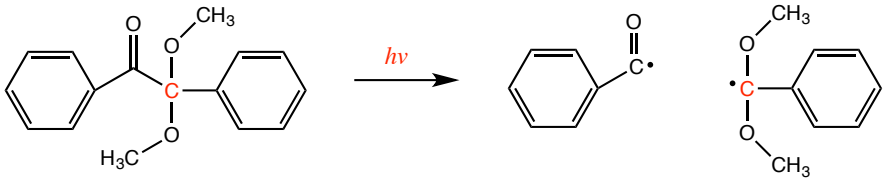

Figure 1.18. Initial bond cleave of DMPA at α-carbon upon illumination.

Type II photo-initiation is comprised of a bimolecular reaction, where a PI requires hydrogen abstraction from an additional molecule, or coinitiatior, in order to produce two radical species. Exposing a type II PI to UV light shifts the PI into an excited triplet state, providing sufficient activation energy to abstract a hydrogen via electron transfer and final dissociate into two radical species [68]. Dependent on the

coinitiator used will affect the initiating efficiency of the radicals in starting radical chain-growth polymerization. For example, the addition of an amine to benzophenone type II initiator in the presence of 300-400 nm light will significantly increase initiating efficiency, while an alcohol may only enhance efficiency slightly. Benzophenone is able to abstract a hydrogen from a thiol compound to produce a thiyl and ketyl radical, as is commonly done in past thiol-ene studies (Figure 1.19) [35], [56], [69].

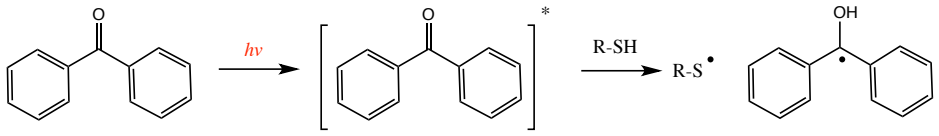

Figure 1.19. Exciplex formation of BP upon illumination and radical formation with thiol.

2. EXPERIMENTAL PROCEDURE

All work was performed at Lawrence Livermore National Laboratory under authority of each lab's responsible individual. A ventilated hood, safety glasses and surgical nitrile gloves were utilized throughout all formulation studies.

2.1. Resin Constituents

Commercial 1,2-polybutadiene (PB, Nisso America Incorporated) in the form of both neat (B-1000, 1,100 (g mol^{-1})) and difunctional urethane methacrylate end groups (TE-2000, 2,500 (g mol^{-1}), hexane (anhydrous, 95%, Sigma Aldrich), 2-Hydroxy-2-methylpropiophenone (Irgacure, 97%, Sigma Aldrich), 2,2-Dimethoxy-2-phenylacetophenone (DMPA, Sigma Aldrich), 1,5-pentanedithiol (PD, 96%, Sigma Aldrich), 1,6-hexanedithiol (HD, 96%, Sigma Aldrich), 1,8-octanedithiol (OD, 97%, Sigma Aldrich), 1,9-nonanedithiol (ND, 95%, Sigma Aldrich), and 1,10-decanedithiol (DD, 95%, Alfa Aesar) were purchased and used without further purification.

B-1000 was the lowest molecular weight 1,2-PB that was commercially available, where TE-2000 had the additional bifunctional methacrylate end groups to aid in forming a dense network (Figure 2.1). Reported T_g values for B-1000 and TE-2000 were -44°C and -9°C, respectively. According to manufacturers specifications of B-1000, at least 85% of the polybutadiene chain is composed of 1,2-butadiene units and a maximum of 15% is 1,4- units. TE-2000 acryl equivalent was listed as ranging from 1,600 to 2,300 g/eq [70]. The estimated number of vinyl groups available for cross-linking reaction was determined by back calculating the number of mers from the manufacturers given number-average molecular weight. Dividing the molecular weight

of the polymer by the molecular weight of each mer provided the estimated number of butadiene monomers in sequence. For B-1000, approximately 20 vinyl groups were calculated, and 35 for TE-2000 (including that of the dimethacrylate end groups).

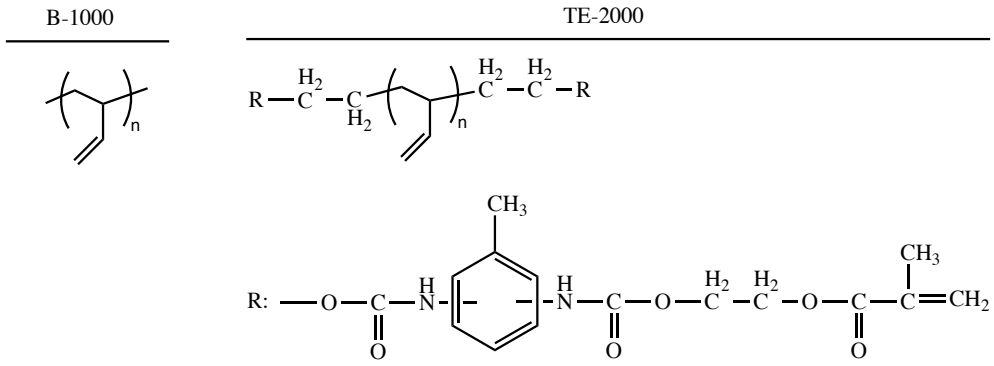

Figure 2.1. B-1000 and TE-2000 PB representative molecular structures.

A maximum thiol compound functionality of two was experimentally found compatible in PB resins, as any greater functionality was insoluble. All formulations produced and studied were with PB and dithiols. Two base resin formulations were prepared: the first for direct application to displays for sealing, encasing and encapsulation and the second for real-time studies of the varying dithiol chain length studies. Display resins varied in increasing weight percentage of Irgacure (0.25 – 1 wt%) and increasing thiol/vinyl molar ratios (0.05 to 0.2) with B-1000, TE-2000, and a hybrid polymer of both. All display resins were diluted in 30 wt% hexane. Dithiol carbon chain length (CL) study resins were simplified to only using a 1:1 thiol to vinyl molar ratio of B-1000 and 1 wt% Irgacure to better study the direct effects of dithiol CL. Table 2.1 provides the series of dithiol CLs and respective molecular weights (MW) to be presented in section 3.4.

Table 2.1. Respective dithiol molecular weight differences

# Carbon (acronym)	5 (PD)	6 (HD)	8 (OD)	9 (ND)	10 (DD)
MW (g/mol)	136.3	150.3	178.4	193.4	204.4

2.2. Device Preparation

Three ways of preserving the display suspension with the formulated elastomer resin has been implemented: edge sealant, spacer, and encasing. Sealing the perimeter of rigid displays was the preliminary, simple approach, however the use of kapton tape as a spacer between electrodes was proven disadvantageous. Using resin as a spacer was thought to act as a more efficient seal, but could also effectively adhere two electrodes together after curing and provide an aesthetically pleasing transparent appearance. Fixing electrodes in place without an external binding mechanism was necessary, as rigid electrodes had previously been held together with binder clips. In the transition from rigid to flexible electrodes the spacer resin will still be used, but encasing the entire flexible display was thought to provide a thorough seal and added device durability. The following procedures explain how each preservation technique was implemented.

2.2.1. Sealing

Of the most simplistic of the discussed preservation techniques, edge sealing will be presented first. Sealant resin was dispensed around the perimeter of two electrodes via a 0.61 mm diameter syringe needle (Figure 2.2), while two binder clips held electrodes together. A 550 μW/cm^2 365 nm light source was used to cure the edge seal for 2 minutes, in which post cure the binder clips could be removed.

2.2.2. Spacing

Preserving electrodes via the implementation of an elastomer spacer is versatile for both rigid and flexible electrode application. Spacer resin was applied to one electrode via a micrometer tunable doctor blade at a 25-μm thickness. A cotton swab dipped in hexane was utilized to form a circular window area, and was repeated until no residual resin was left. EPD NP suspension was then pipette into the window area and the second electrode was placed on top. While holding electrodes in place, the spacer resin was cured under the 550 μW/cm^2 same light source for two minutes, thus adhering the two electrodes together and subsequently sealing the NP suspension from the ambient environment (Figure 2.2).

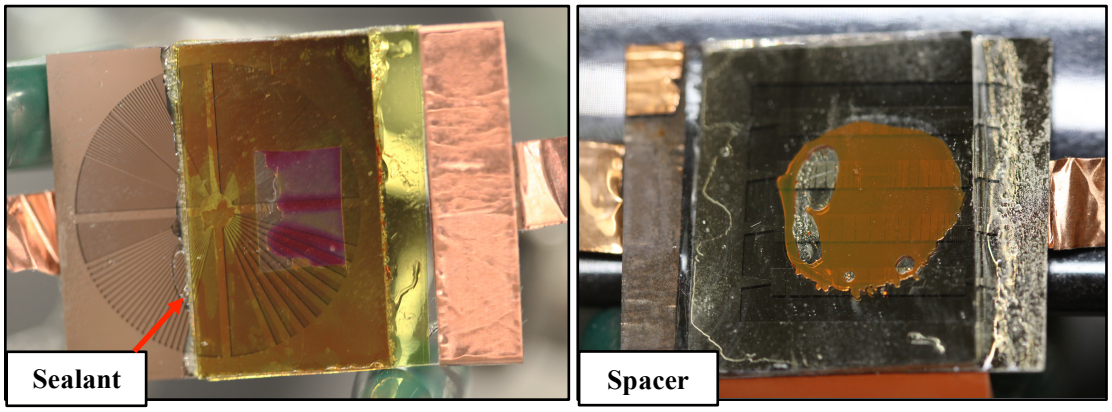

Figure 2.2. Sealant polymer with kapton tape spacer (left) and spacer polymer replacement (right).

2.2.3. Encasing

Encasing flexible displays enables a durable protective shell, but was also thought to ease the fabrication process. As discussed in section 1.1.2, introducing flexibility causes difficulty in maintaining the display suspension in a locally defined area, as the suspension flows quickly in the direction of electrode bending during device fabrication. Thus, building a flexible display in a layer-by-layer approach and initially adhering the

bottom electrode to a rigid surface via a layer of photosensitive elastomer, was thought to overcoming initial bending issues during fabrication. Figure 2.3 illustrates flexible display fabrication steps via elastomer encasing. First, an initial layer of resin is deposited on a glass slide via doctor blade and cured for five minutes under a 365 nm light (550 μW/cm^2). A piece of mylar film (1.6"x1.4") is then placed on top of the cured layer and subsequently covered by an additional layer of resin and cured. Mylar film allows ease of removal once the entire display is encased. Next, a flexible ITO/PET substrate assembled with copper tape electrical contact is place on top. Step four involves implementing the spacer material via section 2.2.2 procedure, followed by pipetting NP suspension in the provided area. Prior to curing the spacer resin, the top ITO/PET electrode is placed on top and cured while held in place. After two minutes of UV light exposure, the flexible display is then entirely filled with resin and cured for another five minutes. Excess resin surrounding the perimeter of the flexible display is removed via a razor blade and encased display is peeled off from the mylar film.

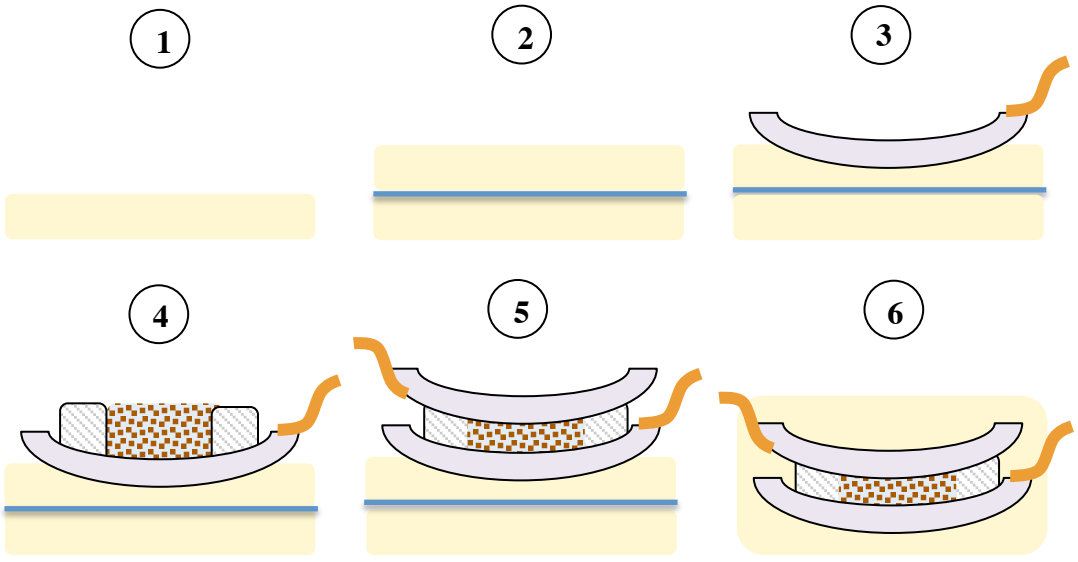

Figure 2.3. Illustrated procedure of encasing flexible electrodes with elastomer resin.

2.3. Encapsulation via Microfluidics

Yet another preservation technique directed towards the advancement of flexible displays is encapsulating the display suspension within a cured elastomer shell. A schematic of in-line UV cure encapsulating microfluidic set up is presented in Figure 2.4. All input fluids were filtered via a 0.5 μm filter prior to running through microfluidic device. As α-Fe_2O_3/SiO_2 core/shell NPs require extensive time to fabricate, a Boron suspension in propylene carbonate was used as the capsule core fluid. Boron has been found to deposit via an electric field and thus acts as a good testing replacement. Flow parameters input into a 100/400-μm inner biaxial capillary diameter microfluidic device were 0.9, 1.5, and 18 mL/hour for core, shell and continuous fluids, respectively. UV cure chamber light (365 nm) intensity was set to 135 mW/cm^2 to cure capsules flowing through the chamber prior to reaching the output capsule capture vial (~ 8 seconds of UV exposure).

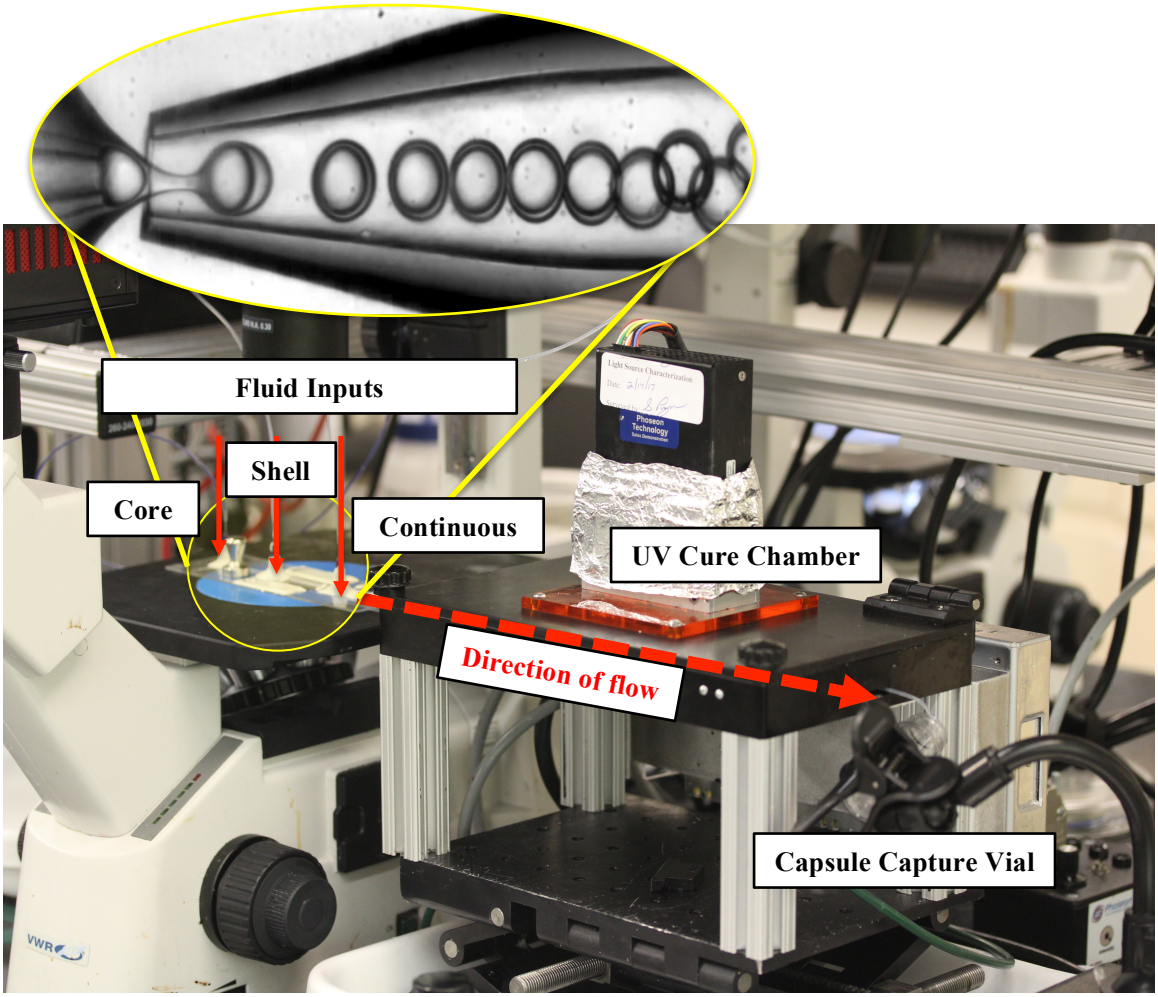

Figure 2.4. NP suspension microencapsulation schematic via microfluidics.

2.4. Instrumental Methods of Analysis

2.4.1. Dynamic Mechanical Analysis

Compression elastic moduli and loss tangent were measured with TA Instruments RSA-G2 dynamic mechanical analyzer (DMA). Circular holes of 8 mm diameter were die cut into 0.5 mm thick silicon sheets to act as a mold in order to cure samples. Silicon molds were set on top of a glass slide, filled with photosensitive resin, and sandwiched with another glass slide. Samples were cured under a 365 nm UV light (550 μW/cm^2 intensity) for 2 minutes. In order to make maximum surface area contact with samples

that experienced warping during curing, 2mm diameter punches were taken from each cured sample disc and utilized for compression testing. DMA oscillation amplitude proceeded at a frequency of 1 Hz while increasing strain percentage from 0.1 to 7%. Test parameters were chosen such that measurements were taken in the linear viscoelastic region, from which the measured elastic moduli and loss tangent were derived. At least seven sample replicates were performed for each PB resin formulation.

2.4.2. Swell Testing

The swell test experiment followed ASTM D2765. DMA samples of 8 mm diameter were weighed with a Mettler Toledo microbalance and recorded as the initial weight, W_o. Hexane used in the formulation was assumed to evaporate from the sample during curing. Each sample was placed into a vial of hexane and let soak for 24 hours at room temperature. Samples were then removed from hexane and instantly weighed after excess hexane dripped off. Weight of swollen polymer (W_{sp}) was recorded and swell percentage was calculated (Equation 2.1). Swollen samples were left for 24 hours to allow remaining trapped hexane or dissolved polymer leave the elastomer system. The remaining insoluble sample (W_{dp}) was weighed again and the gel percentage was calculated and recorded (Equation 2.2). At least three samples per PB resin formulation were swell tested to gain an average swell and gel percentage.

$$Swell\ \% = \frac{W_{sp} - W_o}{W_o} \tag{2.1}$$

$$Gel\ \% = \frac{(W_{sp} - W_{dp})}{W_o} \tag{2.2}$$

2.4.3. Real-Time Fourier Transform Infrared Spectroscopy

Real-time Fourier transform infrared spectra (RT-FTIR) were obtained from a custom horizontal absorbance apparatus with Bruker Tensor II FTIR spectrometer (Figure 2.5). Polymer formulations were pipette onto a 32 mm round (3 mm thick) NaCl crystal polished discs with 30 μm double-sided PET adhesive tape on the edges and sandwiched between another NaCl crystal. Cross-linking was initiated via an Omnicure S2000 light guide with a 356 nm filter. A CON-TROL-CURE silver line radiometer measured 0.2 mW/cm^2 at the surface of a blank NaCl sandwich prior to acquiring data. Series scans were recorded, with spectra taken at the rate of approximately 1 spectra every 10 seconds. Samples were irradiated and spectra was recorded until no change was observed in the peak of interest. One spectral scan of blank NaCl sandwich, B-1000 sandwiched between NaCl, and B-1000 with 1 wt% Irgacure sandwiched between NaCl were taken as backgrounds. IR spectra was used to monitor conversion of polybutadiene vinyl groups (910 cm^{-1}) , thiol groups (2560 cm^{-1}) and the benzyl radical reaction (3076 cm^{-1}) (Figure 2.6). Conversion (x) of each group was calculated with Equation 2.3:

$$x = \frac{A_o - A_t}{A_o} \tag{2.3}$$

where A_o is the initial area under the peak and A_t is the area at time t (seconds).

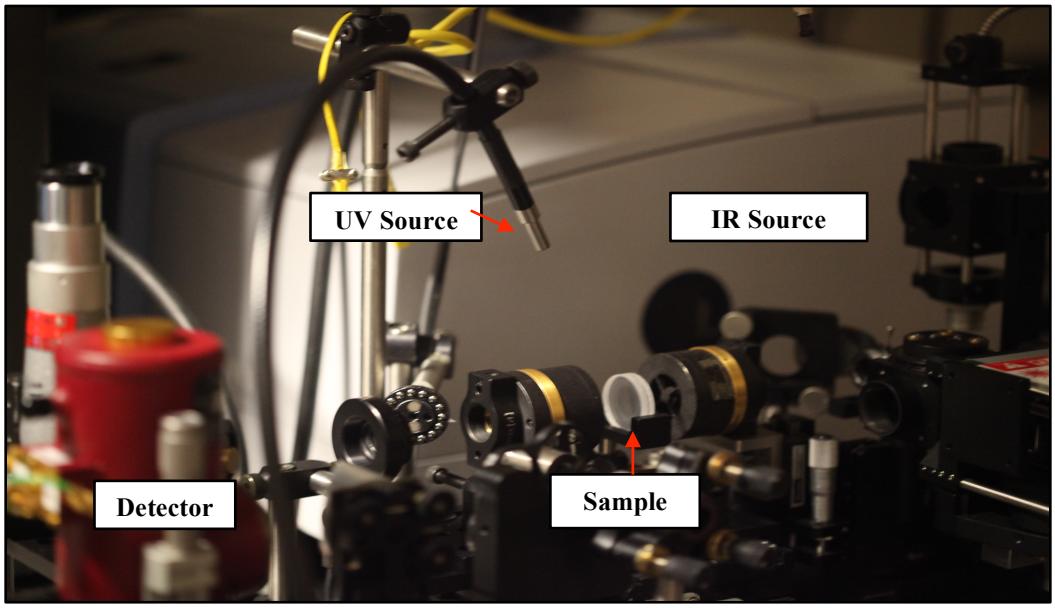

Figure 2.5. Horizontal absorbance apparatus used for RT-FTIR experimentation.

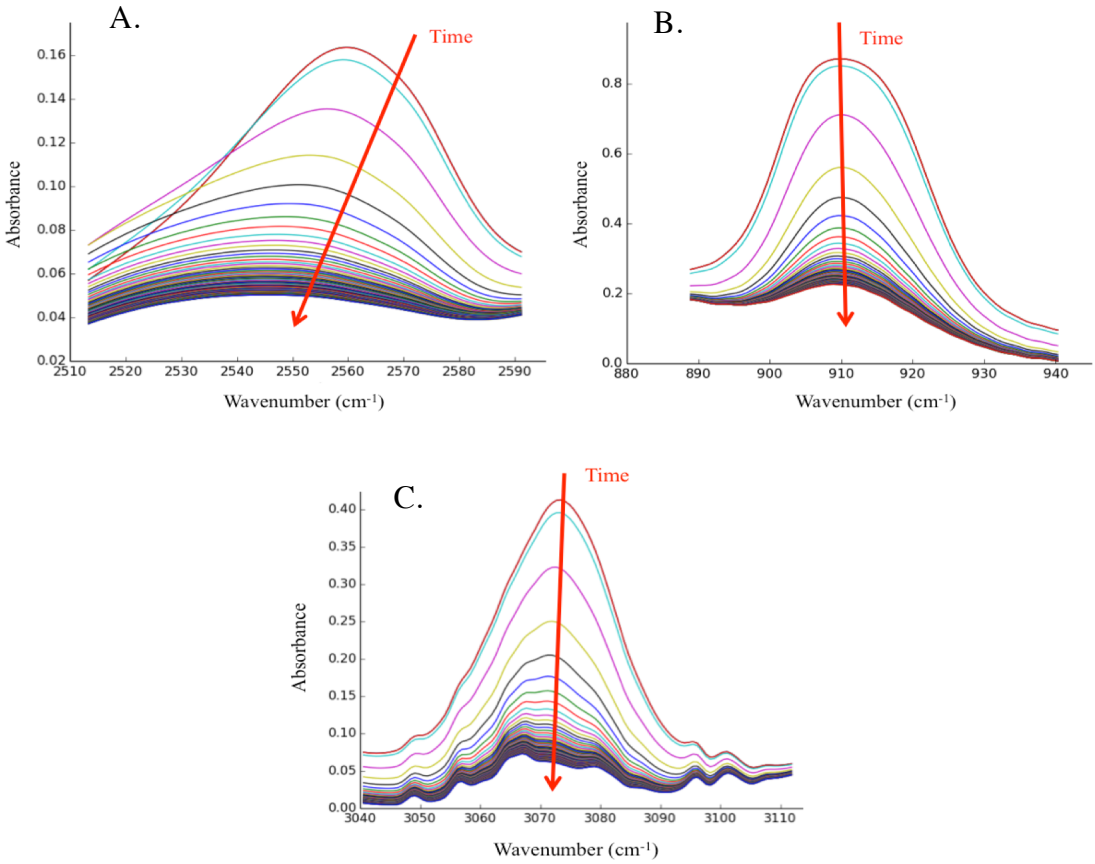

Figure 2.6. Thiol (A.), PB vinyl (B.), and benzyl radical peak (C.) conversions with UV exposure time.

2.4.4. Rheology

Real-Time Dynamic Oscillatory Experiment

A TA instruments AR2000ex was equipped with a UV light-guide attachment and disposable parallel plate fixtures for in-situ monitoring of curing. UV curing attachment schematic (Figure 2.7) shows the bottom-up curing through the clear acrylic bottom plate. The same Omnicure S2000 lightguide, 365 nm filter and radiometer from the RT-FTIR experiments were utilized, ensuring that 0.2 mW/cm^2 light intensity was attained at the surface of the bottom acrylic plate prior to each experiment. Sample resin was placed on top of the acrylic plate and sandwiched with the top aluminum plate geometry with 30μm spacing. All experiments were conducted at ambient temperature conditions, which varied within a couple degrees from 25±2˚C.

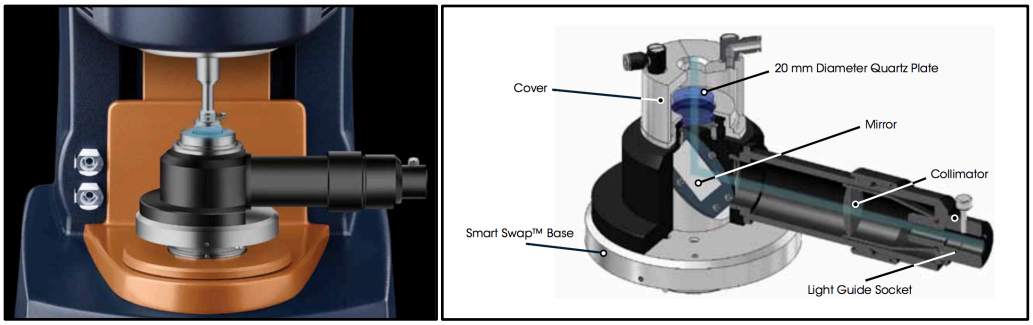

Figure 2.7. RT-Rheology diagram of bottom-up curing of resin between two parallel plates. From TA Instruments product guide.

Dynamic oscillatory experiments were performed as a function of time with constant strain percentage and frequency set to 5% and 1 rad/s, respectively. Parameters were chosen on the basis of linear viscoelastic regions during strain and frequency sweeps. Application of low strain was assumed to not dramatically disturb the curing network, for later comparison with RT-FTIR kinetic data. All experiments were exposed

to UV light after a 100 second stabilization period, and G' and G" were recorded for 400 seconds thereafter. GP was determined and recorded when $\tan\delta$ was equal to one (Equation 2.4), as well as the strength at GP (Equation 1.2) [38]. Shear stress (τ) as a function of G' and G" with increasing UV exposure time was recorded in order to measure stress distribution variance between increasing dithiol CL formed network [45].

$$\tan\delta = \frac{G"}{G'} = 1 \tag{2.4}$$

$$\tau = \gamma_o[G'(sin\omega t) + G"(cos\omega t)] \tag{2.5}$$

Viscosity Determination

Flow sweeps were performed on resin samples and base polymers prior to UV exposure via stainless steel 2˚ cone and plate geometrical set-up. Flow sweeps were performed at room temperature (25˚C) from 0.1 to 1050 s^{-1} at a 50-μm gap spacing. All reported viscosities were recorded at 1000 s^{-1}.

First Normal Stress Measurement

Axial force control was utilized to maintain a 30-μm gap while measuring the normal stress of the upper parallel plate geometry as the photosensitive resin cured. First normal stress measurements verified volumetric shrinkage due to network formation and a greater final network displacement in high thiol conversion resin systems. The same light intensity (0.2 mW/cm^2) was used to expose resin, however no flow was applied during curing.

3. RESULTS AND DISCUSSION

3.1. Preliminary Investigation

Initially, spin coating was investigated as a method to apply the spacer to the electrode surface. Spin coating is able to deposit uniformly thick layers by controlling the spin speed (revolutions per minute) and the volume of resin applied to the surface. However, the resin formulations were too viscous to evenly flow across the electrode surface (Figure 3.1). Doctor blade and wire-round rods were found to be the method of choice for deposition of the sealant layer. The doctor blade device is fitted with a micrometer in order to deposit a wet resin layer of known thickness. Two 10 μm and 20 μm wet resin thickness wire-round rods were used for deposition. "Back of the envelope" shear rate calculation for doctor blade deposition was performed to estimate shear rates at which viscosity measurements should be made. Dividing measured coating velocity (~0.01 m/s) by the thickness of the coating, shear rate range was estimated to be 400 to 1000 s^{-1}.

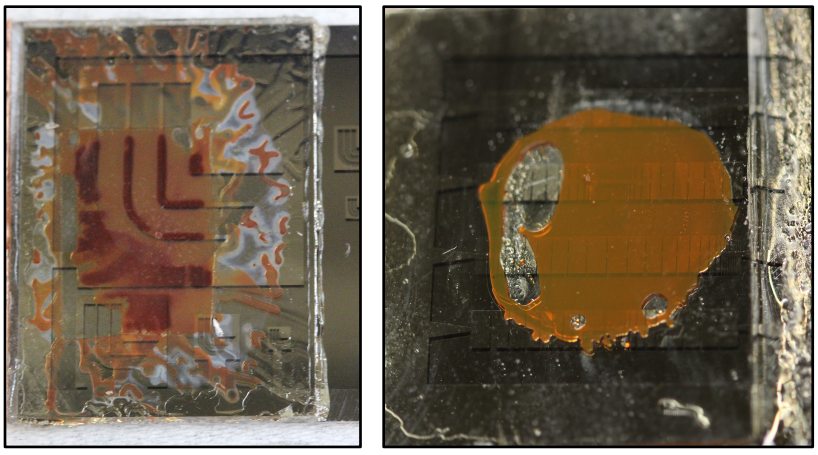

Figure 3.1. Spacer elastomer layer uniformity comparison of spin coating deposition (left) vs doctor blade deposition (right).

A general understanding of the necessary dithiol concentration to form dense cross-link network structure was obtained by successive drop-wise addition of 1,6-hexanedithiol into either a TE-2000 or B-1000 matrix until round swell samples appeared non-tacky. This method prompted a 0.2:1 thiol to vinyl molar ratio in TE-2000 with 50% hexane and 1 wt% DMPA for initial sealant and spacer material. Following the spacer procedure (section 2.2.1) allowed for good adhesion between two rigid electrodes post curing, preventing electrode separation in attempting to pull electrodes apart. Formulations based on B-1000 was estimated to require 10 wt% hexane and a 0.1:1 thiol to vinyl molar ratio for encasing purposes, as B-1000 was more flexible than TE-2000. The sides of TE-2000 encased devices fractured off more easily upon bending the flexible encased displays, however, the edges of B-1000 encasing crumbled off while handling. This is hypothesized to be due to a weak PB backbone. Formulations produced for encasing flexible electrodes could subsequently be used as a sealant between rigid and flexible electrodes, as similar viscosities were used for either application.

Choosing the correct photoinitiator was a vital to producing densely cross-linked networks. Although a complete study was not performed, comparing type I and type II initiators, visual estimates distinguished that type I initiators were more efficient. Thus, the decision is between Irgacure and DMPA, as both were deemed as efficient and compatible with 365 nm light. Melting temperature of Irgacure is below room temperature, while DMPA is commercially available as a crystal solid. Additional processing was required to dissolve DMPA in resin formulations, sometimes requiring the addition of heat. Thiol-ene chemistry is also catalyzed by heat, posing a potential to form an unstable resin prior to UV exposure. Additionally, stable resin chemistry is

required for microencapsulation to prevent increased viscosity that resists fluid flow or that may suggest curing inside the microfluidic device. DMPA was used in all initial samples as the absorbance sensitivity peak was directly at 365 nm, however, as thiol-ene is a fast reaction, cross-linking appeared to occur too quickly. As Irgacure absorbance peak is closer to 300 nm and absorbs less 365 nm light, thiol-ene reaction is slowed enough to better meet microfluidic cell requirements. Irgacure is thus the preferred initiator in further formulations.

The first successful attempt at encapsulating propylene carbonate was with TE-2000 diluted in 50% hexane with 1 wt% Irgacure. Hexane is used as the nonpolar solvent as polybutadiene is soluble and hexane is not miscible with propylene carbonate. High concentrations of hexane were necessary with TE-2000 to reduce the viscosity below 0.5 Pa.s. However, the capsule shell displayed microscopic cracks due to the high viscosity of TE-2000 producing imperfections in the capsule shell and from hexane leaving behind voids during evaporation (Figure 3.2). Subjecting capsules to compression between two glass slides resulted in a seemingly brittle fracture, failing to meet microcapsule design criteria. In attempting to use B-1000 with a lower viscosity and an expectedly more elastically active structure, no gelling was observed with 1 wt% Irgacure. However, attempting to add 0.2 thiol molar ratio of 1,6-hexanedithiol to the system introduced instability, as resin was extremely sensitive to any visible light and cured in the dark after 24-hours. Thus, a comprehensive study was performed to find stable and efficient concentrations of dithiols and Irgacure, as well as quantify mechanical properties of TE-2000 and B-1000 under compressive loads.

Figure 3.2. Imperfections in capsule shell surface due to high viscosity of TE-2000 and voids.

Light intensity also had to be taken into account as a substantial amount of shrinkage stress was found in using a high intensity light source. An Omnicure AC 475 light source with 2.5 W/cm^2 light intensity was able to cure encased flexible display cells within two seconds per layer. However, extreme warping of the entire device resulted. As the intensity of absorbed light is directly proportional to the number of propagating chains initiated per light photon absorbed, a higher cross-linking rate causes higher internal network stress with greater intensity light [49]. Equivalent curing doses between light intensities were not performed, as time to cure each encasing layer for 151 minutes with 550 μW/cm^2 light would be too long. A bar light of 500 μW/cm^2 light intensity was then used to cure flexible device encasings in five minutes per depositing layer (following section 2.2.2 procedure). Five minutes provided a cured, non-tacky layer, showing 151 minutes would not be necessary. Figure 3.3 displays a flat encased device with slower curing, directing further studies to use the lower intensity bar light.

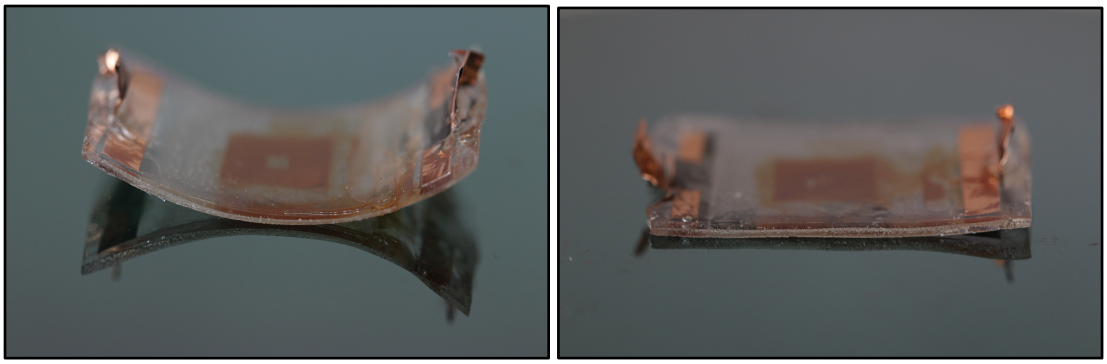

Figure 3.3. Increased polymerization stress from a two second cure with 2.5 W/cm^2 light (left) opposed to a five minute cure from a 550 μW/cm^2 light (right).

3.2. Effect of Thiol and Initiator Concentration on Functionalized and Non-Functionalized Polybutadiene

As TE-2000 was hypothesized to produce a denser cross-linked network of greater stiffness than B-1000, B-1000 was hypothesized to be more elastically active and flexible. This study lends support to these hypotheses through increasing amounts of HD and Irgacure, and attempts to produce a hybrid polymer to encompass both strength and elastomeric property in future EPD display elastomer. The HD purposes as a cross-linker and increasing the concentration can provide more links between PB chains. Increasing the Irgacure concentration can maximize light absorption to initiate thiol compounds at a faster rate. However, cross-linking rate improvements do not linearly increase by increasing the HD and Irgacure concentrations. Dependent on the polymer-based system, increasing initiator and cross-linker components too much can decrease elastomer physical and mechanical properties. Manipulating the HD and Irgacure concentrations in a systematic approach is thus studied to maximize elastomer properties.

Figure 3.4 demonstrates the recommended reaction pathway that radical benzene and radical tetracarbon take after Irgacure is irradiated by UV light. It has been confirmed (see section 3.4.1) that the two disassociated Irgacure radicals do not attack the vinyl groups protruding off the backbone of B-1000, but do initiate urethane methacrylate and thiol functional groups. Once initiated, it is assumed that acrylate end groups undergo cross-linking reaction with both thiol groups as well as B-1000 vinyl groups, essentially acting as a high molecular weight cross-linker. Post initiation of dithiol compound into a thiyl radical at one end enables the attack of both acrylate end groups as well as B-1000 vinyl groups, producing carbon radicals at either end. Past studies have shown that methacrylates are consumed at an initially faster rate than thiols by initiator radicals, consuming 4.9 methacrylate units per every one thiol [46]. Additionally, higher initial methacrylate conversion has been attributed to higher reactivity towards homopolymerization than that of reacting with thiols [27].

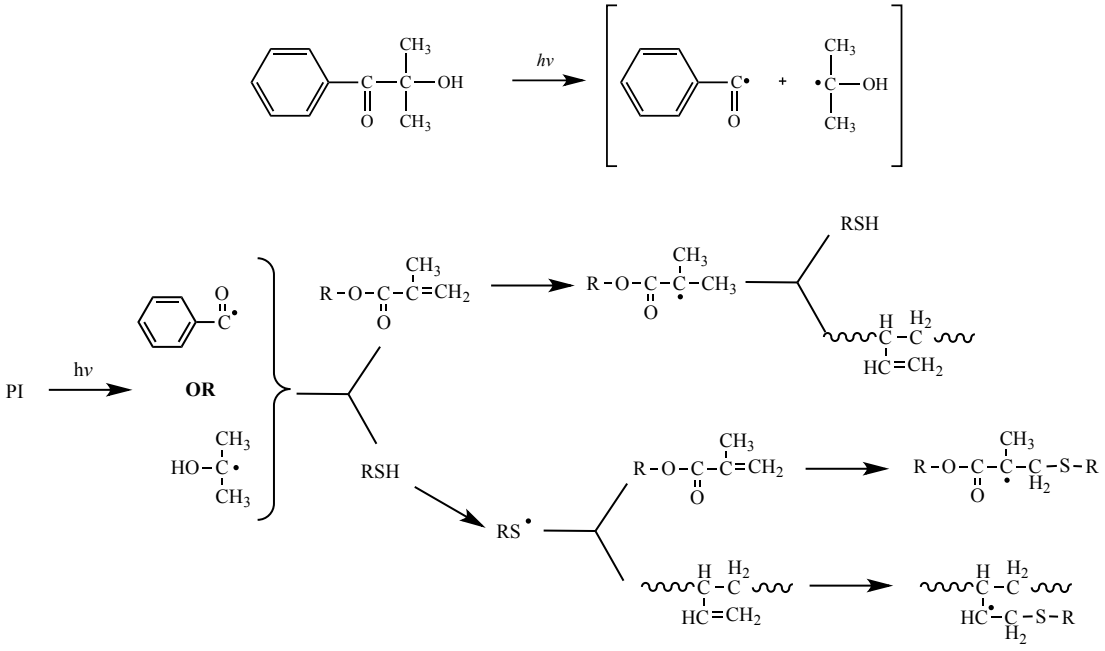

Figure 3.4. Radical reaction pathway in difunctionalized PB after excitation via UV light.

3.2.1. Cross-linking Density Determination

A high percentage of swelling indicates a loose polymer network, as can be seen especially in B-1000 resins with lower thiol to C=C molar ratios. For example, the highest amount of swelling was detected in B-1000 with only 0.05 thiol to C=C molar ratio, where samples swelled to over twice the initial size (Figure 3.5). Increasing the ratio of thiols in B-1000 resins significantly decreased swelling by an average of 120% when increasing from 0.05 to 0.1 moles of thiol, and then an additional 41 % when increasing to 0.15 moles thiol. Increasing the thiol molar ratio to 0.2 decreased swelling an additional 11%, showing a decaying change in swell percentage from the initial 0.05 molar thiol ratio to between 0.15 and 0.2. A tighter cross-link network subsequently forms with an increasing concentration of thiols to form intermolecular cross-links between polybutadiene chains. Increasing the weight percentage of Irgacure did not significantly decrease swell percentages throughout constant thiol molar ratios in B-1000 samples. This is due to the initiator radical's ability to only attack the dithiol compounds and not the vinyl groups of the polybutadiene. Initial presumptions would expect the increase from 0.15 to 0.2 thiol molar ratio to produce a more significant decrease in swell percentage, however, due to the intramolecular homopolymerization occuring between neighboring 1,2-units, further increasing thiol concentration may increase the number of unreacted thiols in the polymer network. As discussed, this can be disadvantageous as unreacted thiols can cause early onset of degredation, as oxygen, hydrogen and other compounds are able to react within the cross-linked network.

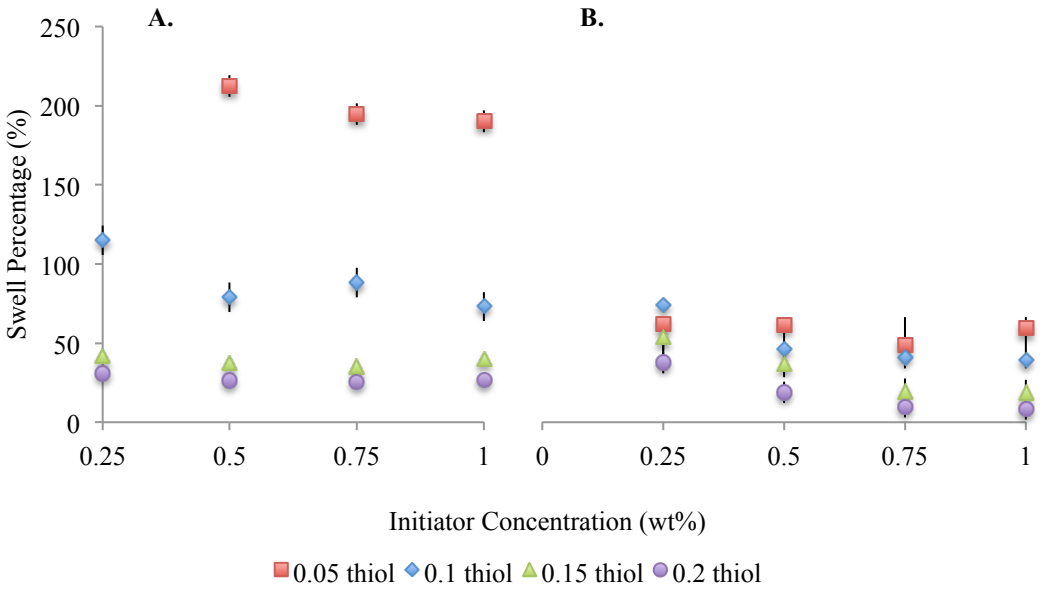

Figure 3.5. Swell percentage comparison between B-1000 (A) and TE-2000 (B).

Gel percentages at 0.01 thiol to C=C molar ratios indicated significant insolubility to hexane, with a floor gel percentage of approximately 68% for 0.01 thiol ratio and gel % increase to a ceiling 91% with 0.2 molar ratio (Figure 3.6). As swelling was severe for 0.05 molar ratio samples in B-1000, gel percentage data was not able to be accumulated as samples promptly shrunk when swelled hexane evaporated. Evaporation of hexane caused excess stress on the loosely formed network, causing the samples to split into pieces. Regardless, with an average of 51% swell difference between 0.1 and 0.2 molar ratios, only an average of 11.4% gel difference was measured. This indicates that although a more loose network was formed with lower thiol to C=C ratios, insoluble fractions from the formation of covalent bonds or via homopolymerization from neighboring vinyl groups resisted chemical breakdown from exposure to hexane.

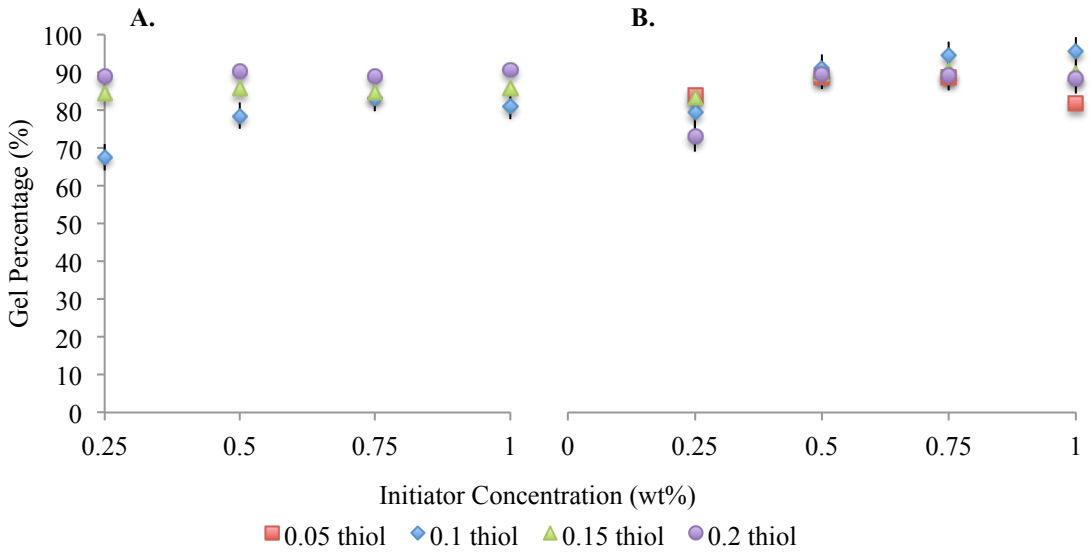

Figure 3.6. Gel percentage comparison between B-1000 (A) and TE-2000 (B)

As expected, TE-2000 samples appeared to form a more dense, tightly cross-linked network at lower thiol to C=C molar ratios when compared to B-1000 at similar ratios. Samples with 0.05 molar thiol ratio exhibited an average of 56% swell, where 0.2 molar thiol ratio only swelled an average of 19%. More dense cross-linked networks are formed as the methacrylate difunctionality of TE-2000 act as a high molecular weight cross-linker in combination to the dithiols. The methacrylate end groups are initiated by both the initiator and thiyl radicals and can react with 1,2 butene units as well as with other methacrylate groups.

The dimethacrylate reactivity of TE-2000 also explains the swell and gel percentage trend effects of both increasing initiator concentration as well as increasing dithiol concentration. With increasing initiator concentration, swell percentage decreases gradually at each thiol conentration, a phenomenon that was not seen with B-1000

samples. However, when increasing initiator concentration from 0.75 wt% to 1 wt%, only an average of 1-3% swell was measured for greater thiol concentrations. TE-2000 samples with 0.05 molar thiol ratio seemed to exhibit more error, potentially due to the looser network structure and more tacky physical properties. Error bars dictate the magnitude of the standard error, signifying that the 0.25 wt% and 1 wt% initiator concentration in 0.05 thiol molar ratio samples may not provide accurate trends. Observing gel percentage of TE-2000 samples demonstrates a similar trend, with increasing gel percentage at higher initiator concentrations and little to no increase between 0.75 wt% and 1 wt% initiator concentration. Gel percentages of TE-2000 samples appear to be around 90%, which is similar to that of the average 0.2 thiol molar ratio in B-1000 samples.

3.2.2. Compressive Material Properties

Cross-linking density differences as thiol and initiator concentrations increased exhibited clear distinctions in physical properties, distinguishable via the naked eye. However, to quantify physical property change, loss tangent and E' data was acquired via DMA compression testing in order to better choose dithiol and initiator concentrations for display resins. As frequency was kept constant throughout all experiments, the magnitude of phase angle is directly proportional to the loss tangent. The data portrays the overall average loss tangent in TE-2000 samples to be 0.42 greater than B-1000 samples, meaning that the ratio of energy lost to energy stored within the polymer network for B-1000 samples is approximately eight times less than TE-2000 samples (Figure 3.7). However, as loss tangent limits range from zero to a theoretical infinity, this 0.42

difference is small. Differences between loss tangent properties will still be discussed. As a perfectly elastic material exhibits a phase change equal to zero, the amount of viscoelastic damping, or the degree of phase change deviating from zero indicates a less elastic material.

A greater change in internal entropy and distortion of covalent bonds is experienced by TE-2000 samples, as the greater concentration of elastically active linked segments dampen oscillatory motion. B-1000 chains dampen oscillations to a lesser degree, signifying a more rigid structure. These results opposed initial hypotheses as B-1000 was expected to provide a more elastically active network than TE-2000. This was thought to be true as benzene rings within TE-2000 end groups may have caused a lower free volume and a lower segmental motion within a cross-linked network. However, with increasing thiol concentration in B-1000 to form a denser cross-linked network, B-1000 may form a less amorphous structure than TE-2000 due to a lack of end group functionality. As discussed, a more amorphous structure is advantageous for elastomers to better dissipate applied stress. Swell testing demonstrated a more densely cross-linked network in cured TE-2000 samples alluding to a greater amount of elastically active cross-links to dissipate oscillatory compression forces. B-1000. High phase angle shift increases the loss tangent. Even the 0.2 molar thiol ratio in B-1000 samples that have a cross-link density comparable to TE-2000 samples, less entropic change was instilled into B-1000 linked segments as a response to oscillatory forces, showing a lower loss tangent. TE-2000 thus shows a greater cooperative motion between segments experiencing deformation when compared to the B-1000 samples.

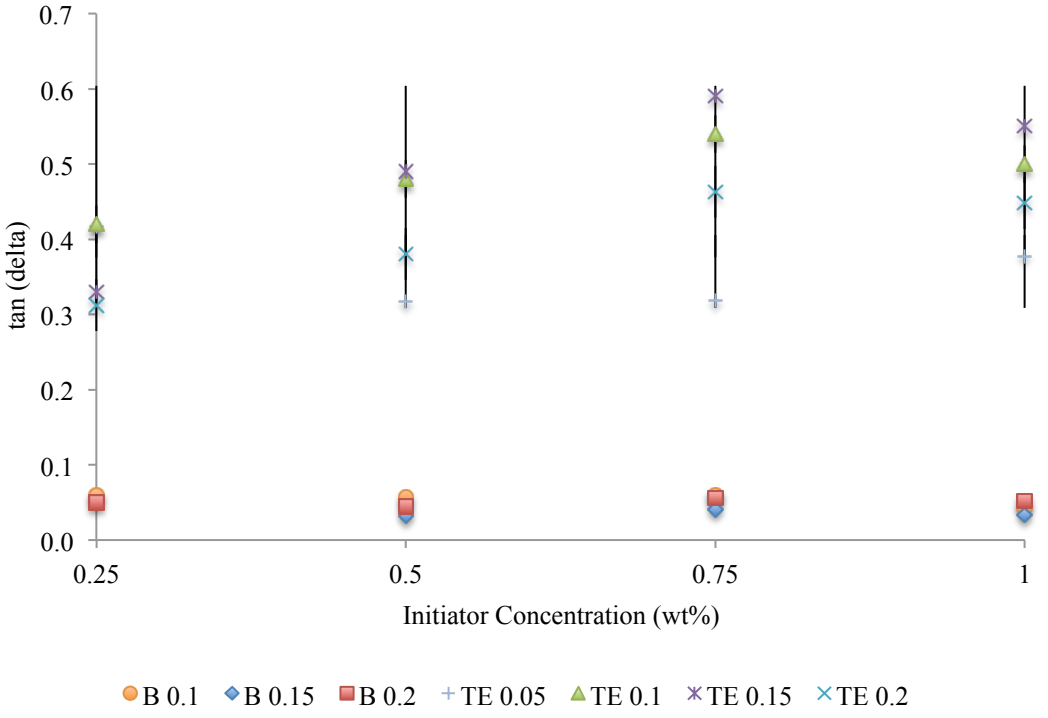

Figure 3.7. Tan delta values displaying more elastic modulus dominated B-1000 samples in comparison to TE-2000 samples.

Poor sample-to-sample repeatability may be caused by defects such as bubbles within cross-linked compression samples, as well as trapped chain entanglements. High-molecular weight polymers pose a high probability of chain entanglements prior to UV exposure that can be incorporated into the cross-linked network post curing. Trapped chain entanglements may show greater elastic moduli as additional restraints and chain friction persist within the network to resist segmental motion [43]. In TE-2000 samples of 8 mm diameter (prior to taking 2mm cut-outs), stress build-up caused contact-shaped warping to occur. It is well known that acrylates and methacrylates gel at low conversions, which causes increased internal and shrinkage stress. Warping degrades

DMA E' accuracy as full contact between upper and lower plate fixtures is not completely flush with all sample surfaces, resulting in error.

As high variability between thiol concentrations obscures any trends within polybutadiene sample groups, each polymer sample group of varying thiol concentrations was averaged to see the effect of increasing initiator concentration on E' (Figure 3.8). As B-1000 samples modeled higher elastic properties in comparison to TE-2000 samples, B-1000 samples also had a lower average elastic modulus. As elastic moduli represents the stiffness of a material, benzene rings within TE-2000 structure exhibit more crystalline portions within the cross-linked network and restrict segmental motion. Increasing initiator concentration from 0.25 wt% to 0.75 wt% demonstrated a significant E' increase of 0.22 MPa in TE-2000 samples. A slight 0.04 MPa E' change was observed in B-1000 samples of the sample initiator concentration increase, although not statistically significant. Further initiator increase to 1 wt% in both TE-2000 and B-1000 samples decreased E' by 18 % in TE-2000 samples and by 23% in B-1000 samples. Any initiator radicals left within the cured network acts as a plasticizer to decrease E'. Thus, utilizing a 0.75 wt% initiator concentration is ideal for the highest stiffness in cured TE-2000 and B-1000.

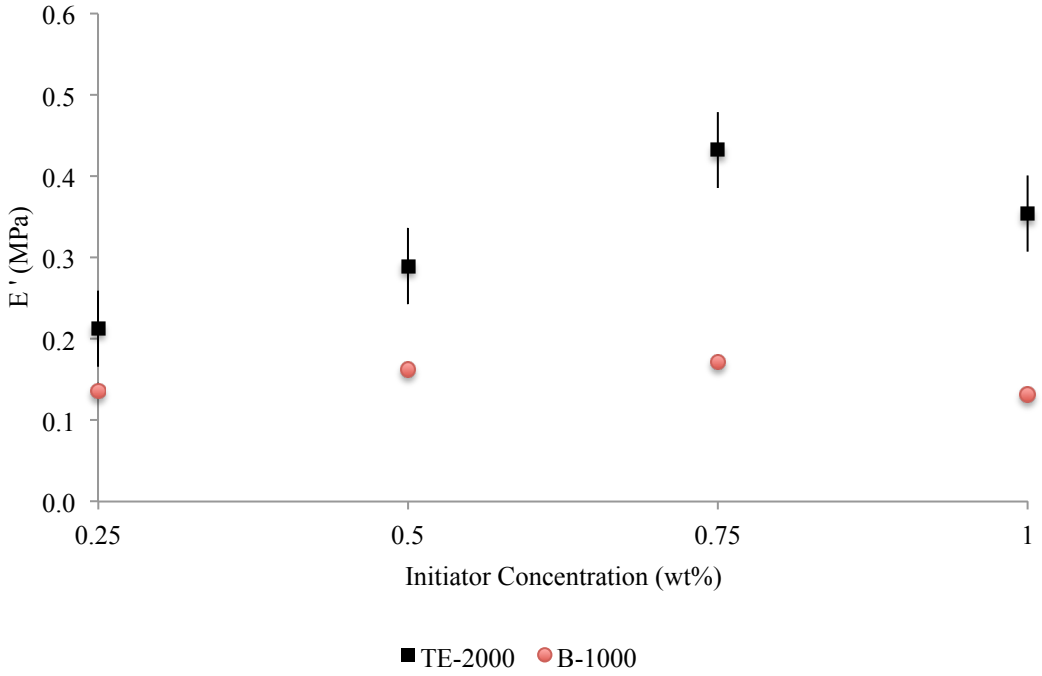

Figure 3.8. Average compressive elastic moduli values for TE-2000 and B-1000 matrix samples.

3.3. Hybrid Polymer

In an attempt to reduce hexane concentration while achieving high cross-linking density and stiffness of TE-2000 samples as well as reduce viscosity of the system by incorporating less viscous B-1000, a TE-2000 and B-1000 hybrid polymer formulation was produced. Initial viscosities of B-1000 and TE-2000 prior to hexane dilution was 9.98 Pa.s at 1x 10^3 s^{-1} and 3.44x10^3 Pa.s at 3 s^{-1}, respectively. The viscosity of TE-2000 is too high for the instrument to probe higher strain rates than 3 s^{-1}. After reducing hexane concentration to 30 wt %, B-1000 was added to TE-2000 in 10 wt% increments and the viscosity was measured at 1000 s^{-1}, a shear rate equivalent to that expected in microfluidic chips. B-1000 diluted in 30% hexane was measured to be 68.33 mPa.s in comparison to TE-2000 in hexane at 1120.54 mPa.s. A cloudy solution resulted in co-

polymer ratios surpassing 30 wt% B-1000 addition, however, a viscosity of under the maximum 500 mPa.s for usage in microfluidic cells was obtained (Figure 3.9).

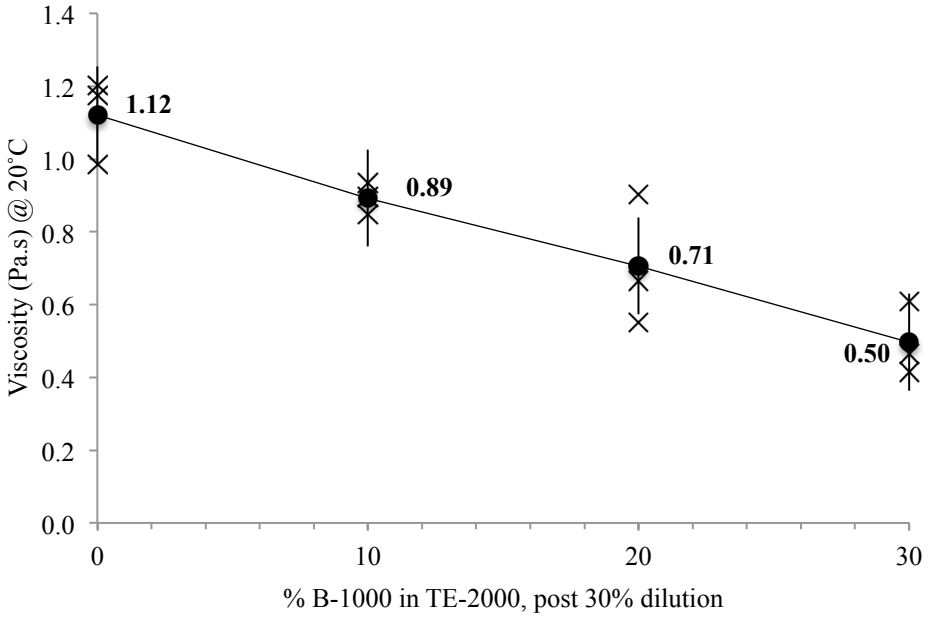

Figure 3.9. Decreasing hybrid polymer viscosity with increasing B-1000 concentration at 1000 s^{-1}.

Hybrid polymer (HP) of 70/30 TE-2000/B-1000 ratio was used with an initiator concentration of 0.75 wt% as determined from initial testing of TE-2000 and B-1000 samples previously. Swell testing showed a decrease in swelling by 50% with increasing thiol concentration from 0.05 to 0.2 molar thiol ratio and a concurent increase in gel percentage by 13% (Figure 3.10). HP samples without dithiol were cure tested resulting in some gelling, however gelling was insufficient for a stable sample of 0.5 mm thickness. A 25 μm layer of HP without dithiol successfully cured but was not swell tested due to sample inconsistency. The gelling observed is attributed to initiator radicals attacking TE-2000 urethane methacrylate end groups, thus acting as a cross-linker to B-1000 and with itself. Comparing HP swell percentage and loss tangent data to that of TE-

2000 and B-1000 samples results in HP data lying in between. HP resin showed a significantly more dense cross-linking network than B-1000 at lower thiol molar ratios, and a similar swelling percentage of both TE-2000 and B-1000 at high thiol molar ratios. Average results demonstrate a minimum HP swelling percentage of 18.7% at 0.2 thiol molar ratio, in comparison to 25.6% and 9.85% for B-1000 and TE-2000 samples, respectively. Gel percentages were also comparible, with no significant differences throughout all thiol molar ratios.

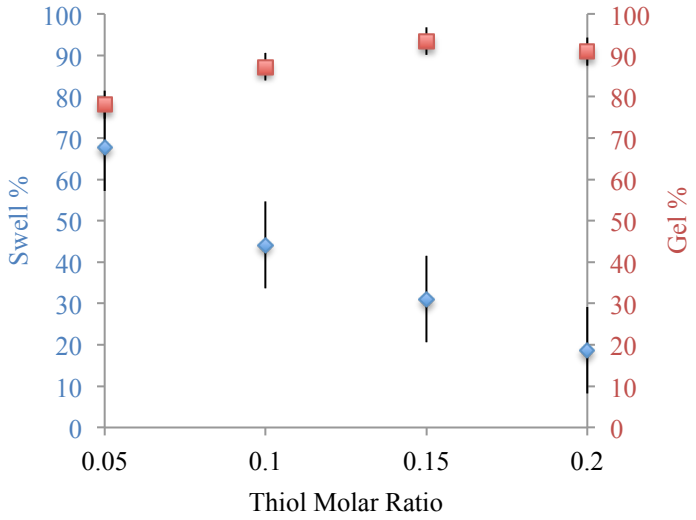

Figure 3.10. Cross-linking density determination via swell testing shows a decrease in swelling with increasing thiol percentage and subsequent increase in gel percentage.

The HP achieved high stiffness from TE-2000 and a reduced viscosity with B-1000, however as cross-linking density was slightly decreased from TE-2000 samples, a lower loss tangent resulted. At low thiol molar ratios, HP showed a higher E' than TE-2000, which is assumed to be due to both dithiols and methacrylate end groups acting as cross-linkers (Figure 3.11). With B-1000 reducing the viscosity of the system, high MW TE-2000 chains are able to more efficiently react. Increasing thiol molar ratios of 0.15

and 0.2 decreased HP stiffness lower than that of TE-2000, as increasing dithiol concentration enabled TE-2000 chain mobility, increasing cross-linking density, and thus further increasing network stiffness. Overall, the HP stiffness did not change dramatically with increasing HD concentration as did TE-2000 samples, averaging 0.36 ± 0.05 MPa. HP loss tangent data followed more closely to B-1000 data, relaying a more characteristically elastic cured elastomer than TE-1000 samples. With more lower molecular weight PB chains without urethane methacryalte end groups, TE-2000 can act as an additional cross-linker to dithiols to form a denser cross-linked network while still inheriting higher chain mobility when subject to applied compressive forces. It appears that the B-1000 incorporation with TE-2000 made a more significant impact in loss tangent than in cross-linking density, potentially due to the slowing of urethane methacrylate reactivity with dithiols as less steric hendrance to B-1000 butene units persisted for dithiol reaction.

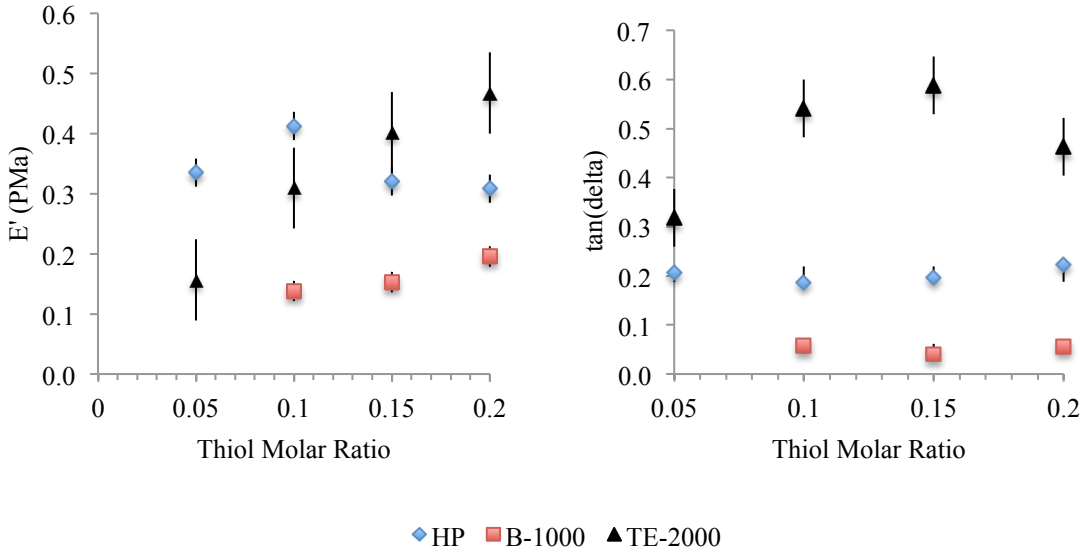

Figure 3.11. Stiffness and loss tangent properties of hyrbid polymer falling between those of TE-2000 and B-1000 samples.

HP usage in a 100-μm/400-μm capillary sized double emulsion microfluidic cell was successful at encapsulating a boron suspension, with propylene carbonate as the solvent. The first microfluidic encapsulation attempts with HP were without dithiol in the resin formulation to ensure viscosity parameters were met. Encapsulation of boron suspension resulted in stable shell-core capsules of approximately 17 μm shell thickness, however the elastomer shell appeared weak when compressed between two glass slides and tacky when sticking to neighboring capsules in continuous solution (Figure 3.12). Drying capsules via vacuum filtration resulted in concaved capsules, although boron suspension remained in the core.

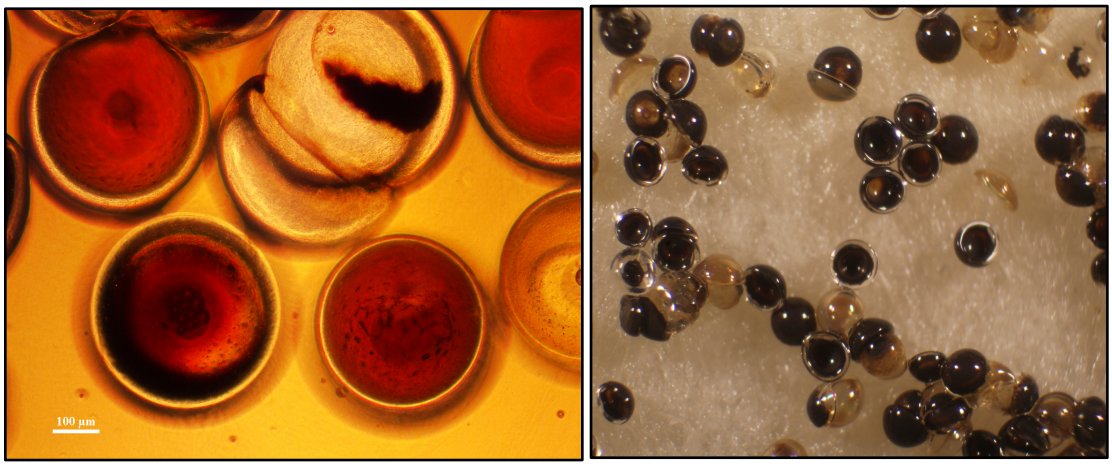

Figure 3.12. Encapsulation with HP lacking dithiols resulted in stable capsules in the continuous fluid (left) and concaved capsules after drying (right). Shell thickness ~ 17 μm.

Using HP formulation with 0.05 molar thiol ratio resulted in stable capsules which could withstand multiple tests of compression between two glass slides and did not stick to neighboring capsules whilst suspended in deionized water (Figure 3.13). After drying, many capsules maintained a spherical shape, however some capsules did appear

collapsed. Shell thicknesses were approximately 31 μm, which may pose potential for a lesser degree of curing towards the interface of boron suspension and shell layer when compared to the outer shell layer interface in direct contact to UV light. However, caving may be attributed to the osmotic pressure build-up, as the curing of the capsule shell initially acts semipermeable, but shifts to an assumed impermeable thin film once cured. With increased pressure at the core/shell interface, studies have shown that increasing pressure causes an increase in polymerization rate [71]. Although characterization of this phenomenon was not performed, an increase in polymerization rate towards the core would increase shrinkage stress, thus causing the concaving of the spherical capsules.

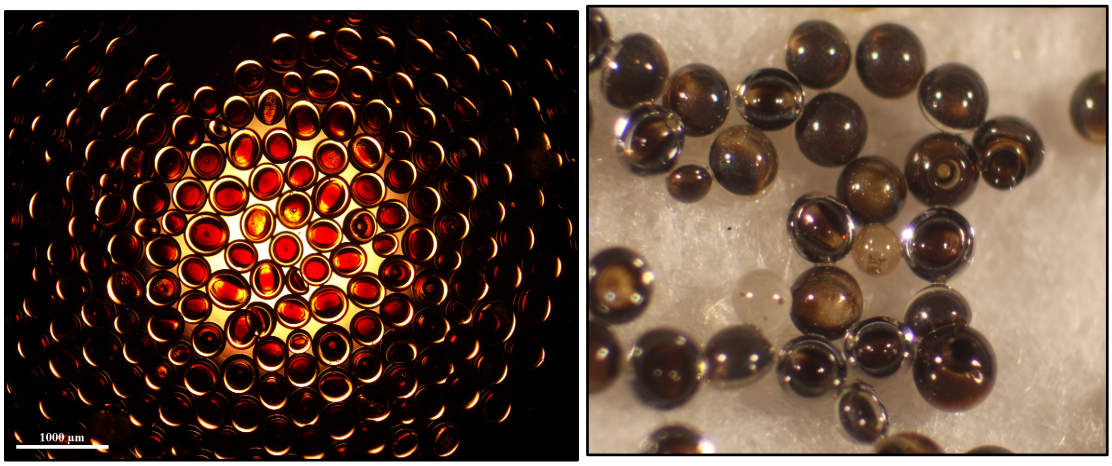

Figure 3.13. HP with 0.05 molar thiol ratio encapsulating boron suspension when suspended in DI water (left) and spherical capsules post drying (right).

Surpassing 0.05 molar thiol ratio in the HP resulted in unstable resin formulations. Resin formulation stability was tested by covering vials of 0.05, 0.10, 0.15, and 0.2 molar thiol ratio in HP with foil and checking the viscosity in the vial post 24 hours. All formulations over 0.05 molar thiol ratio were partially or entirely cured when checked after 24 hours, indicating evidence of dithiol dark curing (see section 1.5.2). By

increasing thiol concentration, more thiol and C=C bond collisions occur, thus resulting in a higher probability for thiyl radical formation. Radical stabilizers such as diazabicyclo-2,2,2-octane or hydroquinone monomethyl ether may be necessary in order to further increase thiol concentration in formulations and acquire a higher network cross-link density [57], [72].

3.4. Cross-linking Variation Among Dithiol Carbon Chain Length

Few literature papers provide detail on cross-linking differences, and varying mechanical and physical properties thereafter, as a result of varying carbon chain length (CL) between dithiol compounds [73]. Initial formulations for encasing of flexible EPD cells revealed a fatal difference between utilizing DD vs HD, resulting in macroscopic cracking in DD formulations (Figure 3.14). These two formulations and preparation parameters varied only by the dithiol cross-linker used, sparking further investigation via real time FTIR and rheology. A past study performed a computer simulation and simultaneous finite-element analysis on stresses occurring between the shrinkage stress of a curing polymer on top of a flexible polymer that deemed interfacial stress as triaxial. Simulations indicated strong shearing stress as a result of simultaneous tensile and compressive forces of the underlying flexible PET substrate [74]. Hypotheses on the matter were as follows: (1) poor conversion was occurring in longer carbon CL dithiols to produce a weaker network, and (2) longer CL dithiol resins experienced an increase in

internal stress build-up as cross-linking proceeded.

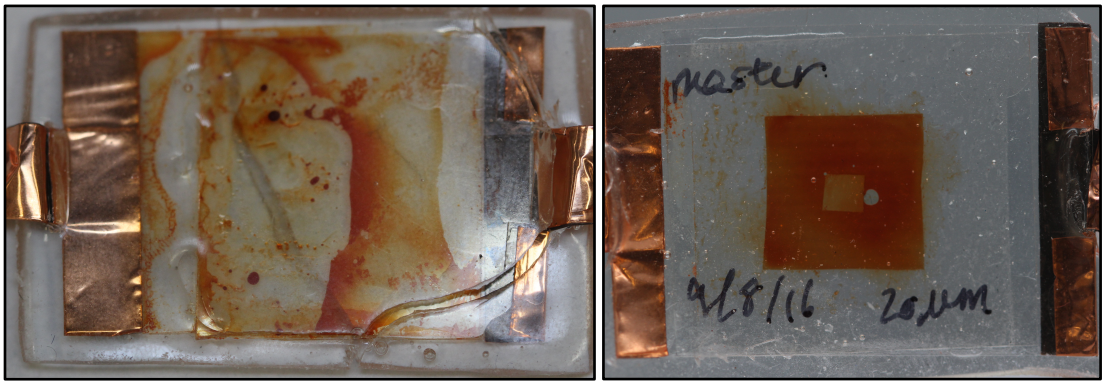

Figure 3.14. Cracking within flexible EPD cell resin encasing, as a result of long dithiol chain length (left) in comparison to short chain length dithiol resin (right).

3.4.1. Real-time Fourier Transform Infrared Spectroscopy

Thiol conversion as a function of exposure time enables network structure comparison between increasing CL dithiol compounds used in B-1000 PB resins (Figure 3.15). The series of dithiol compounds characterized represent a range of potential dithiols that could be incorporated into resin formulation for encapsulation, encasing, and sealing of EPD devices. Each thiol conversion plot is measured independently via Equation 2.3. Results show an increase in maximum thiol conversion in decreasing CL dithiol compounds. PD resin system had approximately 8 times greater thiol conversion than did DD, with PD and DD formulations at a maximum thiol conversion of 86% and 11.3%, respectively. OD dithiol system appeared to exhibit error at low thiol conversions, suggesting some radical reaction prior to recording spectra.

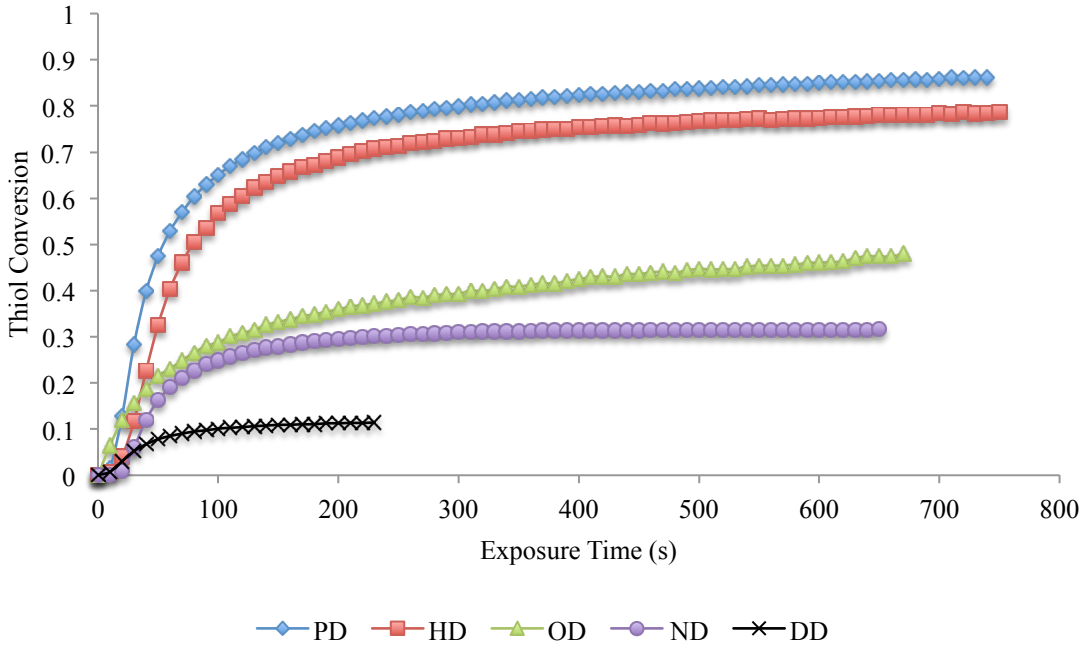

Figure 3.15. Thiol conversion comparison of increasing carbon CL as a function of time.

Plotting thiol conversion against time presented three stages of polymerization, representing the initial constant rate at low conversions (I), the increased polymerization rate due to the gel effect stage (II), and the terminal constant rate at high conversions (III) [49], [75]. Initial rates at low conversions ($x < 6\%$) appear to abide by Flory's step-growth kinetic theory (except for OD system), although an insufficient number of data points could be gathered to fully define stage I during the short reaction period (~10 seconds). As the shift from stage I to stage II occurred in a linear transformation, a second-order kinetic model is assumed. If a linear transition proceeded with no change in slope, a first-order kinetic model would have been assumed. After taking the derivative, the degree of cross-linking (Equation 3.1) was then applied to thiol conversion data and graphed against time to confirm the assumed kinetic model. Additionally, to verify the thiol-ene step-growth reaction mechanism as a result of chain-transfer reactions, degree

of cross-linking was graphed as a function of thiol conversion (Figure 3.16). Instead of demonstrating chain-growth behavior of an almost instantaneous increase in the degree of cross-linking at low thiol conversions, a steady increase in degree of crosslinking was observed, followed by a greater degree of cross-linking at higher thiol conversions. However, chain-growth behaviors, such as the gel effect, are still observed, which prevent the thiol-ene reactions presented here from following an entirely step-growth behavior. Step-growth kinetics are still followed as the best fit representation to calculate rate constants.

$$Degree\ of\ Crosslinking = \frac{1}{(1-x)} = k_x t + 1 \qquad (3.1)$$

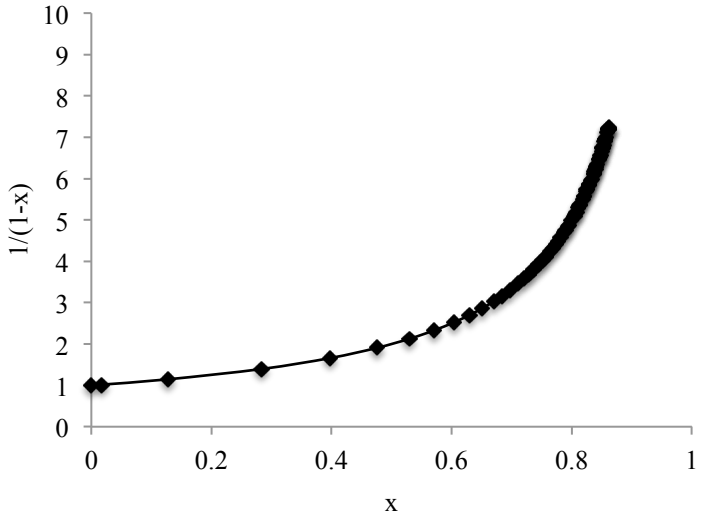

Figure 3.16. Displaying step-growth trend in thiol conversion for 1,5-pentanedithiol resin system.

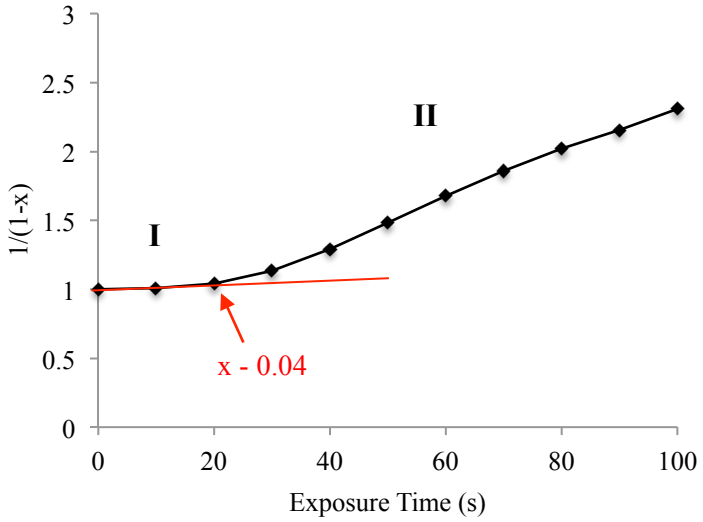

Figure 3.17. Linear slope transition from stage I polymerization (~20 seconds) to stage II in representative HD resin system.

The representative plot of HD reveals a linear transition as a function of degree of conversion in stages I and II of polymerization (Figure 3.17). Rate constants for initiation of thiols and vinyl consumption were then determined via fitting a linear fit to respective graphs. Photochemical initiation rate was calculated via Equation 1.9 (see sec 1.5.2), with initiator efficiencies for each dithiol system empirically calculated by dividing stage I rate constant of thiol consumption by that of the initiator species. Production of initiator radical species commences activation of thiyl radicals from the dithiol compounds with rate constant k_s and rate R_s (Equation 1.13). R_s was calculated and compared for stage II polymerization (after 20 seconds and before stage III transition). Stage II to III conversion percentage transition is listed in Table 3.1, along with calculated kinetic rates.

Thiyl radicals attack vinyl groups protruding off the polybutadiene backbone, instigating either cross-linking and chain transfer or homopolymerization with neighboring 1,2-butadiene units. Resulting vinyl consumption rate, R_v (Equation 3.2),

encompasses both heterogeneous cross-linking reaction constant k_X , and homopolymerization rate constant k_H. Thiyl radicals can be subject to chain transfer or be consumed via a termination reaction. As chain transfer is an inherent reaction of thiols to proceed, the rate at which thiyl radicals react with vinyl groups and the rate at which chain transfer occurs to produce a new thiyl radical is assumed to be nearly equal.

$$R_v = k_x[RS^*][C=C] + k_H[C^*][C=C] \quad (3.2)$$

As both the rate of cross-linking and chain transfer have been assumed equivalent by both LeCamp et al. [46] and Cramer and Bowman [56], Equation 3.3 was employed to calculated the relative consumption rate of homopolymerization to thiyl consumption:

$$\frac{d[C=C]}{d[SH]} = 1 + \left(\frac{k_H}{k_x}\right)\left(\frac{[C=C]}{[SH]}\right) \quad (3.3)$$

Graphing vinyl conversion against thiol conversion provides insight to the extent of homopolymerization in relation to the extent of cross-linking, and thus enables an understanding of the developed network uniformity and structure (Figure 3.18). The more linear the slope and the closer the slope of the line approaches unity, the more uniformly cross-linked network with less homopolymerization occurring. Relative reactivity ratios of each dithiol system was calculated after stage I polymerization (after ~20 seconds) and listed in Table 3.1. Butadiene units of 1,2-unit conformation undergo homopolymerization and copolymerization with the thiol, but 1,4-"trans" units only react with thiyl radicals and do not pose the potential for homopolymerization. Therefore, when calculating the relative consumption rates, only 85% of measured thiol conversion was considered as approximately 85% of B-1000 is composed of 1,2-units.

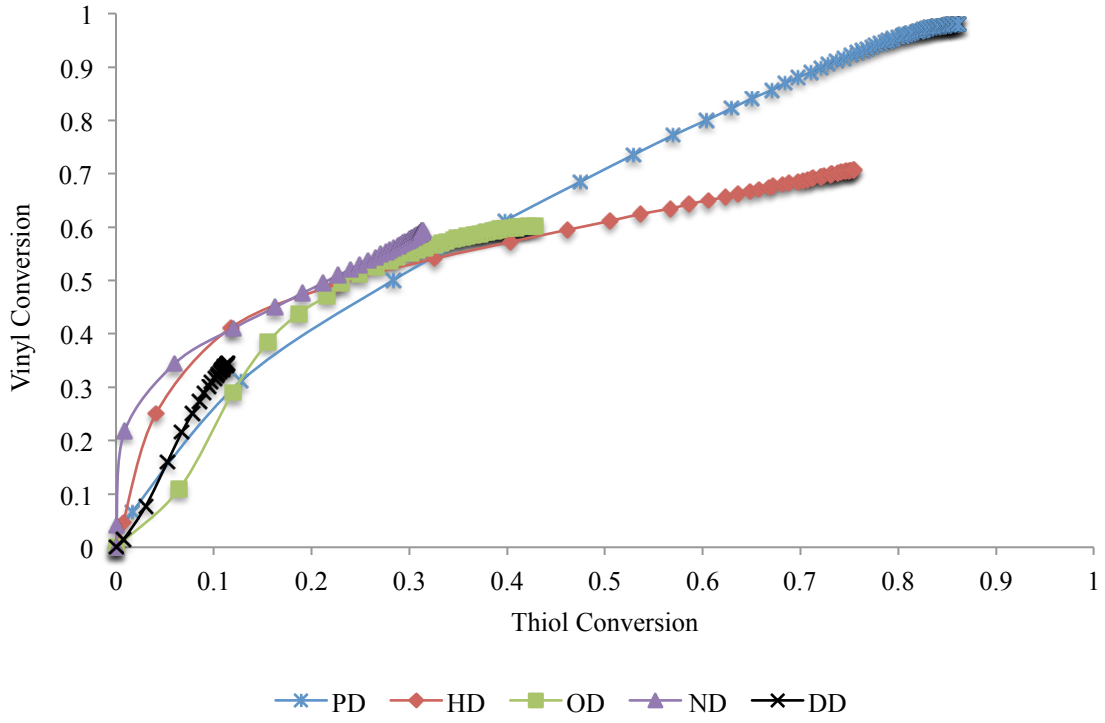

Figure 3.18. Vinyl vs thiol conversion graph displaying an increased C=C reactivity for higher molecular weight dithiols.

Table 3.1. Rate, conversion and relative reactivity ratio comparison between dithiol systems

# Carbon	**5**	**6**	**8**	**9**	**10**
∈ (L/mol cm)	41.25	42.08	47.87	50.77	40.06
R_i (mol/Ls)	1.49E-06	9.43E-07	2.42E-06	2.47E-07	5.83E-07
R_s - *II* (mol^2/L^2)	6.8E-03	5.2E-03	7.8E-04	9.2E-04	4.2E-04
X% (II - III)	73.7	65.7	32.6	29.7	8.5
K_H/K_x	1.46	1.49	1.81	2.12	4.39

Rate of photolysis of Irgacure did not show significant trends with increasing dithiol CL, which is to be expected. As each resin mixture is low in viscosity at low conversions, initiator radicals are able to efficiently attack thiol compounds at a

comparative rate as diffusivity is high. Additionally, as no solvent is present, besides dithiol compounds acting as a reactive diluent, and RT-FTIR characterization did not detect butadiene peak change due to Irgacure radicals alone, initiation of thiols is expected to be dependent on thiol mobility and availability. Irgacure conversion was monitored to react throughout the duration of thiol conversion. Low concentrations of initiator species (1 wt%, 0.06 M) are required for initiation of thiyl radicals, as chain transfer enables further initiation of thiol compounds throughout propagation. Once thiyl radicals are produced, the dithiol compound is the sole means of radical initiation of butadiene groups, signifying that vinyl conversion is thus dependent on dithiol mobility efficiency as well. B-1000 and increasing dithiol CL initial viscosities were measured and reported in Table 3.2 to represent decreasing dithiol mobility with increasing dithiol CL. Rate of dithiol initiation as a function of initiator concentration during stage II polymerization exposed a decreasing rate with increasing dithiol CL. ND dithiol resin system portrayed a 0.85 greater thiyl reaction rate than OD resin system, of which may be attributed to lack of sample replicates and will be studied further. However, for the sake of the end thiol conversion data recorded and the diffusion-limitation model to be discussed, greater ND R_s rate is attributed to error. In addition, gel effects appeared to be most pronounced for shorter CL dithiols, which may be attributed to dithiol mobility.

Table 3.2. Dithiol resin system initial viscosities at $1x10^3$ s^{-1}

# Carbon	**5**	**6**	**8**	**9**	**10**
***η* (mPa.s)**	19.0	25.5	31.0	41.5	46.9

Diffusion limitations are assumed to be the determining factor towards bimolecular thiol termination, increasingly so in long CL dithiol compounds. Termination rates were not calculated as the probabilities of thiyl radical collisions were not measured, and thus specific rate constants for diffusion termination could not be accurately calculated. Viscosity measurements of 1:1 molar ratio of thiols to butadiene groups in B-1000 were used as initial diffusion coefficient estimates, related to the Perrin's derivation of the Stokes-Einstein equation for prolate and oblate ellipsoids (Equation 3.4):

$$D = \frac{kT}{6\pi\eta r(\frac{f}{f_o})} \tag{3.4}$$

where k is Boltzmann's constant, T is the absolute temperature, η is the viscosity of the resin, and f/f_o is the frictional ratio [76]. As f/f_o increases with the increase in carbon CL between dithiols, and as viscosity increases as well, the diffusion coefficient subsequently decreases with increasing dithiol CL.

The rapid increase in stage II conversion due to the gel effect does not occur in long CL dithiols as segmental diffusion dominates when two radicals become sufficiently close. Long CL dithiols have a greater chance to entangle with each other and PB chains, thus posing a higher potential for thiol termination. Table 3.1 lists the conversion percentage of thiols towards the end of stage II polymerization, once conversion rates begin to plateau. DD resin only reaches a conversion of 8.5 percent prior to assumed segmental diffusion leading to an overwhelming termination. Additionally, not all radicals may be consumed and may be left trapped within the cured network. With increasing degree of cross-linking, viscosity increases as the active diluent is consumed, thus increasing segmental diffusion in long CL dithiols. Short CL dithiols such as PD and HD have high mobility to maintain a distance from other propagating thiyl radicals. Even

when subject to translational diffusion of two propagating thiyl radicals, thiyl radicals pose a greater affinity towards butadiene units than each other, decreasing the probability of termination at low conversions [46].

The probability of each end thiol in dithiol compounds to react with itself is significantly low. Dithiol compounds are not likely to undergo direct cyclization with thiol functional groups at each end of the compound, in place of performing a cross-linking reaction. Especially for shorter CL dithiols with five and six carbons, forming a ring would not be thermodynamically or kinetically favorable due to high ring strain. For higher molecular weight dithiols, the probability is still unlikely as torsional and transannular strain arise from cyclic conformation on adjacent atoms of the ring and repulsive interaction between hydrogen and sulfur [49]. However, in the slim case that a longer CL dithiol were to be entangled either with another dithiol or polymer chain, combination termination between dithiols may persist, but would be due to segmental diffusion.

In comparing butadiene conversion to thiol conversion, initial reaction rates of C=C bonds appear greater, on average, than thiol reaction rates. Short induction periods during thiol-ene chemistry have been characterized throughout literature studies to be due to oxygen side-reactions, where dissolved oxygen has a retarding effect on thiyl reaction [77], [78]. Not all dithiols will be retarded in the case of oxygen side reactions, in which some thiyls will successfully attack butadiene units. However, if an insufficient number of dithiol compounds are available for chain transfer, the probability of homopolymerization between neighboring 1,2-butadiene units is higher, thus leading to a potentially higher initial butadiene peak conversion on average. Calculated relative

consumption rates indicate that DD resin systems are approximately three times more likely than PD to propagate via homopolymerization than chain transfer reaction. Rates indicate that kinetic feasibility for efficient high thiol cross-linking conversion requires shorter CL dithiols. Additionally, higher relative reactivity rates pertained to greater homopolymerization that may affect the final cross-linked network microstructure. Figure 3.19 displays the two main paths a thiyl radical can venture, either towards cross-linking and producing an additional thiyl radical, or undergoing homopolymerization with a neighboring 1,2-butadiene unit. A significantly greater degree of homopolymerization will produce a weaker, less dense cross-linked network, diminishing physical bulk properties of the final cured elastomer.

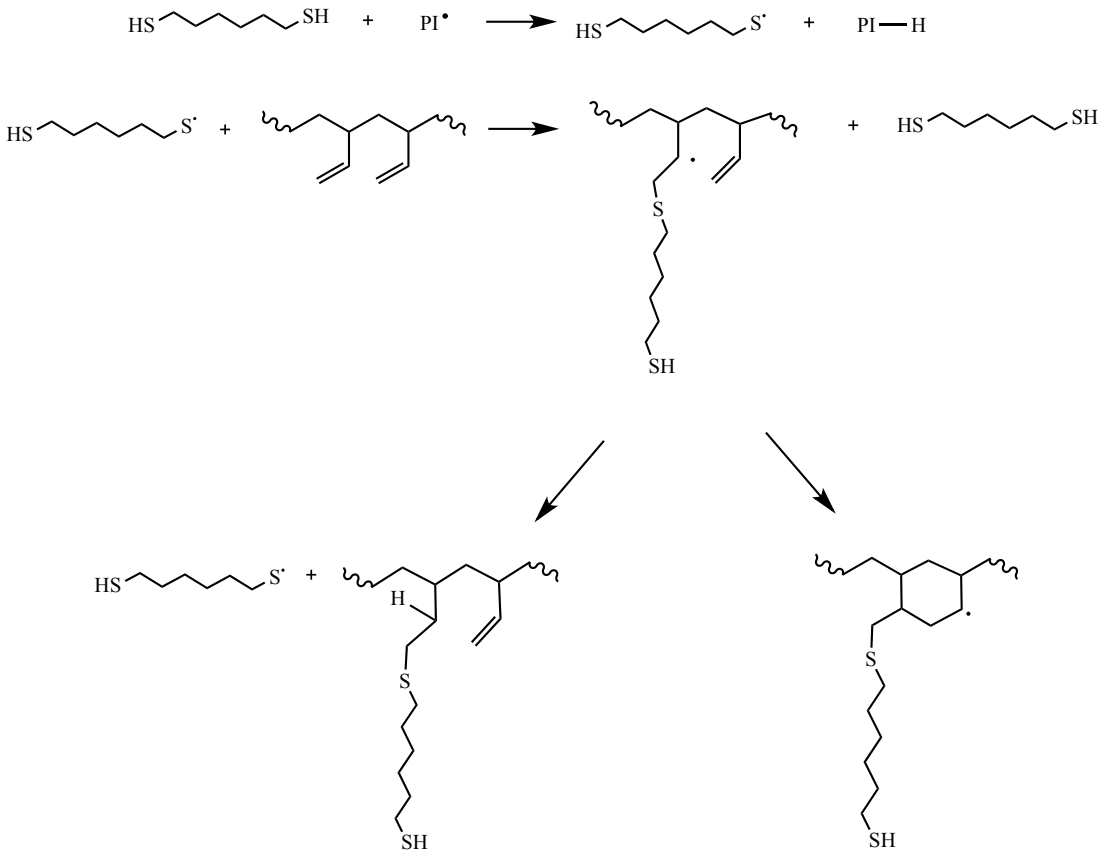

Figure 3.19. Copolymerization vs homopolymerization of 1,2-butadiene vinyl groups

Oxygen related side reactions were suspected during FTIR characterization of thiol conversion, as recorded peak showed constructive absorbance of two functional groups (Figure 3.20). As –OH stretch peak can be detected in 2500-3300cm^{-1} range, the second peak (~2570 cm^{-1}) next to the thiol peak (2560 cm^{-1}) may be attributed to oxygen. When comparing DD to PD resins, PD peak shape appears less symmetric, indicating potentially less oxygen effects in PD resin systems. Therefore, low thiol conversions of short CL dithiols remains to be understood by stage I conventional kinetics. An insufficient number of data points was able to be gathered between zero and 20 seconds of exposure time, leading to inability in deciphering if stage I is due to oxygen effect or by hypothesized conventional kinetics. As initial recorded IR peaks display –OH stretch peak presence, it appears oxygen reacts with thiol prior to UV exposure, potentially due to dark reaction. OD resin characterization may have experienced dark reaction prior to UV exposure, as some reaction prior to characterization was previously mentioned. The potential "induction period" may have been due to consuming the concentration of oxygen in the thin-film, followed by cross-linking once all oxygen had been reacted [29]. Further evidence was shown when comparing initial thiol conversion to that of the initiator benzyl radical conversion (Figure 3.21). No significant induction period was observed in the initial benzyl radical conversion, confirming reaction. Supplementary characterization will be performed in the future to gather quantitative oxygen effect results.

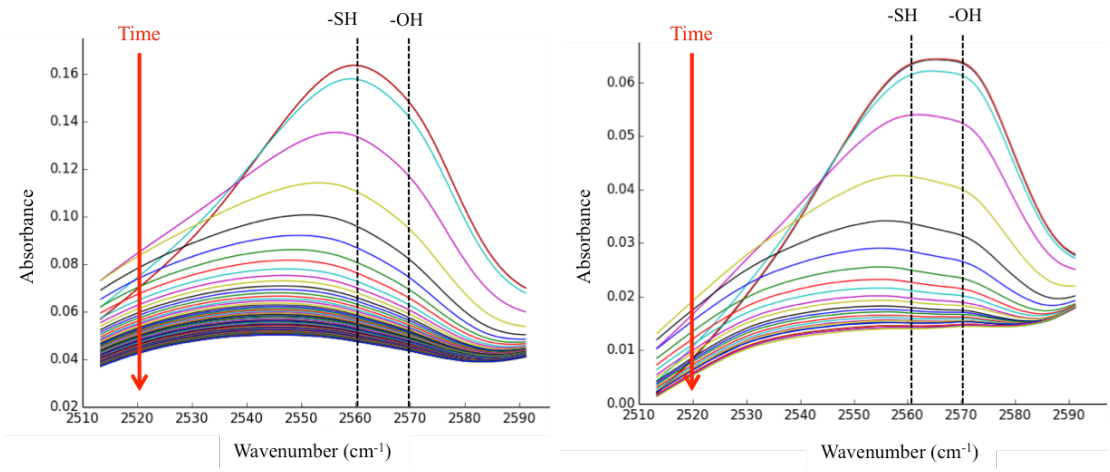

Figure 3.20. Shoulder on thiol peak due to suspected oxygen side reaction in PD (left) and DD (right) resin systems.

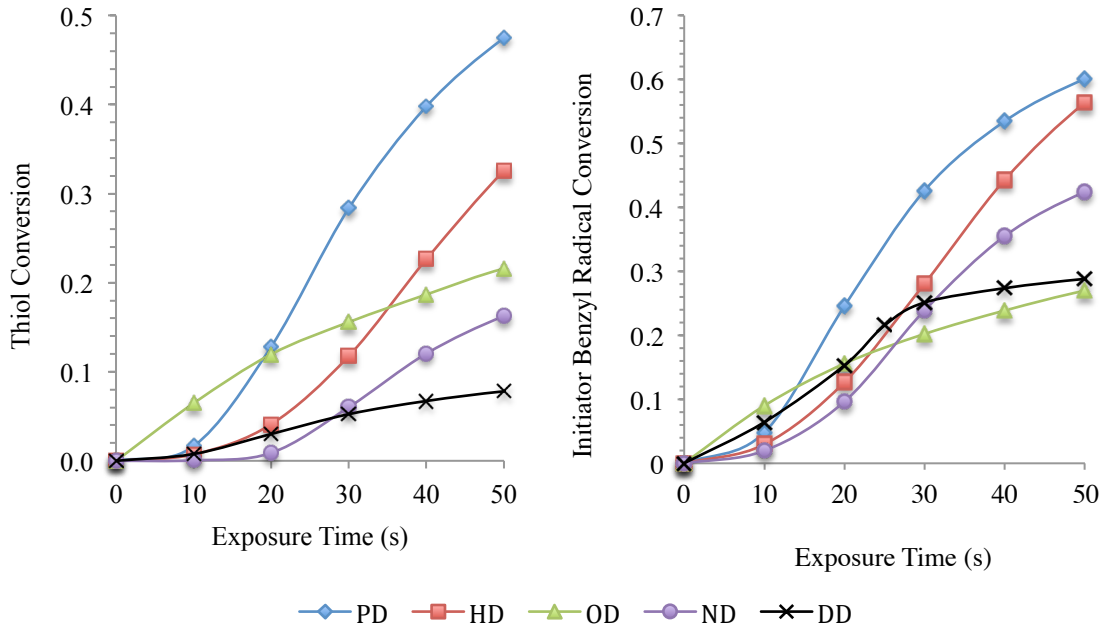

Figure 3.21. No significant initiator benzyl radical inhibition when compared to that of thiol conversion during early exposure times.

3.4.2. Real-time Rheology

The initial hypothesis suggested a shorter gelation point for long dithiol CL resin systems, as it was apparent that there was an increase in internal stress. With less time until gel point (GP), network formation rate would be higher, thus causing an increase in shrinkage stress. Internal stress was assumed to be due to increased shrinkage stress as a result of network formation, or to external stresses caused by the underlying PET substrate. Figure 3.22 displays a representative plot of a dynamic oscillatory rheology experiment against time, where G" is initially above G' indicating more viscous-like properties of the resin. Once the resin is exposed to UV light, G' was non-dominate until near the GP when the displacement of larger molecules commenced.

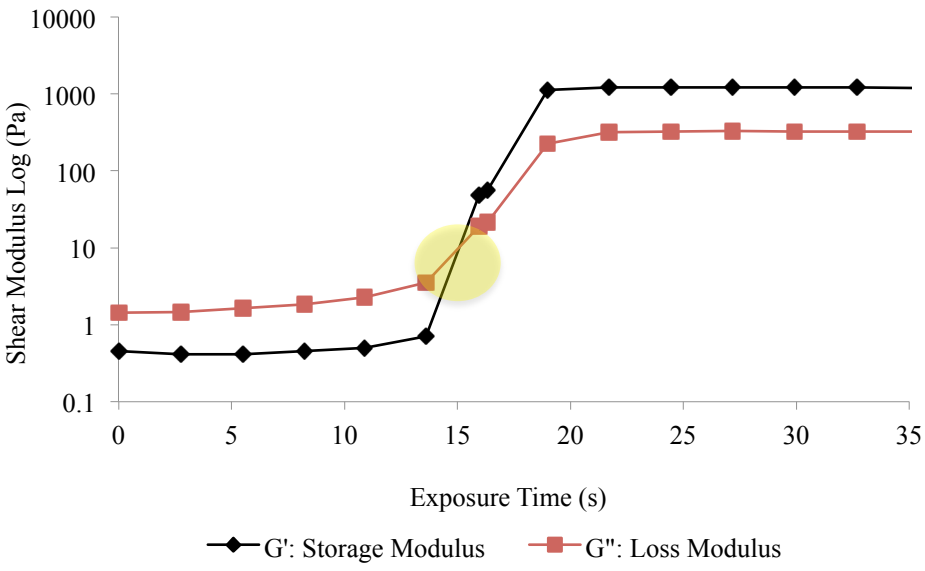

Figure 3.22. Representative dynamic oscillatory rheology plot vs. UV exposure time, highlighting the gelation point of when G' crosses G".

Utilizing the Winter-Chambon criterion to determine the GP, each dithiol resin system displayed a GP of 16 ± 2.5 seconds with no significant trend. Additionally, no

trend was presented in the strength of each dithiol resin network at GP, as the calculated strength was 2.8 Pa $s^{-0.5}$ on average, with a consistent 2.24 Pa G'. For comparison purposes to the degree of conversion slope change from stage I to stage II occurring around ~20 seconds, the calculated thiol conversion at GP using Flory-Stockmayer's theory of gelation was 0.23. Although RT-FTIR data was unable to measure precisely at 16 seconds of UV exposure, none of the resin systems reached further than 0.13 thiol conversion at 20 seconds of UV exposure. This contradicts that Flory's theory applies to the reaction system prior to the GP. More precise and rapid data accumulation is required to define initial rate kinetics.

Applying oscillations of a constant frequency and strain percentage resulted in dramatic shear stress increase within long CL dithiol networks. As a low degree of thiols convert and a higher degree of homopolymerization between neighboring 1,2-butadiene units persist, applying oscillatory stresses causes plastic deformation to occur within weakly cross-linked networks. Impinged cross-links lead to accumulation of densely populated chain entanglement that resists applied shearing forces. As polymer chains cannot easily move to elastically respond to the applied shearing force, continued shearing results in internal stress build up, even at low thiol conversions. With high thiol conversion and a densely cross-linked network, oscillatory shearing force is more efficiently distributed throughout the network, exhibiting elastic deformation. Shear stress was calculated with Equation 2.5 and positive values were plot against exposure time. Although shear stress distribution appears to gradually increase with increased exposure time in dithiol of 10 carbon atoms and increases at a dramatically steep rate for dithiol of five carbon atoms, stress distribution trend was best illustrated by G' vs thiol

conversion (Figure 3.23). As strain was kept constant, increasing G' slope vs thiol conversion shows the growing network's ability to distribute energy rather than store applied stress. Taking the slope of increasing G' as a function of thiol conversion enabled quantification of network ability to distribute applied shearing force with increasing thiol conversion. Table 3.3 provides the rate of increased stress storage as a function of time for varying dithiol molecular weight resins. Data displays a significant increase in stored stress as a function of thiol conversion in long CL dithiol resins, in particular that of DD. When excluding DD and comparing PD to ND resins, PD is 60.4% more efficient at distributing applied shearing stress than ND.

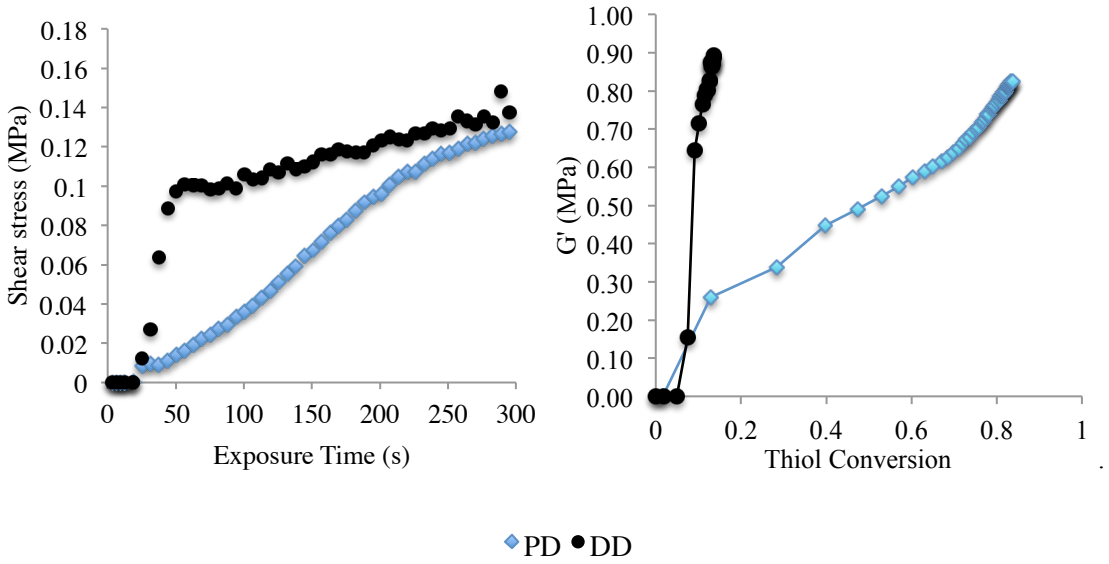

Figure 3.23. Representative plots show positive values of calculated shear stress distribution with time (left) and elastic shear modulus increase with increasing thiol conversion (right).

Table 3.3. Stage II polymerization network stress build-up as a function of thiol conversion

# Carbon	**5**	**6**	**8**	**9**	**10**
G'/x **(MPa/s)**	0.69	0.72	0.85	1.73	264.89

Increasing viscosity with thiol conversion may have also contributed to internal stress build up. As discussed, dithiols act as a reactive diluent. With increasing degree of cross-linking, mobility of free dithiol monomers and polymer chains decrease significantly, resulting in an increase in diffusion-related termination. By monitoring the complex viscosity during RT-Rheology measurements, viscosity data increased in a manner directly proportional to G' (Figure 3.24). This confirmed greater entanglement within long CL dithiol network, as dithiol mobility was restricted with a lesser-recorded degree of cross-linking.

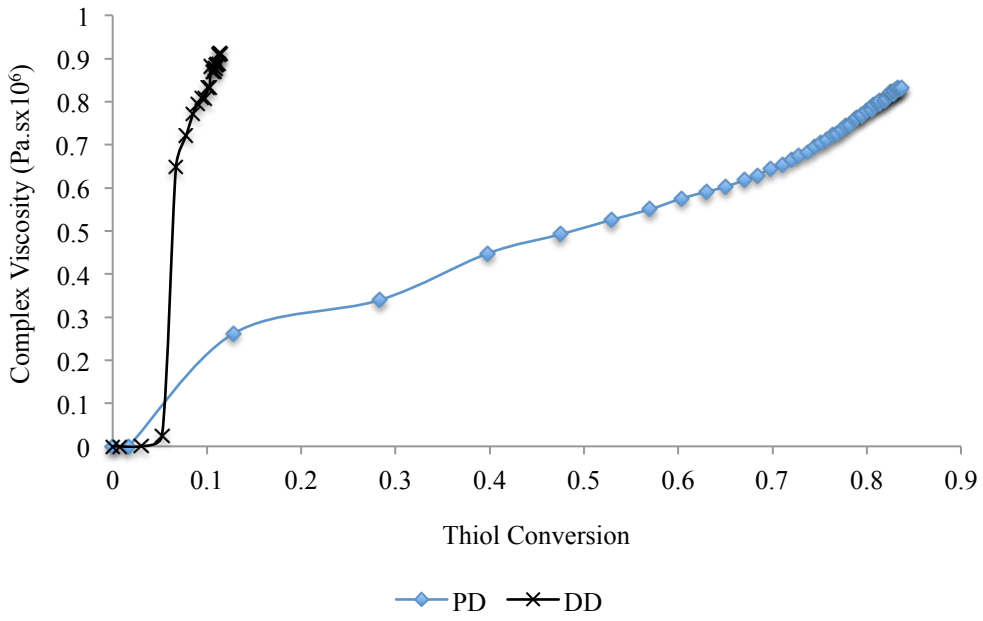

Figure 3.24. Complex viscosity as a function of thiol conversion for PD and DD resin systems follow similar trends to that of increasing G' as a function of thiol conversion.

3.4.2.1. Internal Network Stress Variation

Monitoring the axial force acting on the upper plate geometry of the rheometer during network formation confirmed a greater internal stress with a weakly cross-linked

network in long CL dithiol resin systems. Figure 3.25 displays the change in axial force during network formation after zeroing the initial force of each resin. No change in axial force is detected until reaching the GP as chains can flow past each other, followed by a drastic decrease in axial force. Inducing covalent bond formation between PB chains implements an overall contraction in the curing elastomer, causing a negative axial force. Once the network has formed, flow is restricted between chains and elastically active linked segments experience forced conformation change with shear, causing a positive axial force. Depending on segment orientation, network segments will be compressed or stretched. Increasing positive axial force has been attributed mostly to stretched segments [42], where cyclic structures and entanglements within long CL dithiol systems show a greater axial force than the more uniformly linked network formed via short CL dithiol resins. Chain entanglements can act similarly to a cross-link, but can cause shorter linked segments depending on where the entanglement occurs. With a shorter segment being stretched or compressed, a greater amount of stress results, causing an overall greater internal stress in the network. Additionally, regions of dangling chain ends cause weak locations within the network, enabling network impingement and plastic deformation with shear.

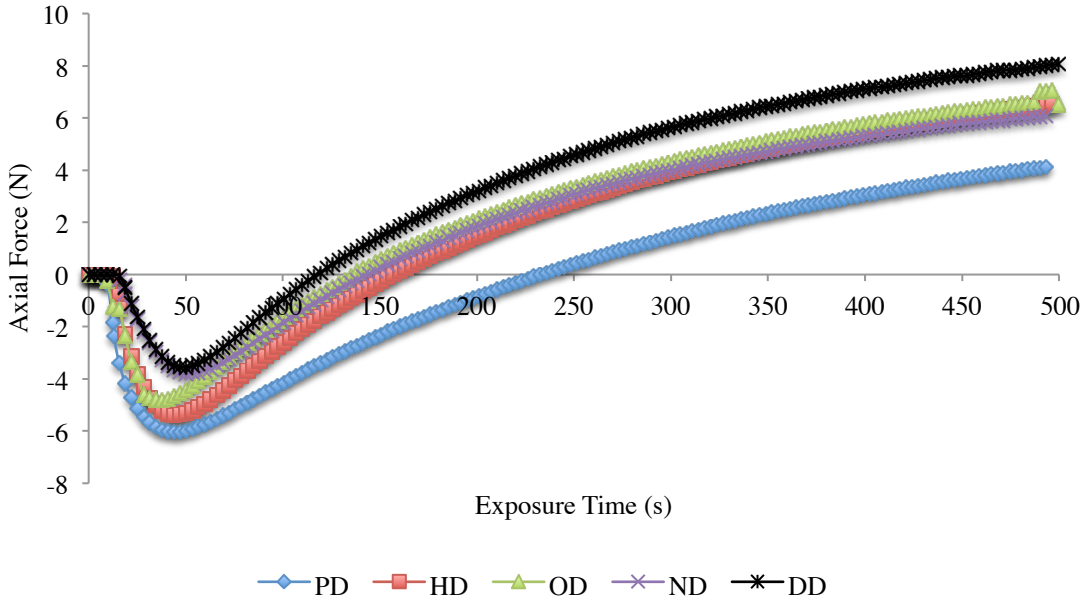

Figure 3.25. Axial force change due to increasing dithiol CL displaying greater network contraction in short CL dithiols, and greater stress in long CL dithiols.

Negative axial forces due to contraction of network formation were confirmed by measuring the first normal force of DD and HD resin systems (Figure 3.26). A higher degree of thiol conversion (79%) measured during FTIR in HD resin results in a greater shrinkage stress than DD resins, signified by the more negative normal stress values. Negative normal stress values are attributed to the stress in the y-direction, while positive stress values are those perpendicular to the parallel plate. Positive normal stress values measure the displacement of large molecules, specifically those forming an elastomer network. Higher thiol conversion in HD with a lower relative reactivity ratio towards homopolymerization produced a denser cross-linked network, resulting in a greater positive normal stress than DD. Positive normal stress reaches a maximum and remains constant, indicating the termination of network formation. Axial force

measurements during oscillatory shear did not plateau at a maximum value. With oscillatory shear, cross-link segments experience repeated stretching and compression to a magnitude dependent on their orientation with respect to the upper geometry. If chain entanglements are trapped within the network, entanglements cause an increase in axial force due to increased friction against linked polymer segments [43]. Comparing the first normal stress data to axial force measurements confirms a greater internal network friction and stress within DD resins as a less dense network was detected.

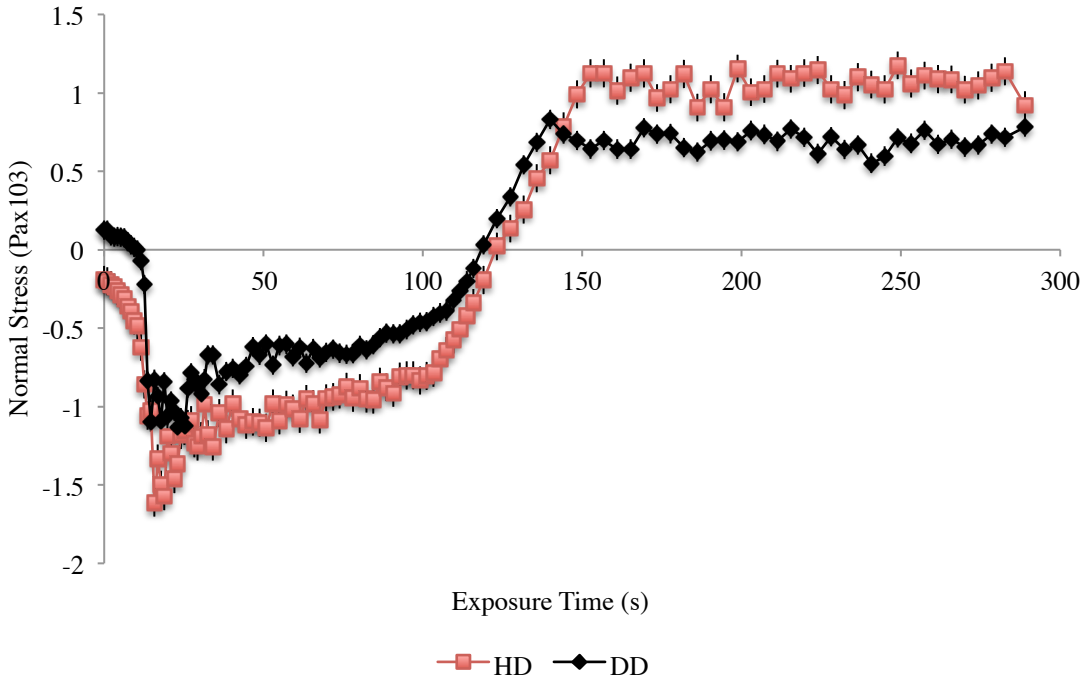

Figure 3.26. Greater shrinkage stress in HD compared to DD, verified via first normal stress measurements.

Macroscopic cracking within DD resin encasing has been explained due to a weakly cross-linked network and inability to effectively dissipate stress during oscillatory

shear application. The compression and tensile forces of the underlying PET electrode acting on the cured DD elastomer caused internal stress build-up that the non-uniform network was unable to dissipate, resulting in elastomer failure. Resin systems containing PD as the cross-linker presented the highest thiol conversion, lowest relative reactivity ratio to homopolymerize, and was able to effectively distribute stress within the network. PD resin systems, or at least short CL dithiol systems, should be utilized throughout all elastomer formulations in preserving the lifetime of EPD displays.

4. RESEARCH OUTLOOK

Uniformity of cross-linked networks can be compared between TE-2000 and B-1000 samples with temperature DMA to better characterize the low loss tangent observed in B-1000 samples [73]. The WLF equation will be used to describe relaxation time in relation to free volume. Microstructural differences of varying dithiol CL as well as varying PB functionality can thus be studied, as well as gather quantitative network relaxation values. DMA with increasing temperature will be performed with tensile samples to reduce error found from DMA compression testing.

Additionally, enthalpy differences associated with dithiol CL can be studied with temperature DMA or differential scanning calorimetry (DSC). A clear T_g has been characterized during preliminary DSC studies of cured TE-2000 samples (Figure 4.1). Initial tests determined the effect of a lack of HD vs adding 0.05 molar ratio HD in formulations with 1 wt% Irgacure 1173, diluted in 30 wt% hexane. T_g shifted from -9.27 ˚C to -4.63 ˚C in formulations without and with HD. Additionally, a significant exothermic peak was observed in formulations without HD, with less of the effect seen with the addition of 0.05 molar thiol ratio. Addition of HD acted to reduce the viscosity of the system, even if minutely, enabling a greater degree of cross-linking. This effect has been seen in other studies [11], [46], where autoacceleration is delayed and the propagation rate is increased. Without dithiols the system viscosity is high, enabling diffusion limitation within propagation and termination, thus decreasing the both rates. This explains the greater exothermic peak in formulations without HD, as higher temperatures enable acrylates to continue propagating. Temperature DMA will thus be utilized to further understand network response to oscillatory tensile stress, and can be

used in conjunction with DSC for characterizing uncured and cured thiol-polybutadiene samples.

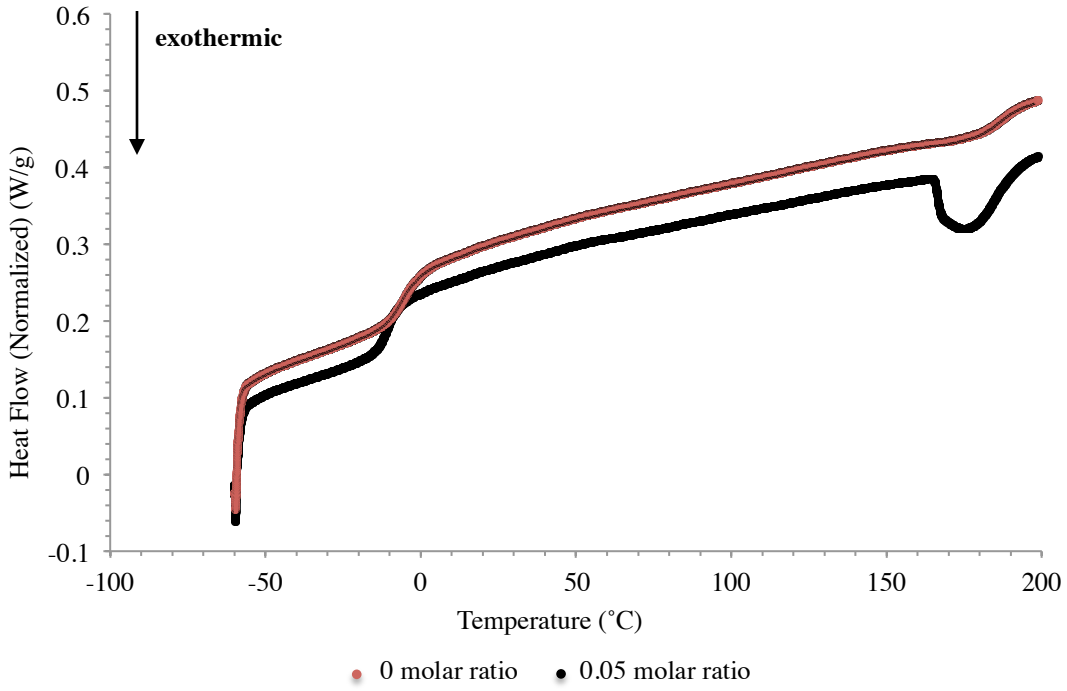

Figure 4.1. Preliminary DSC characterization of TE-2000 without thiol and with 0.05 molar ratio thiol:vinyl addition.

More RT-FTIR replicates will be performed in obtain a higher confidence in the observed decrease in thiol conversion with greater dithiol CL. However, solid-state nuclear magnetic resonance (NMR) spectroscopy may also be used to verify RT-FTIR results for cured B-1000 resins of increasing dithiol CL. Solid-state ^{13}CNMR spectroscopy of acrylate reactions have been utilized in past studies to characterize degree of cross-linking, homopolymerization kinetics and unreacted double bonds within a network [79], [80]. Although an ex-situ method, solid-state NMR can be used after stopping thiol-polybutadiene photopolymerization after sequential time intervals and

characterizing. Additionally, ^{1}HNMR studies will be performed on uncured resins after sitting in the dark for incremental periods of time to measure resin instability due to oxygen effects (dark reaction) [29]. Additional stabilizers such as hydroquinone monomethyl ether will be added in an attempt to scavenge activated oxygen prior to reacting [72]. Solid-state NMR can also be utilized to more closely examine any effects of oxygen and aging post curing.

5. CONCLUSIONS

In summary, thiol-polybutadiene formulations are promising for preserving propylene carbonate in EPD displays. Utilizing TE-2000 as PB base exhibited denser cross-linked networks with a higher compressive elastic modulus than did B-1000. Overall, B-1000 and TE-2000 reached swell percentage minimums of 25.6% and 9.85%, respectively, at 0.75 wt% Irgacure 1173. However, maximum calculated gelation percentages did not vary significantly between either PB base, as both were approximately 90% insoluble fraction at 0.2:1 molar thiol ratio. DMA average loss tangent results signified that TE-2000 network exhibited an eight times more elastically active network than B-1000, potentially due to a denser network of elastically active cross-linked segments. Although B-1000 was found to be more elastic, microstructure of TE-2000 showed a 2.5 times greater stiffness at 0.75 wt% than B-1000 samples.

In an attempt to combine both elasticity and strength and produce a dense cross-link network, a hybrid resin of 70/30 TE-2000/B-1000 ratio with 0.75 wt% Irgacure 1173 was developed. Swell and compression testing results of the cured hybrid resin samples fell right between that of B-1000 and TE-2000, reaching a minimum swell percentage of 9.84% and elasticity two times less than TE-2000. The hybrid resin was high in viscosity (496.5 mPa.s), but was still able to successfully encapsulate a propylene carbonate suspension in the microfluidic apparatus. The best results were seen with a 0.05:1 thiol:vinyl ratio.

Encasing resin formulations were improved by indicating that PD resin systems had approximately eight times greater thiol conversion than did DD, with PD and DD formulations reaching a maximum thiol conversion of 86% and 11.3%, respectively. Low

thiol conversion and three times the homopolymerization reaction in DD dithiol resin compared to PD resin resulted in encasing failure. Oscillatory rheological experiments confirmed a more uniform network to better dissipate applied shear in short chain length dithiol systems, as long chain length dithiols relayed a steep internal stress build-up due to less cross-links, a higher degree of homopolymerization and chain entanglements. Thus, utilizing short CL dithiols will produce more robust elastomers in encasing, as well as encapsulating EPD NP suspension.

This work has been focused on improving the cross-linking density and mechanical properties of thiol-polybutadiene resins for use to seal, encase flexible devices, and to form an elastomeric shell around EPD NP suspension. Initial development of display resins has led to improvement in EPD flexible displays. This work shows how critical it is to understand curing kinetics and network microstructure formation within elastomers and can be applied to future thiol-polybutadiene based elastomer resin systems.

6. REFERENCES

[1] "E Ink: Technology: Display Products." [Online]. Available: http://www.e-ink.com/display_products.html. [Accessed: 08-Mar-2017].

[2] B. R. Yang, "Overview of design considerations for electrophoretic e-paper and strategies for achieving full-color," in *2016 23rd International Workshop on Active-Matrix Flatpanel Displays and Devices (AM-FPD)*, 2016, pp. 81–84.

[3] A. P. Tarun, P. Wang, A. Girouard, P. Strohmeier, D. Reilly, and R. Vertegaal, "PaperTab: An Electronic Paper Computer with Multiple Large Flexible Electrophoretic Displays," in *CHI '13 Extended Abstracts on Human Factors in Computing Systems*, New York, NY, USA, 2013, pp. 3131–3134.

[4] L. Besra and M. Liu, "A review on fundamentals and applications of electrophoretic deposition (EPD)," *Prog. Mater. Sci.*, vol. 52, no. 1, pp. 1–61, Jan. 2007.

[5] J. Ge and Y. Yin, "Magnetically Tunable Colloidal Photonic Structures in Alkanol Solutions," *Adv. Mater.*, vol. 20, no. 18, pp. 3485–3491, Sep. 2008.

[6] J. Ge, Y. Hu, T. Zhang, T. Huynh, and Y. Yin, "Self-Assembly and Field-Responsive Optical Diffractions of Superparamagnetic Colloids," *Langmuir*, vol. 24, no. 7, pp. 3671–3680, Apr. 2008.

[7] M. G. Han *et al.*, "Full Color Tunable Photonic Crystal from Crystalline Colloidal Arrays with an Engineered Photonic Stop-Band," *Adv. Mater.*, vol. 24, no. 48, pp. 6438–6444, Dec. 2012.

[8] "Polarity Index." [Online]. Available: http://macro.lsu.edu/howto/solvents/Polarity%20index.htm. [Accessed: 14-Mar-2017].

[9] C. Ye, A. Chen, P. Colombo, and C. Martinez, "Ceramic microparticles and capsules via microfluidic processing of a preceramic polymer," *J. R. Soc. Interface*, p. rsif20100133, May 2010.

[10] M. J. Kade, D. J. Burke, and C. J. Hawker, "The power of thiol-ene chemistry," *J. Polym. Sci. Part Polym. Chem.*, vol. 48, no. 4, pp. 743–750, Feb. 2010.

[11] C. E. Hoyle, T. Y. Lee, and T. Roper, "Thiol–enes: Chemistry of the past with promise for the future," *J. Polym. Sci. Part Polym. Chem.*, vol. 42, no. 21, pp. 5301–5338, Nov. 2004.

[12] C. R. Morgan and A. D. Ketley, "The effect of phosphines on thiol/ene curing systems," *J. Polym. Sci. Polym. Lett. Ed.*, vol. 16, no. 2, pp. 75–79, Feb. 1978.

[13] "Norland Products, Inc. | Interferometric Microscopes for Multifiber Connectors." [Online]. Available: http://www.norlandproducts.com/. [Accessed: 19-Feb-2017].

[14] N. B. Cramer and C. N. Bowman, "Kinetics of thiol–ene and thiol–acrylate photopolymerizations with real-time fourier transform infrared," *J. Polym. Sci. Part Polym. Chem.*, vol. 39, no. 19, pp. 3311–3319, Oct. 2001.

[15] N. B. Cramer, J. P. Scott, and C. N. Bowman, "Photopolymerizations of Thiol–Ene Polymers without Photoinitiators," *Macromolecules*, vol. 35, no. 14, pp. 5361–5365, Jul. 2002.

[16] N. B. Cramer, T. Davies, A. K. O'Brien, and C. N. Bowman, "Mechanism and Modeling of a Thiol–Ene Photopolymerization," *Macromolecules*, vol. 36, no. 12, pp. 4631–4636, Jun. 2003.

[17] B.-S. Chiou and S. A. Khan, "Real-Time FTIR and in Situ Rheological Studies on the UV Curing Kinetics of Thiol-ene Polymers," *Macromolecules*, vol. 30, no. 23, pp. 7322–7328, Nov. 1997.

[18] B.-S. Chiou, R. J. English, and S. A. Khan, "Rheology and photo-cross-linking of thiol-ene polymers," *Macromolecules*, vol. 29, no. 16, pp. 5368–5374, 1996.

[19] H. Lu, J. A. Carioscia, J. W. Stansbury, and C. N. Bowman, "Investigations of step-growth thiol-ene polymerizations for novel dental restoratives," *Dent. Mater.*, vol. 21, no. 12, pp. 1129–1136, Dec. 2005.

[20] J. W. Stansbury, M. Trujillo-Lemon, H. Lu, X. Ding, Y. Lin, and J. Ge, "Conversion-dependent shrinkage stress and strain in dental resins and composites," *Dent. Mater.*, vol. 21, no. 1, pp. 56–67, Jan. 2005.

[21] M. Braem, P. Lambrechts, G. Vanherle, and C. L. Davidson, "Stiffness Increase During the Setting of Dental Composite Resins," *J. Dent. Res.*, vol. 66, no. 12, pp. 1713–1716, Dec. 1987.

[22] L. C. C. Boaro, F. Gonçalves, T. C. Guimarães, J. L. Ferracane, A. Versluis, and R. R. Braga, "Polymerization stress, shrinkage and elastic modulus of current low-shrinkage restorative composites," *Dent. Mater.*, vol. 26, no. 12, pp. 1144–1150, Dec. 2010.

[23] R. R. Braga, R. Y. Ballester, and J. L. Ferracane, “Factors involved in the development of polymerization shrinkage stress in resin-composites: A systematic review,” *Dent. Mater.*, vol. 21, no. 10, pp. 962–970, Oct. 2005.

[24] J. G. Kloosterboer, “Network formation by chain crosslinking photopolymerization and its applications in electronics,” in *Electronic Applications*, Springer, Berlin, Heidelberg, 1988, pp. 1–61.

[25] M. U. Kahveci, A. G. Yilmaz, and Y. Yagci, “Photoinitiated Cationic Polymerization: Reactivity and Mechanistic Aspects,” in *Photochemistry and Photophysics of Polymer Materials*, N. S. Allen, Ed. John Wiley & Sons, Inc., 2010, pp. 421–478.

[26] C. Decker and T. Nguyen Thi Viet, “Photocrosslinking of functionalized rubbers IX. Thiol-ene polymerization of styrene-butadiene-block-copolymers,” *Polymer*, vol. 41, no. 11, pp. 3905–3912, May 2000.

[27] T. Y. Lee, J. Carioscia, Z. Smith, and C. N. Bowman, “Thiol–Allyl Ether–Methacrylate Ternary Systems. Evolution Mechanism of Polymerization-Induced Shrinkage Stress and Mechanical Properties,” *Macromolecules*, vol. 40, no. 5, pp. 1473–1479, Mar. 2007.

[28] C. Decker and T. N. T. Viet, “Photocrosslinking of functionalized rubbers, 8. The thiol-polybutadiene system,” *Macromol. Chem. Phys.*, vol. 200, no. 8, pp. 1965–1974, Aug. 1999.

[29] J.-P. Fouassier and J. F. RABEK, *Radiation Curing in Polymer Science and Technology*. Springer Science & Business Media, 1993.

[30] V. S. Khire, Y. Yi, N. A. Clark, and C. N. Bowman, "Formation and Surface Modification of Nanopatterned Thiol-ene Substrates using Step and Flash Imprint Lithography," *Adv. Mater.*, vol. 20, no. 17, pp. 3308–3313, Sep. 2008.

[31] V. Mucci and C. Vallo, "Efficiency of 2,2-dimethoxy-2-phenylacetophenone for the photopolymerization of methacrylate monomers in thick sections," *J. Appl. Polym. Sci.*, vol. 123, no. 1, pp. 418–425, Jan. 2012.

[32] A. E. Rydholm, C. N. Bowman, and K. S. Anseth, "Degradable thiol-acrylate photopolymers: polymerization and degradation behavior of an in situ forming biomaterial," *Biomaterials*, vol. 26, no. 22, pp. 4495–4506, Aug. 2005.

[33] A. F. Senyurt, H. Wei, C. E. Hoyle, S. G. Piland, and T. E. Gould, "Ternary Thiol–Ene/Acrylate Photopolymers: Effect of Acrylate Structure on Mechanical Properties," *Macromolecules*, vol. 40, no. 14, pp. 4901–4909, Jul. 2007.

[34] I. Sideridou, V. Tserki, and G. Papanastasiou, "Effect of chemical structure on degree of conversion in light-cured dimethacrylate-based dental resins," *Biomaterials*, vol. 23, no. 8, pp. 1819–1829, Apr. 2002.

[35] C. Decker, "Kinetic Study and New Applications of UV Radiation Curing," *Macromol. Rapid Commun.*, vol. 23, no. 18, pp. 1067–1093, Dec. 2002.

[36] P. C. Painter and M. M. Coleman, *Fundamentals of polymer science : an introductory text*. Lancaster [etc.]: Technomic, 1997.

[37] M. Shimbo, M. Ochi, and Y. Shigeta, "Shrinkage and internal stress during curing of epoxide resins," *J. Appl. Polym. Sci.*, vol. 26, no. 7, pp. 2265–2277, Jul. 1981.

[38] H. H. Winter, "Gel Point," in *Encyclopedia of Polymer Science and Technology*, John Wiley & Sons, Inc., 2002.

[39] H.H. Winter and F. Chambon, “Analysis of Linear Viscoelasticity of a Crosslinking Polymer at the Gel Point,” *J. Rheol.*, vol. 30, no. 2, pp. 367–382, Apr. 1986.

[40] C. D. Han and K.-W. Lem, “Chemorheology of thermosetting resins. I. The chemorheology and curing kinetics of unsaturated polyester resin,” *J. Appl. Polym. Sci.*, vol. 28, no. 10, pp. 3155–3183, Oct. 1983.

[41] T. G. Mezger, *The Rheology Handbook: For Users of Rotational and Oscillatory Rheometers*. Vincentz Network GmbH & Co KG, 2006.

[42] P. A. Janmey, M. E. McCormick, S. Rammensee, J. L. Leight, P. C. Georges, and F. C. MacKintosh, “Negative normal stress in semiflexible biopolymer gels,” *Nat. Mater.*, vol. 6, no. 1, pp. 48–51, Jan. 2007.

[43] W. W. Graessley, “The entanglement concept in polymer rheology,” in *The Entanglement Concept in Polymer Rheology*, Springer Berlin Heidelberg, 1974, pp. 1–179.

[44] R.S. Lakes, “Viscoelastic measurement techniques,” *Rev. Sci. Instrum.*, vol. 75, no. 4, pp. 797–810, Mar. 2004.

[45] R. S. Lakes, *Viscoelastic Solids*. CRC Press, 1998.

[46] L. Lecamp, F. Houllier, B. Youssef, and C. Bunel, “Photoinitiated cross-linking of a thiol–methacrylate system,” *Polymer*, vol. 42, no. 7, pp. 2727–2736, Mar. 2001.

[47] I. M. Ward and J. Sweeney, *Mechanical Properties of Solid Polymers*. John Wiley & Sons, 2012.

[48] J. D. Ferry, *Viscoelastic Properties of Polymers*. John Wiley & Sons, 1980.

[49] G. G. Odian, *Principles of polymerization*, 4. ed. Hoboken, NJ: Wiley-Interscience, 2004.

[50] R. F. Boyer, "Dependence of mechanical properties on molecular motion in polymers," *Polym. Eng. Sci.*, vol. 8, no. 3, pp. 161–185, Jul. 1968.

[51] K. Matyjaszewski and T. P. Davis, *Handbook of Radical Polymerization*. John Wiley & Sons, 2003.

[52] A. Von Raven and H. Heusinger, "Radiation-induced crosslinking and cyclization in 1, 2-polybutadiene," *J. Polym. Sci. Polym. Chem. Ed.*, vol. 12, no. 10, pp. 2255–2271, 1974.

[53] J. Justynska, Z. Hordyjewicz, and H. Schlaad, "Toward a toolbox of functional block copolymers via free-radical addition of mercaptans," *Polymer*, vol. 46, no. 26, pp. 12057–12064, Dec. 2005.

[54] B. M. Mandal, *Fundamentals of Polymerization*. World Scientific, 2013.

[55] H. H. Szmant, A. J. Mata, A. J. Namis, and A. M. Panthananickal, "The thiol-olefin co-oxidation (TOCO) Reaction—IV : Temperature effects on product distribution in the toco reaction of indene and aromatic thiols," *Tetrahedron*, vol. 32, no. 22, pp. 2665–2680, 1976.

[56] N. B. Cramer and C. N. Bowman, "Kinetics of thiol–ene and thiol–acrylate photopolymerizations with real-time fourier transform infrared," *J. Polym. Sci. Part Polym. Chem.*, vol. 39, no. 19, pp. 3311–3319, Oct. 2001.

[57] E. Klemm, S. Sensfuß, U. Holfter, and H. J. Flammersheim, "Free-Radical stabilizers for the thiol/ene-systems," *Angew. Makromol. Chem.*, vol. 212, no. 1, pp. 121–127, Nov. 1993.

[58] T. M. Lovestead, K. A. Berchtold, and C. N. Bowman, “Modeling the Effects of Chain Length on the Termination Kinetics in Multivinyl Photopolymerizations,” *Macromol. Theory Simul.*, vol. 11, no. 7, pp. 729–738, Sep. 2002.

[59] M. Buback, H. Frauendorf, F. Günzler, F. Huff, and P. Vana, “Determining Initiator Efficiency in Radical Polymerization by Electrospray-Ionization Mass Spectrometry,” *Macromol. Chem. Phys.*, vol. 210, no. 19, pp. 1591–1599, Oct. 2009.

[60] P. J. Halley and M. E. Mackay, “Chemorheology of thermosets—an overview,” *Polym. Eng. Sci.*, vol. 36, no. 5, pp. 593–609, Mar. 1996.

[61] C. Decker and T. Nguyen Thi Viet, “Photocrosslinking of functionalized rubbers. X. Butadiene–acrylonitrile copolymers,” *J. Appl. Polym. Sci.*, vol. 82, no. 9, pp. 2204–2216, Nov. 2001.

[62] C. Decker and T. N. T. Viet, “Photocrosslinking of functionalized rubbers, 7. Styrene-butadiene block copolymers,” *Macromol. Chem. Phys.*, vol. 200, no. 2, pp. 358–367, Feb. 1999.

[63] E. Rabinowitch, “Collision, co-ordination, diffusion and reaction velocity in condensed systems,” *Trans. Faraday Soc.*, vol. 33, no. 0, pp. 1225–1233, Jan. 1937.

[64] H. K. Mahabadi and K. F. O’Driscoll, “Termination rate constant in free-radical polymerization,” *J. Polym. Sci. Polym. Chem. Ed.*, vol. 15, no. 2, pp. 283–300, Feb. 1977.

[65] S. Połowiński, “Template polymerisation and co-polymerisation,” *Prog. Polym. Sci.*, vol. 27, no. 3, pp. 537–577, Apr. 2002.

[66] P. Hayden and H. Melville, “The kinetics of the polymerization of methyl methacrylate. I. The bulk reaction,” *J. Polym. Sci.*, vol. 43, no. 141, pp. 201–214, Mar. 1960.

[67] M. Uygun, M. A. Tasdelen, and Y. Yagci, “Influence of Type of Initiation on Thiol–Ene ‘Click’ Chemistry,” *Macromol. Chem. Phys.*, vol. 211, no. 1, pp. 103–110, Jan. 2010.

[68] H. F. Gruber, “Photoinitiators for free radical polymerization,” *Prog. Polym. Sci.*, vol. 17, no. 6, pp. 953–1044, 1992.

[69] C. E. Hoyle and C. N. Bowman, “Thiol–Ene Click Chemistry,” *Angew. Chem. Int. Ed.*, vol. 49, no. 9, pp. 1540–1573, Feb. 2010.

[70] “NISSO-PB | Nippon Soda Co., Ltd.” [Online]. Available: http://www.nippon-soda.co.jp/pb/list.html#b. [Accessed: 17-Jan-2017].

[71] P. W. Moore, F. W. Ayscough, and J. G. Clouston, “γ-radiation-initiated polymerization of bulk styrene at high pressure,” *J. Polym. Sci. Polym. Chem. Ed.*, vol. 15, no. 6, pp. 1291–1308, Jun. 1977.

[72] H. Becker and H. Vogel, “The Role of Hydroquinone Monomethyl Ether in the Stabilization of Acrylic Acid,” *Chem. Eng. Technol.*, vol. 29, no. 10, pp. 1227–1231, Oct. 2006.

[73] J. W. Chan, H. Zhou, C. E. Hoyle, and A. B. Lowe, “Photopolymerization of Thiol-Alkynes: Polysulfide Networks,” *Chem. Mater.*, vol. 21, no. 8, pp. 1579–1585, Apr. 2009.

[74] G. A. Laughlin, J. L. Williams, and J. D. Eick, “The influence of system compliance and sample geometry on composite polymerization shrinkage stress,” *J. Biomed. Mater. Res.*, vol. 63, no. 5, pp. 671–678, Jan. 2002.

[75] S. K. Soh and D. C. Sundberg, “Diffusion-controlled vinyl polymerization. I. The gel effect,” *J. Polym. Sci. Polym. Chem. Ed.*, vol. 20, no. 5, pp. 1299–1313, May 1982.

[76] J. T. Edward, “Molecular volumes and the Stokes-Einstein equation,” *J. Chem. Educ.*, vol. 47, no. 4, p. 261, Apr. 1970.

[77] C. E. Hoyle, R. D. Hensel, and M. B. Grubb, “Laser-initiated polymerization of a thiol-ene system,” *Polym. Photochem.*, vol. 4, no. 1, pp. 69–80, Jan. 1984.

[78] C. R. Morgan, F. Magnotta, and A. D. Ketley, “Thiol/ene photocurable polymers,” *J. Polym. Sci. Polym. Chem. Ed.*, vol. 15, no. 3, pp. 627–645, Mar. 1977.

[79] J. E. Dietz, B. A. Cowans, R. A. Scott, and N. A. Peppas, “Solid-State NMR Spectroscopy for Characterization of Acrylate Reactions,” in *Photopolymerization*, vol. 673, 0 vols., American Chemical Society, 1997, pp. 28–34.

[80] W. F. Jager, A. Lungu, D. Y. Chen, and D. C. Neckers, “Photopolymerization of Polyfunctional Acrylates and Methacrylate Mixtures: Characterization of Polymeric Networks by a Combination of Fluorescence Spectroscopy and Solid State Nuclear Magnetic Resonance,” *Macromolecules*, vol. 30, no. 4, pp. 780–791, Feb. 1997.